

# Quantum many-body dynamics of driven-dissipative Rydberg polariton systems

Von der Fakultät für Mathematik und Physik  
der Gottfried Wilhelm Leibniz Universität Hannover  
zur Erlangung des Grades

Doktor der Naturwissenschaften  
Dr. rer. nat.

genehmigte Dissertation von

**Dipl.-Phys. Tim Pistorius**

Referent: Priv.-Doz. Dr. Hendrik Weimer

Korreferent: Prof. Dr. Klemens Hammerer  
Prof. Dr. Michael Fleischhauer

Tag der Promotion: 08.02.2021





# Abstract

Rapid advancements in the experimental realisation of large many-body systems also leads to the necessity for better theoretical descriptions of them. In this thesis, I present the successful solution of the notoriously hard but experimentally highly relevant many-body problem of driven-dissipative Rydberg polaritons in an optical lattice. The setup uses two counter-propagating light fields to produce a standing light field inside the lattice in combination with another control laser field to excite Rubidium atoms into the Rydberg states. From the continuous model, we derive a dispersion relation and construct the respective Wannier functions of the bands. We identify two dark-state polaritons and derive a Bose-Hubbard-like model in consideration of the interaction with the surrounding bright-state polariton bands. We then study the dynamics of this system with the Lindblad master equation to also include dissipative processes. To solve it, we use a variational approach in combination with a hard-sphere constraint to describe the Rydberg blockade. First, we compare these results with the solution from a Monte-Carlo wave function simulation where we find a good agreement between the two solutions for larger system sizes. We then use the variational approach to obtain a result for a system size of  $N = 40$ , which far exceeds the possible site number obtainable via Monte-Carlo simulations. In the end, we also study the time correlation between measurements of two photons leaving the system after they travelled through the entire lattice. The problem of the description of the infinite Hilbert space that occurs in bosonic fields is also a highly relevant topic in the context of many-body systems. Here, we show a new way to use the variational principle to describe any bosonic field by the usage of the P-representation of the density matrix in combination with the formulation of the master equation in terms of equations of motion. By investigating the bistability region of the driven-dissipative Jaynes-Cummings model, we show that our method exceeds conventional mean-field descriptions. We then extend the new approach by adding correlation functions as additional variational parameters to describe correlations between different parts of the Hilbert space. This allows us to investigate the effective three-boson model which describes Rydberg atoms inside a driven cavity with dissipation channels for the atoms and the cavity. The Rydberg-

Rydberg interaction leads to correlations between the atoms which in turn cause a squeezing effect of the different bosonic modes. By a transformation of the model into the polariton picture, we show how the squeezing mostly affects the dark-state polaritons and its scaling with the pumping rate of the cavity.

The last part focuses on the dissipative Ising model and its realisation through the coupling of internal states of ions and their vibrational modes. We present the analysis of the system with the novel approach to combine mean-field solutions with the variational norm to deepen the understanding of the phase diagram of the model. We also look for traces of the different phase transitions between a ferromagnetic and a paramagnetic phase if we are far from the thermodynamical limit. Furthermore, we present a measurement protocol that reduces unwanted detuning terms that can arrive from systematic errors in experiments, which will allow a better comparison between the theoretical and experimental analysis of the dissipative Ising model.

## Keywords

Open quantum systems

Offene Quantensysteme

Nonlinearity

Nicht-Linearitäten

Polaritons

Polaritonen

Dissipative Rydberg gases

Rydberg Gase

Ising model

Ising Modell





# Contents

<b>Introduction</b>	<b>9</b>
<b>1. Theoretical Background</b>	<b>13</b>
1.1. Open quantum systems . . . . .	14
1.1.1. Master equation in Lindblad form . . . . .	15
1.1.2. Variational Principle . . . . .	19
1.2. Quantum description of light . . . . .	22
1.3. Quasiprobability distributions . . . . .	29
1.4. Light-Matter interaction . . . . .	35
1.5. Rydberg atoms . . . . .	38
1.6. Optical lattices . . . . .	42
<b>2. Quantum many-body dynamics of driven-dissipative Rydberg polaritons</b>	<b>47</b>
2.1. Setup . . . . .	47
2.1.1. Dispersion relation . . . . .	49
2.1.2. Hamiltonian . . . . .	53
2.1.3. Influences of the environment . . . . .	55
2.1.4. Long-range interaction . . . . .	57
2.2. Time evolution . . . . .	64
2.2.1. Temporal correlations . . . . .	72
<b>3. The variational method for bosonic fields</b>	<b>75</b>
3.1. P-representation of the density matrix in the variational approach . . . . .	76
3.2. Jaynes-Cummings Model . . . . .	82
3.3. Rydberg atoms in a cavity . . . . .	88
3.4. Outlook . . . . .	92
3.5. Summary . . . . .	93
<b>4. Dynamical decoupling in the dissipative Ising model</b>	<b>95</b>
4.1. Phase transitions in the dissipative Ising model . . . . .	96
4.2. Mean-field solution and the phase diagram . . . . .	101
4.3. Measurement protocol . . . . .	101

*Contents*

<b>5. Summary</b>	<b>109</b>
<b>A. Pumping with a forward propagating wave</b>	<b>113</b>
<b>B. Fokker-Planck-equation for the damped harmonic oscillator</b>	<b>115</b>

# Introduction

The duality of light to behave like an electromagnetic field and a particle is one of the cornerstones of quantum mechanics. Nowadays, these particles, called photons, are back in the spotlight of a large research field. With progress in the fields of signal processing, quantum information and communication also came the possibility to use them as transmitters of informations[1, 2, 3, 4].

Almost lossless movement with the speed of light is a useful feature in the classical but also in the quantum world. On the other hand, photons do not only show almost no interaction with their environment but also with other photons which makes their usage for quantum gates, transistor, switches etc. hard as these devices rely on that interaction between the particles. Early research by Kerr showed that the application of an electric field can manipulate the optical properties of a medium. Even though researchers knew that these nonlinear effects can cause interaction between photons, they thought that the effects are only relevant for high levels of light intensities and not usable at the level of a single atom with only a few photons [4, 5]. The first major step to overcome the weak interaction between a photon and the atom was to drastically increase the time of interaction between atoms and photons by the usage of a cavity with a high-quality factor which enhances the probability that the two particles interact with each other [6, 7].

Another approach was the development of strongly nonlinear media which was achieved by the discovery of the electromagnetically induced transparency (EIT) effect, which creates strong nonlinearities even at a level of only a few quanta. If a three-level system is driven by a probe field and further excited to a metastable state by another control laser, then the interferences between different excitation patterns can allow photons to move through the medium. Therefore, EIT turns a normally opaque medium into a transparent one in a very narrow spectral window which causes the large nonlinearities. Furthermore, the photons that now pass through the system form quasi-particles with the atoms called polaritons [8]. These particles have a drastically reduced group velocity compared to pure light which depends on the ratio of light and matter in the composition of the polaritons. Because this can be changed by the control laser, these systems also find application in the field of

## *Contents*

quantum memories and storing of quantum informations by transforming light to matter and vice versa.

The control of the transmission on the level of a single photon was achieved by introducing Rydberg states as the third level in the EIT scheme. This change in the level architecture maps the dipole-dipole interaction of the Rydberg atoms onto the photons [9]. Responsible for this mapping process is the Rydberg blockade effect. The interaction strength detunes the atom out of the two-photon resonance necessary for EIT. The detuning can even exceed the control laser linewidth in an area around the Rydberg atom. Other atoms within the blockade radius of the Rydberg atom become two-level systems because they can no longer reach the Rydberg state. The interacting atoms inside the sphere form a mesoscopic superatom with an enhanced coupling to light [10, 11, 12, 13]. By also considering EIT in this description, the medium becomes transparent to single photons and opaque to pairs of photons. Multiple experimental groups confirmed the theoretical predictions later on [14, 15, 16, 17].

The emergence of different Rydberg polariton systems showed the need for better theoretical descriptions [9, 14, 15, 18, 19, 20, 21, 22, 23, 24, 25, 26, 27]. The interplay between external drive, a natural dissipation channel from the Rydberg state and strong dipole-dipole interaction can lead to interesting dynamics that are not found in closed systems [28, 29]. However, the analysis of open quantum many-body systems is extremely difficult [30]. Different attempts so far, are either limited by the number of polaritons in the system [24] or neglect the decay channel of the Rydberg state [25, 26, 27].

This thesis wants to offer new ways to study these open many-body systems with the usage of the variational principle for open quantum systems. The first chapter covers most of the theoretical concepts that build the foundation of this thesis. It focuses on the theory for open quantum systems and how the variational principle can be adapted to it. We also give a brief summary on how to describe light in the quantum mechanical context which also includes its representations in terms of quasi-probability distributions and the examples of some of the most prominent states of light. In the end, we discuss the distinctive properties of Rydberg atoms which also leads to the formation of EIT, dark states and polaritons if they interact with light.

The second chapter then investigates the dynamics of Rydberg polaritons in an optical lattice potential. We will first derive the dispersion relation of the system by solving the single-particle problem, which allows us to obtain a Bose-Hubbard-like

Hamiltonian with long-range hopping. We then move on to study the influences of an environment and also how the long-range interactions affect our system. We will use this knowledge to adapt the variational principle for the system and compare it to other common numerical methods to see how it performs. The variational approach then allows us to probe our model for larger system sizes than otherwise possible. In the end we observe the time dynamics in the system, especially on the last site, which has a connection to the photon output of our system. Furthermore, we also look at the time correlation function which will give us information about the quantum nature of the emitted light.

In the next chapter, we turn to a wider problem of how to treat bosonic fields in an open quantum system. To tackle the problem, we will look at the convolution of phase-space representations of the density matrix and how to calculate expectation values without knowing the full expression of these convoluted distribution functions. Based on that, we formulate a variational principle in terms of expectation values with the P-distribution to describe bosonic fields. We then test it on the well-known Jaynes-Cummings model and compare it again with other methods. We then extend the newly developed method even further by also allowing correlation between different modes. In the last section of this chapter we look at an effective model for Rydberg atoms in a cavity. We study how the Rydberg-Rydberg interaction affects the squeezing of the polariton particles and we also look at particle numbers that are very hard to obtain with other methods to see how the same scale with cavity pumping.

In the last part of this thesis, we turn our attention to a different many-body system in the form of the dissipative Ising model. Extensive studies of the model with the variational principle showed an interesting and rich phase diagram that exceeds previous assumptions based on the mean-field approach or the closed version of the system [31, 32, 33, 34]. We will look at a system of two trapped ions that are coupled with each other through their vibrational modes which causes an Ising-like interaction between the ions. There are two questions we are concerned with. The first one is if the mean-field solutions can be used to find both second and first-order transitions if combined with the variational principle. The second one is if we can find traces of the phase transitions between a ferromagnetic and a paramagnetic phase in an experimentally realistic setup which means far from the thermodynamical limit. To lower possible errors for these systems we also present a measurement protocol to minimize unwanted systematic error.



# 1. Theoretical Background

We want to use this section to discuss some basic concepts we will need throughout the thesis. The concepts and methods for describing open quantum systems will serve us as a starting point. First, we will establish the description of quantum systems with mixed states via the density operator. We use this to describe the dynamics of systems that couple to an external bath which leads us to the Lindblad master equation and the generalised Ehrenfest equation, which offers an equivalent description but in terms of expectation values. We also introduce the concepts of the variational principle for open quantum systems as an efficient method to solve driven-dissipative many-body problems.

Afterwards, we give a brief overview of the quantum description of light. We will give a few examples of possible states in which we can encounter light or bosonic fields in general and follow this up with the introduction of quasiprobabilities distributions to describe these bosonic fields.

We then want to look at some coherence and interference effects that stem from the interaction of atoms with light, including the electromagnetically induced transparency (EIT), the creation of dark states and at the end the introduction of polaritons.

Hereafter we shift our attention towards the systems we will encounter in the following chapters. First and foremost, this will include Rydberg atoms, their properties and also a short overview of how these atoms connect to the previously mentioned effects in combination with light. In the end, we apply the Bloch theorem to a general lattice system, which will be our foundation for the theoretical description of Rydberg atoms in a lattice.

## 1.1. Open quantum systems

From quantum mechanics, we know that a system can be described by its wave function  $\Psi$  and its dynamics are given by [35]

$$\hat{H} |\Psi\rangle = \hat{E} |\Psi\rangle. \quad (1.1)$$

Eq. (1.1) is the most general form of the Schrödinger equation with  $\hat{H}$  as the Hamilton operator and  $\hat{E} = i\hbar \frac{\partial}{\partial t}$ . This description of quantum systems is only valid as long as it is isolated from its environment, an impossible task in any realistic situation.

In this section we want to discover how we can include the influences of the environment to the system we are interested in. We will see that a single wave function is in general not sufficient enough to describe the system, which will lead us to the introduction of the density matrix. This obviously implies that we cannot use the Schrödinger equation in the form of Eq. (1.1) to describe the dynamics of an open quantum system. Instead, we will give a brief derivation of the Lindblad master equation and its description of the dynamics of systems with dissipation channels. In the last part, we will introduce the variational principle for open quantum systems and how to solve the master equation with it.

Let us first discuss why wave functions are not appropriate to describe open quantum systems. The state  $|\Psi\rangle$  in Eq. (1.1) is an eigenvector of the Hamiltonian that describes a system. Such a state is also called a pure state. The interaction with an environment that we do not have full knowledge about and also cannot control can lead to a mixture of different pure states. A convenient way to write this mixture is to sum over the projection operators  $P_i = |\Psi_i\rangle \langle \Psi_i|$  for each pure state  $|\Psi_i\rangle$  and weight it with the probability  $p_i$  to find the system in this specific eigenstate. The operator

$$\rho = \sum_i p_i |\Psi_i\rangle \langle \Psi_i| \quad (1.2)$$

that we obtain in that way is semi-positive ( $\rho \geq 0$ ) and hermitian ( $\rho = \rho^\dagger$ ) and is called the *density operator* or in its matrix form the *density matrix*. The sum over all possible states of the system in 1.2 also implies the constraint

$$\sum_i p_i = 1 \quad (1.3)$$

for the probabilities.

With the definition in Eq. (1.2) we can write the expectation value  $\langle \hat{A} \rangle$  of an operator



$\hat{A}$  as

$$\hat{A} = \sum_i p_i \langle \Psi_i | \hat{A} | \Psi_i \rangle = \text{Tr} \{ \hat{A} \rho \}. \quad (1.4)$$

Here, we used the trace function  $\text{Tr} \{ \cdot \}$  which is defined as

$$\text{Tr} \{ A \} = \sum_{k=1}^d \langle \phi_k | A | \phi_k \rangle. \quad (1.5)$$

for any d-dimensional quadratic matrix  $A$  and orthonormal basis set  $|\phi_k\rangle$ . Even though any basis set is sufficient enough to fulfill the definition in Eq. (1.5), it is often convenient to choose the eigenstates  $|\Psi_i\rangle$ .

In many cases, we can split up the Hilbert space in subsystems  $\mathcal{H}_1$  with eigenstates  $|\phi_i\rangle$  and  $\mathcal{H}_2$  with eigenstates  $|\phi_j\rangle$ . The composite Hilbert space is then given by the tensor product of the subsystems  $\mathcal{H} = \mathcal{H}_1 \otimes \mathcal{H}_2$ . The same is also possible for the density matrix  $\rho = \rho_1 \otimes \rho_2$  under the condition that the two subsystems are uncorrelated. We want to write the states of compound Hilbert space as  $|\Psi_i\rangle \otimes |\phi_j\rangle = |ij\rangle$ . If we are now only interested in one of the subsystems, that is if we look at observable of the form  $\hat{A} \otimes I$  or  $I \otimes \hat{A}$ , we can also use the reduced density matrix of the corresponding subsystem by defining the partial trace of the full density matrix like

$$\rho_1 = \text{Tr}_2 \{ \rho \} = \text{Tr}_\chi \{ \rho \} = \sum_{ii'} \sum_j \langle ij | \rho | i'j \rangle | \Psi_i \rangle \langle \Psi_{i'} |. \quad (1.6)$$

The different expressions in Eq. (1.6) have the same meaning but can be useful in different contexts. For example,  $\text{Tr}_2 \{ \rho \}$  just means to take the partial over subsystem 2, whereas  $\text{Tr}_\chi \{ \rho \}$  means that we are taking the partial trace over all subsystems except 1, which is especially useful when dealing with a large amount of subsystems.

### 1.1.1. Master equation in Lindblad form

So far, we only discussed how the density matrix can be useful to describe a quantum system in case its states become mixed by the interaction with the environment. Now, we want to investigate how exactly we can describe these interactions and especially what influences they have on the dynamics of our system.

First, we want to have a look at the Liouville-von Neumann equation as a generalisation of the Schrödinger equation for the density operator. For convenience reason, we will set  $\hbar = 1$  and if not mention it otherwise will keep it that way throughout

## 1. Theoretical Background

the thesis. The equation then reads as

$$\dot{\rho} = \frac{d}{dt}\rho = -i[\hat{H}, \hat{\rho}] = \mathcal{L}(t)\hat{\rho} \quad (1.7)$$

where we introduced the notion of superoperators that act on other operators. The Liouville superoperator  $\mathcal{L}$  maps the density operator  $\rho$  to its time derivative  $\dot{\rho} = \frac{d}{dt}\rho$ . We can use Eq. (1.7) to obtain the dynamics of the full systems, that include the system we are interested in, with the Hilbert space  $\mathcal{H}_S$ , and also its environment with  $\mathcal{H}_E$ . The complete Hilbert space can also be written as a composition of the two subsystems like

$$\mathcal{H} = \mathcal{H}_S \otimes \mathcal{H}_E. \quad (1.8)$$

In many cases, we are not interested in the complete dynamical processes that happen in the environment but only its impact on the system S. Therefore, we want to obtain a similar equation like Eq. (1.7) but for the reduced density matrix  $\rho_S = \text{Tr}_E \{\rho\}$ .

A complete derivation of the master equation in Lindblad form can be found in [36]. Here, we want to focus ourselves on the approximations used to get the result and a few key steps to understand its meaning.

For this purpose let us first take a step back. If we take the full system into account, the unitary time evolution operator

$$\rho(t) = U(t)\rho(0)U(t)^\dagger \quad (1.9)$$

realises the time evolution of the the density matrix  $\rho(0)$  to a time  $t$ . For the partial density matrix  $\rho_S$  of the subsystem  $S$ , that means

$$\rho_S(t) = \text{Tr}_E \left\{ U(t)\rho(0)U^\dagger(t) \right\} = \mathcal{V}(t)\rho_S(0). \quad (1.10)$$

Our goal is therefore to obtain the dynamical map  $\mathcal{V}(t)$ . This map does not describe any longer the unitary time evolution of a closed system, instead it describes the dynamical changes of an open system.

To obtain a microscopic derivation, we use as the starting point the Liouville-von Neumann equation in Eq. (1.7). The Hamiltonian  $H = H_S + H_E + H_{\text{int}}$  consists of the system Hamiltonian  $H_S$ , the Hamiltonian of the environment  $H_E$  and the interaction between the two systems  $H_{\text{int}}$ . For simplicity, we want to work in the interaction picture which we obtain by using the unitary transformation  $\tilde{\rho} = U(t)\rho U^\dagger(t)$  with  $U(t) = \exp[-(H_S + H_E)t]$  and insert this into Eq. (1.7) which allows us to rewrite

the equation to

$$\frac{d}{dt}\tilde{\rho} = -i[H_I(t), \tilde{\rho}] \quad (1.11)$$

with

$$H_I(t) = U^\dagger(t)H_IU(t). \quad (1.12)$$

A formal solution can be given through integration in the form of

$$\tilde{\rho}(t) = \tilde{\rho}(0) - i \int_0^t dt' [H_I(t'), \tilde{\rho}(t')] \quad (1.13)$$

We now need the first important approximation which is the *Born approximation*. Its basic assumption is that the interaction between the two subsystems is small and especially that the environment is not influenced by the smaller system S. Then we assume  $\rho_B$  to be constant. Let us further assume that we start in a product state of the two subsystems, that is without any correlations between them. Inserting Eq. (1.13) back into Eq. (1.11) and taking the partial trace over the environment yields the Redfield master equation

$$\frac{d}{dt}\rho_S(t) = - \int_0^t dt' \text{Tr}_E \{ [H_I(t), [H_I(t'), \rho_S(t) \otimes \rho_B]] \}. \quad (1.14)$$

To get to the Markovian master equation we need to take care of the fact that the reduced density matrix still depends on its starting condition at  $t = 0$ . Therefore we substitute  $t'$  by  $t - t'$  and shift the upper limit of the integral to infinity. This is possible as long as the integrand disappears fast for  $t' \gg \tau_E$  with  $\tau_E$  being the timescale over which correlations in the environment decay. This then leads to

$$\frac{d}{dt}\rho_S(t) = - \int_0^\infty dt' \text{Tr}_E \{ [H_I(t), [H_I(t - t'), \rho_S(t) \otimes \rho_B]] \}. \quad (1.15)$$

Here, we replaced  $\rho_S(t')$  by  $\rho_S(t)$  which means that the dynamics of the system at time  $t$  only depends on its present state  $\rho_S(t)$ . This is known as the *Markov approximation* and is valid as long as correlations in the environment decay quickly enough to neglect any memory effects of the environment that could influence the system.

The last approximation we need to apply to obtain a generator of the dynamics in our system is the *rotating frame approximation* or secular approximation. We will not carry out the full calculation and focus on the main point of it: The interaction Hamiltonian between bath and system can be decomposed into eigenoperators of

## 1. Theoretical Background

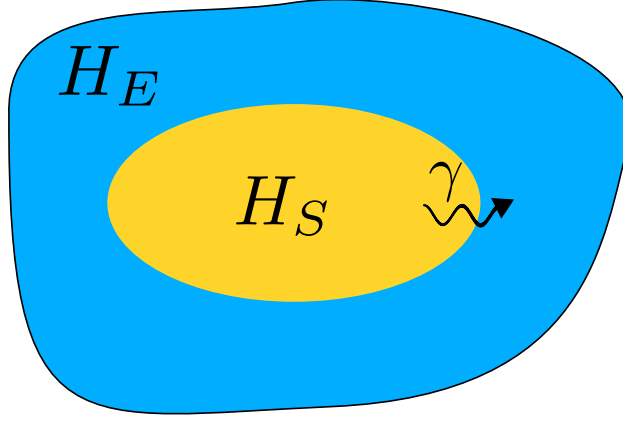


Figure 1.1.: Scheme of an system  $S$  with Hamiltonian  $H_S$  embedded in its environment  $E$  with Hamiltonian  $H_E$ . Energy can leave the system  $S$  by different dissipation channels with rates  $\gamma$  that arise from the interaction with the environment.

the system Hamiltonian and can then be written as

$$H_I(t) = \sum_{\alpha, \omega} e^{i\omega t} A_{\alpha}^{\dagger}(\omega) \otimes B_{\alpha}^{\dagger}(t) \quad (1.16)$$

with  $A_{\alpha}^{(\dagger)}$  being eigenoperators of the system and  $B_{\alpha}^{(\dagger)}$  of the environment. The system operators depend on the frequency  $\omega = \epsilon - \epsilon'$  which is defined as the fixed energy difference between the eigenvalues  $\epsilon, \epsilon'$  of the system Hamiltonian. The secular approximation comes into play if we insert the decomposed interaction Hamiltonian Eq. (1.16) back into Eq. (1.15) which yields

$$\frac{d}{dt} \rho_S(t) = \sum_{\omega, \omega'} \sum_{\alpha, \beta} e^{i(\omega' - \omega)t} \Gamma_{\alpha\beta}(\omega) (A_{\beta}(\omega) \rho_S(t) A_{\alpha}^{\dagger}(\omega') - A_{\alpha}^{\dagger}(\omega') A_{\beta}(\omega) \rho_S(t)) + h.c.. \quad (1.17)$$

Here we also introduced the Fourier transform of the reservoir correlation function as

$$\Gamma_{\alpha\beta}(\omega) = \int_0^{\infty} ds e^{i\omega t} \langle B_{\alpha}^{\dagger}(t) B_{\beta}(t - t') \rangle. \quad (1.18)$$

Neglecting now all fast oscillating terms in  $\omega$ , that is all terms for which  $\omega' \neq \omega$ , is known as the secular approximation and after some more algebra allows to write the master equation as

$$\frac{d}{dt} \rho(t) = \mathcal{L}(\rho) = -i[H(t), \rho(t)] + \sum_i \left( c_i \rho c_i^{\dagger} - \frac{1}{2} \{c_i^{\dagger} c_i, \rho\} \right). \quad (1.19)$$

In the derivation of the master equation for the density matrix  $\rho$  we already shifted

from the Schrödinger picture to the interaction picture. A natural question would be how Eq. (1.19) looks like in the Heisenberg picture. Therefore, we need to find the time evolution of an operator  $\hat{A}$  which is also known as an equation of motion. We start from the definition of the expectation value in terms of the density matrix in the Schrödinger picture which gives us

$$\langle A \rangle = \text{Tr} \{ A(0) \rho(t) \}. \quad (1.20)$$

The formal solution for  $\rho(t)$  from solving the Master equation

$$\frac{d\rho}{dt} = \mathcal{L}[\rho] \quad (1.21)$$

is given by

$$\rho(t) = e^{\mathcal{L}t} \rho(0) \quad (1.22)$$

if we define the adjoint Liouvillian  $\mathcal{L}^\dagger$  as

$$\text{Tr} \{ P \mathcal{L}[Q] \} = \text{Tr} \{ \mathcal{L}[P] Q \} \quad (1.23)$$

for the two arbitrary operators  $P$  and  $Q$ . With that, we can transform the expectation value to

$$\text{Tr} \{ A(0) \rho(t) \} = \text{Tr} \{ A(0) e^{\mathcal{L}t} [\rho(0)] \} = \text{Tr} \{ e^{\mathcal{L}^\dagger t} [A(0)] \rho(0) \}. \quad (1.24)$$

From there we can define the generalised Ehrenfest equation as

$$\frac{d}{dt} \langle \hat{A} \rangle (t) = i \langle [H, \hat{A}] \rangle + \sum_i \langle \left( c_i \hat{A} c_i^\dagger - \frac{1}{2} c_i^\dagger c_i, \hat{A} \right) \rangle. \quad (1.25)$$

### 1.1.2. Variational Principle

The quantum master equation in Eq. (1.19) we derived in the last section is a powerful tool to analyse open quantum systems but solving it constitutes a big problem for classical computers. Exact numerical calculation are only possible for small particle numbers because of the exponentially growing complexity of the problem with increasing system size. Many tools that were developed for closed many-body problems do not work in the open systems [30]. Even finding the steady state ( $\dot{\rho} = 0$ ) can be difficult because it is in most cases not the ground state of the system but a mixture of many possible states. In this section, we want to discuss how the variational principle can be modified for open quantum systems. In the end we will have a method to calculate both the steady state and the dynamics of open quantum

## 1. Theoretical Background

systems.

The variational principle is a broad concept in physics and it already found application in other fields like optics (Fermat's principle) [37] or classical mechanics (Hamilton's principle) [38, 39]. Finding the extrema of a functional is the basic idea of the variational principle and the Rayleigh-Ritz method is its adaptation to the quantum mechanics. It uses the energy functional  $\langle \Psi | H | \Psi \rangle$  to find an approximated ground state of the system. Like we already stated at the beginning of this section, a single wave function is not sufficient enough to describe open quantum systems. Instead, we need a variational approach for the density matrix and its time derivative  $\dot{\rho}$ . For the sake of simplicity, we first want to focus ourselves on the steady state where the goal is that  $\dot{\rho} = 0$ . To find a variational solution of the steady state, we will need to minimize an appropriate matrix norm of the master equation like

$$\|\dot{\rho}\| = \|\mathcal{L}\rho\| \rightarrow \min. \quad (1.26)$$

A possible class of matrix norms are the Schatten p-norms

$$\|\dot{\rho}\| = \sqrt[p]{\text{Tr} \{|\dot{\rho}|^p\}}. \quad (1.27)$$

It turns out that out of the pool of different norms only the trace norm with  $p = 1$  allows for an unambiguous variational solution. The other choices always converge towards the maximal mixed state for large system sizes in Eq. (1.26), independent of the choice of the Hamiltonian or jump operators [40].

To see the advantage of the variational approach, we want to have a closer look at the norm in Eq. (1.26) by assuming the trial state

$$\rho = \prod_i \text{Tr}_f \{\rho\} = \prod_i \rho_i. \quad (1.28)$$

Here, we introduce the superoperator  $\mathcal{R}$  that transform every unit matrix of any given subsystem into the corresponding density matrix of the subsystem  $\rho_i$ .

The product state is the simplest way to express the density matrix for multiple subsystem because it excludes correlation between them and if we further assume that the interaction only acts on nearest neighbor subsystem, e.g., in a lattice, we can write the time evolution in Eq. (1.19) like

$$\dot{\rho} = \sum_i \mathcal{R}\dot{\rho}_i + \sum_{\langle ij \rangle} \mathcal{R}\dot{C}_{ij}. \quad (1.29)$$

The appearance of the additional term  $\dot{C}_{ij}$  is caused by the evolution of correlation between system  $i$  and  $j$  through the interaction and will also influence the variational solution in Eq. (1.26). A different approach to find steady-state solutions of open quantum systems is to approximate the master equation by local terms instead of an approximation of the density matrix. This approach is known as the mean-field approximation and can be achieved by taking the partial trace of the master equation Eq. (1.19) over the full system except for a single site/particle. The solution of this equation can also be expressed by a product state of local density matrices like in Eq. (1.28). In comparison to Eq. (1.29) does the solution of the master equation in the mean-field approximation not involve the terms  $\dot{C}_{ij}$  and is therefore missing a crucial part of the time-evolution [40].

We now can find the steady state of an open quantum system but we also want to be able to capture dynamical processes in the system with the variational approach. We can write a formal solution of Eq. (1.19) by using standard integration methods like the Euler method. The solution after a time step with size  $\tau$  then reads as

$$\rho(t + \tau) = \rho(t) + \tau \mathcal{L}(\rho(t)) + \mathcal{O}(\tau^2) \quad (1.30)$$

or if we want to reduce the error  $\mathcal{O}(\tau^2)$  we can also use the implicit midpoint integration which leads to

$$\rho(t + \tau) = \rho(t) + \frac{\tau}{2} \mathcal{L}(\rho(t) + \rho(t + \tau)) + \mathcal{O}(\tau^3). \quad (1.31)$$

This allows us to formulate a new variational norm for the trial state  $\rho(t + \tau)$  as

$$D = \|\rho(t + \tau) - \rho(t) - \frac{\tau}{2} \mathcal{L}(\rho(t) + \rho(t + \tau))\| \rightarrow \min. \quad (1.32)$$

The integration error of  $\mathcal{O}(\tau^3)$  is low for appropriate time steps  $\tau$ .

For most many-body systems, the variational parameters of even a product trial state exceed numbers that can be well handled by conventional optimizer routines. We can use the triangle inequality to find an upper bound of the variational norm in Eq. (1.32) like

$$D \leq \sum_{ij} D_{ij} = \sum_{ij} \|\rho_{ij}(t + \tau) - \rho_{ij}(t) - \frac{\tau}{2} \mathcal{L}[\rho_{ij}(t) + \rho_{ij}(t + \tau)]\|. \quad (1.33)$$

We now reduced the problem to a summation over norms that only have the manifold of the two subsystems  $i, j$ . If the system is translationally invariant, we can even drop the summation.

## 1. Theoretical Background

For a inhomogeneous system with  $N$  subsystems, that are each described by  $N_\alpha$  numbers of variational parameters, the minimization of Eq. (1.33) still involves  $N_\alpha \cdot N$  independent, variational parameters. We will quickly reach a computational limitation for large system sizes if we want to minimize them all at once. From Eq. (1.33) we can obtain

$$D_i = \sum_i \|\rho_i(t + \tau) \otimes \rho_j(t) - \rho_{ij}(t) - \frac{\tau}{2} \mathcal{L}[\rho_{ij}(t) + \rho_i(t + \tau) \otimes \rho_j(t)]\| \quad (1.34)$$

by applying the product rule to the time derivative  $\frac{\partial \rho}{\partial t}$  of the product state density matrix and then use another triangle inequality. With Eq. (1.34) we shifted the problem of finding the norm of the full system at once to multiple single subsystem minimization while holding the other subsystems constant. It is important to note that we first need to apply Eq. (1.34) to all subsystems for a time step  $\tau$  before we to the next one. By using this method we have reduced the problem from minimizing  $N_\alpha \cdot N$  parameters at once for a single time step to only  $N_\alpha$  parameters but doing it  $N$  times for each time step [41].

## 1.2. Quantum description of light

The full description of light in the context of quantum theory is a quite complicated matter and is a subject on its own with the quantum field theory. Here, we want to focus ourselves on the basic concept of how to describe light as a quantum field and also look at some of its possible states.

From classical electrodynamics and Maxwell's equations, we can describe both the electric field  $\mathbf{E}$  and the magnetic field  $\mathbf{B}$  by the vector potential  $\mathbf{A}$ . If no sources are present are the equations gauge invariant and can be expressed like

$$\mathbf{E} = -\frac{\partial \mathbf{A}}{\partial t}, \quad \mathbf{B} = \nabla \times \mathbf{A} \quad (1.35)$$

under a Coulomb gauge transformation  $\nabla \cdot \mathbf{A} = 0$  [42]. The operator of this vector potential  $\hat{\mathbf{A}}(\mathbf{r}, t)$  is the basis of describing light in quantum theory.

The operator  $\hat{\mathbf{A}}(\mathbf{r}, t)$  consists of all possible light fields and we can write it as an extension of an orthonormal set of waves  $\mathbf{A}_k(\mathbf{r}, t)$  like

$$\hat{\mathbf{A}}(\mathbf{r}, t) = \sum_k (\mathbf{A}_k(\mathbf{r}, t) \hat{a}_k + \mathbf{A}_k^*(\mathbf{r}, t) \hat{a}_k^\dagger). \quad (1.36)$$



## 1.2. Quantum description of light

The complex functions  $\mathbf{A}_k(\mathbf{r}, t)$  are called modes of the light field with a mode index  $k$  which is in most cases their wavenumber. We also introduced the associated operators  $\hat{a}_k^{(\dagger)}$  to each mode which carries the quantum information of the field. The operators correspond to complex Fourier components in classical electrodynamics. By an appropriate choice in the mode expansion we can assure that the modes obey orthonormality which allows us to use the Bose commutation relations for the operators

$$[\hat{a}_k, \hat{a}_{k'}^\dagger] = \delta_{kk'}, \quad [\hat{a}_k, \hat{a}_{k'}] = 0. \quad (1.37)$$

This choice allows for the description of the dynamical behaviour of the electric field amplitudes by an ensemble of independent harmonic oscillators with the same commutation relations as above [43]. This commutation relation describes all bosonic fields which includes all spin-0 and spin-1 particles. An important consequence is that the operators of different modes commute and therefore the Hilbert space for light is equivalent to the tensor product of the Hilbert space of all modes. Eq. (1.36) and Eq. (1.37) are enough to fully describe the wave-like but also the quantum properties of the light field. From here, we want to define three operators to simplify this description. First, the photon number operator

$$\hat{n} = \hat{a}^\dagger \hat{a} \quad (1.38)$$

is defined in such a way that its expectation value  $\langle \hat{n} \rangle$  returns the number of photons in a mode. The second and the third operators  $\hat{q}, \hat{p}$  as a pair are called the quadratures of the field and are defined as

$$\hat{q} = \sqrt{\frac{\hbar}{2}}(\hat{a}^\dagger + \hat{a}), \quad \hat{p} = i\sqrt{\frac{\hbar}{2}}(\hat{a}^\dagger - \hat{a}). \quad (1.39)$$

These two serve as an equivalent to the position and the momentum quantity of an electromagnetic oscillator and are therefore often called that way.

We now want to look at a few interesting states of light that are either important from a mathematical perspective in describing states in general or have significant physical meaning.

A single mode of light can be described by different quantum states. They are given by their eigenstates and the properties are encapsulated in a few distinct observables like the quadratures or the photon numbers. We will first look at Fock states as one of the fundamental states in quantum optics and then go on to coherent light as it is produced by lasers. In contrast, we will also have a brief look at thermal light and we end with a highly non-classical light in the form of squeezed states.

## 1. Theoretical Background

### Fock state

Fock states are the eigenstates of the previously defined number operator  $\hat{n}$

$$\hat{n} |n\rangle = n |n\rangle. \quad (1.40)$$

The definition Eq. (1.40) implies that each Fock state has a fixed photon number and are therefore hard to produce in experiment as a pure state beyond the single photon Fock state  $|1\rangle$  because of thermal fluctuations or the superposition with other states [44]. The set of all Fock states are complete, that means

$$\sum_{n=0}^{\infty} |n\rangle \langle n| = 1 \quad (1.41)$$

and also orthonormal  $\langle n|n'\rangle = \delta_{nn'}$ . Because of that we can use them as a convenient basis of the Hilbert space and are often used in quantum optics. The effect of the operators  $\hat{a}$  and  $\hat{a}^\dagger$  on a Fock state are

$$\begin{aligned} \hat{a} |n\rangle &= \sqrt{n} |n-1\rangle \\ \hat{a}^\dagger |n\rangle &= \sqrt{n+1} |n+1\rangle \end{aligned} \quad (1.42)$$

which is why we will call  $\hat{a}$  the annihilation and  $\hat{a}^\dagger$  the creation operator. The state  $|0\rangle$  can be identified as the vacuum state of the system which allows us to represent the Fock state also as

$$|n\rangle = \frac{\hat{a}^\dagger^n}{\sqrt{n!}} |0\rangle \quad (1.43)$$

### Coherent light

The definition of a coherent state is based on the eigenstates of the annihilation operator  $\hat{a}$  of the light field, which we defined in the previous section, and reads as

$$\hat{a} |\alpha\rangle = \alpha |\alpha\rangle. \quad (1.44)$$

The eigenvalue  $\alpha$  is complex because  $\hat{a}$  is a non-hermitian operator. We can also define the state in the Fock basis as

$$|\alpha\rangle = e^{-\frac{|\alpha|^2}{2}} \sum_{n=0}^{\infty} \frac{\alpha^n}{\sqrt{n!}} |n\rangle = e^{-\frac{|\alpha|^2}{2}} e^{\alpha \hat{a}^\dagger} e^{-\alpha^* \hat{a}} |0\rangle \quad (1.45)$$

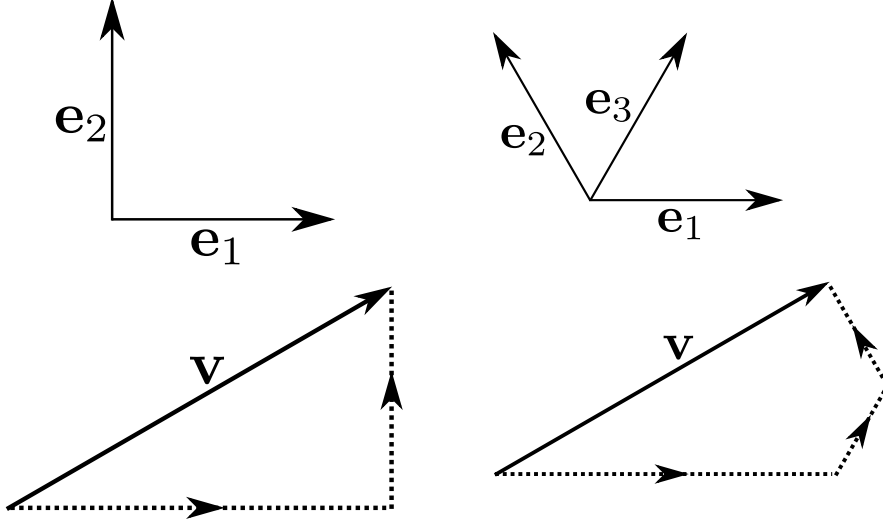


Figure 1.2.: Comparison of the decomposition of vector  $\mathbf{v}$  in an orthonormal basis set  $\mathbf{e}_1, \mathbf{e}_2$  (left) and an overcomplete non-orthogonal basis set  $\mathbf{e}_1, \mathbf{e}_2, \mathbf{e}_3$  (right). This is a visual representation of how the non-orthogonality of the coherent states  $|\alpha\rangle$  leads to an overcomplete basis set.

From Eq. (1.45) we can see that we can also obtain a coherent state by applying the displacement operator

$$D(\alpha) = e^{\alpha a^\dagger - \alpha^* \hat{a}}. \quad (1.46)$$

We used the simplified Baker-Campbell-Hausdorff formula [45]

$$e^{A+B} = e^{-[A,B]/2} e^A e^B \quad (1.47)$$

with  $A = \alpha a^\dagger$  and  $B = -\alpha^* a$  to get from Eq. (1.45) to Eq. (1.46). The simplified version in Eq. (1.47) hold true if  $[A, [A, B]] = [B, [A, B]] = 0$ .

The so defined states form an overcomplete basis set

$$\int_{-\infty}^{\infty} d^2\alpha |\alpha\rangle \langle\alpha| = \pi \quad (1.48)$$

with  $d^2\alpha = d(\text{Re}\alpha)d(\text{Im}\alpha)$  which is a result from the fact that the states are non-orthogonal

$$\langle\alpha|\alpha'\rangle = e^{-\frac{|\alpha|^2}{2} - \frac{|\alpha'|^2}{2} + \alpha'^* \alpha}. \quad (1.49)$$

A visual representation of the difference between an overcomplete set and an orthonormal basis set is depicted in Fig. 1.2.

With the fock representation Eq. (1.45) we can also see that coherent light has a

## 1. Theoretical Background

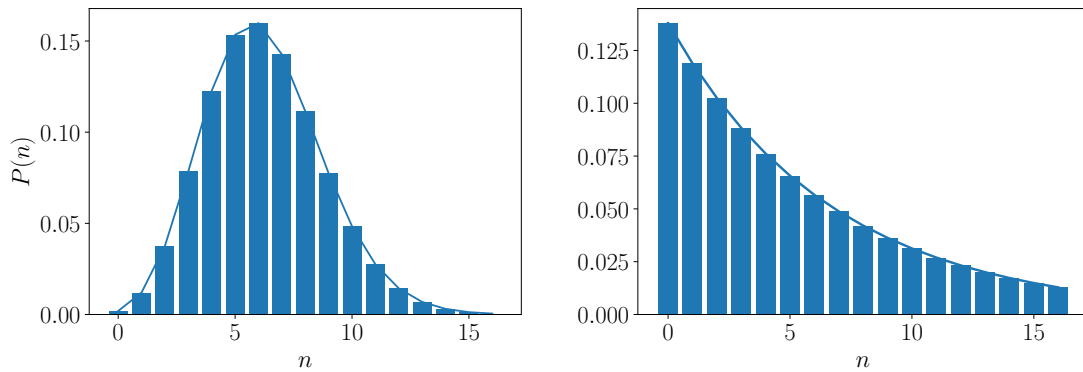


Figure 1.3.: Photon statistics of Poissonian (left) and super-Poissonian light(right). Both distribution have an average photon number of  $\langle n \rangle = 6.25$ .

Poissonian photon statistics, see Fig. 1.3,

$$P(n) = |\langle n|\alpha \rangle|^2 = \frac{|\alpha|^2}{n!} e^{-|\alpha|^2}. \quad (1.50)$$

It should also be mentioned that coherent states belong to the family of states with minimum-uncertainty which means that

$$\Delta p \Delta q = \frac{\hbar}{2} \quad (1.51)$$

with

$$\begin{aligned} (\Delta p)^2 &= \langle p^2 \rangle - \langle p \rangle^2 = \frac{\hbar}{2} \\ (\Delta q)^2 &= \langle q^2 \rangle - \langle q \rangle^2 = \frac{\hbar}{2} \end{aligned} \quad (1.52)$$

being the variances of the quadratures.

### Squeezed coherent states

We mentioned in the previous section about the coherent states that there is a whole family of states that fulfill the minimum-uncertainty relation. The reduction of the noise in one quadrature raises the noise in the other but keeps the product in Eq. (1.51). These states are called squeezed states. They are an important tool in measurement experiments to reduce the uncertainties of the amplitude or the phase of electromagnetic waves caused by quantum fluctuations. An example would be the Laser Interferometer Gravitational-wave Observatory (LIGO) which uses squeezed states to increase the phase sensitivity of their Michelson interferometers[46]. We ob-

## 1.2. Quantum description of light

tain them by expanding the notion in Eq. (1.45) and Eq. (1.46) by another operator  $S(z)$ . This is the squeeze operator for a single mode and is given by

$$\hat{S} = e^{\frac{1}{2}(z^*\hat{a}^2 - z\hat{a}^{\dagger 2})} \quad (1.53)$$

with  $z = re^{i\phi}$ . Therewith we can write the coherent squeezed states as

$$|\alpha, z\rangle = D(\alpha)S(z)|0\rangle. \quad (1.54)$$

If we look again at the uncertainties for these states

$$\begin{aligned} (\Delta p)^2 &= \frac{\hbar}{2}e^{2r} \\ (\Delta q)^2 &= \frac{\hbar}{2}e^{-2r}, \end{aligned} \quad (1.55)$$

we immediately see that the amplitude  $r$  of the complex parameter  $z$  determinate the strength of the squeezing and is therefore also called the squeezing parameter and  $\phi$  rotates the state in the phase-space. The annihilation (creation) operator  $a^{(\dagger)}$  transform to

$$\begin{aligned} S^\dagger(z)aS(z) &= \hat{a} \cosh r - \hat{a}^\dagger e^{-2i\phi} \sinh r \\ S^\dagger(z)a^\dagger S(z) &= \hat{a}^\dagger \cosh r - \hat{a} e^{2i\phi} \sinh r \end{aligned} \quad (1.56)$$

which is important to determine other expectation values like the photon count

$$\langle n \rangle = |\alpha|^2 + \sinh^2 r. \quad (1.57)$$

The first term in Eq. (1.57) is equal to the photon number in a coherent state but from the second term we can see that squeezing can both increase or decrease to total number in the state depending on the squeezing parameter.

## 1. Theoretical Background

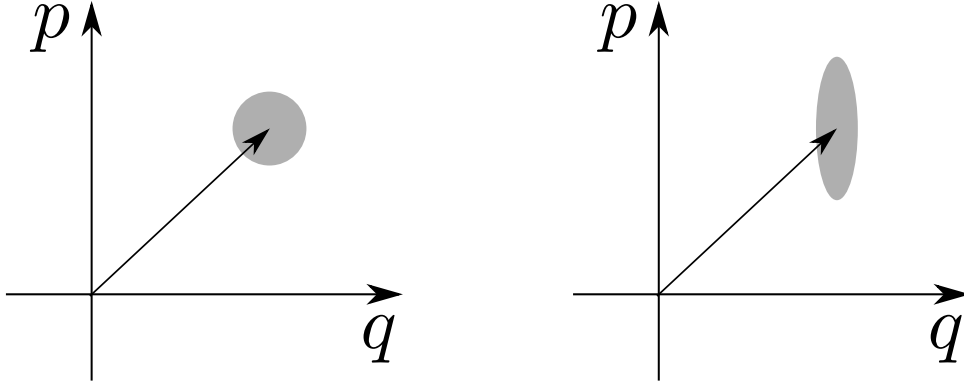


Figure 1.4.: Quadrature uncertainties for a coherent (left) and a squeezed state (right). Both have the same area (the product  $\Delta p \Delta q$  is the same) but the squeezed state has a reduced uncertainty in  $q$  accompanied with the increase noise in  $p$ .

### Thermal states

The states we discussed so far are quite useful in quantum optics and experiments, but most light we encounter in day-to-day life comes from thermal radiation like sunlight. In experiments is thermal light a nuisance most of the time and the experimental setups try to avoid its influences as much as possible. We will later see how exactly a thermal state influences other states of light. The energy and the photon number of thermal light is not fixed but fluctuates. Hence, we will use a description we already introduced in the context of open quantum system which is the density. A Fock state representation of it reads

$$\rho = \sum_n p_n |n\rangle \langle n| \quad (1.58)$$

and allows us to describe the thermal state as a statistical mixture. The state we want to describe is the one with a maximal entropy  $S$  for a given energy  $E$ . This constraint leads to the density matrix

$$\rho = (1 - e^{-\beta}) \sum_{n=0}^{\infty} e^{-n\beta} |n\rangle \langle n| \quad (1.59)$$

with  $\beta = \frac{1}{k_b T}$  as the inverse temperature and  $k_b$  the Boltzmann constant.

The photon statistics can be calculated to

$$P(n) = \frac{1}{\langle n \rangle + 1} \left( \frac{\langle n \rangle}{\langle n \rangle + 1} \right)^n. \quad (1.60)$$

In contrast to coherent light, thermal light follows a super-Poissonian distribution like it is shown in Fig. 1.3.

### 1.3. Quasiprobability distributions

With the beginning of quantum mechanics also came the wish to find a connection between quantum-mechanical operators and classical functions. The goal was to obtain observable with methods of classical statistical physics. To achieve this, we have to find an appropriate representation of the density matrix  $\rho$  in form of a (quasi-)distribution function that depends on the classical correspondence of the operators  $\hat{q}, \hat{p}$  or alternatively  $\hat{a}, \hat{a}^\dagger$  for a bosonic field.

In this section we want to discuss the most prominent examples for such distribution functions. We will also see that for non-classical states, most of the functions are only quasidistributions because they cannot comply with all properties of a real one. Our main focus will be the P-representation as it will later be used to define and expand the variational method for open quantum system to bosonic fields with an infinite Hilbert space. Many properties that we define here also apply to the functions that we also want to discuss afterwards like the Wigner- or Q-function.

#### P-representation

From the last section we know that the coherent states  $|\alpha\rangle$  form a (over-)complete basis set which led to the expression of the density matrix in terms of the diagonal coherent states like

$$\rho = \int d^2\alpha P(\alpha) |\alpha\rangle \langle\alpha|. \quad (1.61)$$

which was established independently by Glauber and Sudarshan in the same year [47, 48]. The expression relies on the non-orthogonality of the coherent states and the idea is to use the P-distribution  $P(\alpha)$  to assign a value to each point in the complex phase-space. Additionally, we know that  $P(\alpha)$  is normalized because

$$\int d^2\alpha P(\alpha) = \text{Tr} \left\{ \int d^2\alpha P(\alpha) |\alpha\rangle \langle\alpha| \right\} \quad (1.62)$$

$$= \text{Tr} \{ \rho \} = 1. \quad (1.63)$$

A general expression of  $P(\alpha)$  can be found by inverting Eq. (1.61) to

$$P(\alpha) = \frac{1}{\pi^2} \int d^2z \text{Tr} \left\{ \rho e^{iz^*a^\dagger} e^{iza} \right\} e^{-iz^*\alpha^*} e^{-iz\alpha}. \quad (1.64)$$

## 1. Theoretical Background

This is the complex Fourier transform of the trace function which we can expand in terms of Fock states to

$$P(\alpha) = \frac{1}{\pi^2} \int d^2z \left( \sum_{n=0}^{\infty} \sum_{m=0}^{\infty} \sum_{k=0}^{\infty} \rho_{n+k, m+k} \frac{\sqrt{(n+k)!} \sqrt{(m+k)!}}{k!} \right) \times \frac{(iz^+)^m (iz^-)^n}{m! n!} e^{-iz^* \alpha^*} e^{-iz \alpha} \quad (1.65)$$

This lengthy expression shows that it is possible to find a P-distribution for any given state if the Fourier transform in Eq. (1.64) exists [49]. Unfortunately, that is only possible if we expand the field of possible functions for  $P(\alpha)$  from ordinary to generalised distributions like the delta distribution  $\delta(x)$ . They are defined as continuous linear functionals over a space of infinitely differentiable functions. An example that is widely used in physics is the delta-distribution  $\delta(x)$ . It is only defined inside an integral acting on a test function  $\phi(x)$  and behaves like the limit of a sequence of Gaussians  $\lim_{n \rightarrow \infty} \frac{1}{\sqrt{\pi n}} e^{-x^2/n}$  which allows us to write  $\int dx \delta(x) \phi(x) = \phi(0)$ . This definition also allows us to define derivatives of generalised functions through partial integration. For the delta-distribution we get

$$\int_{-\infty}^{\infty} \frac{d^n}{dx^n} (\delta(x)) \phi(x) = (-1)^n \int_{-\infty}^{\infty} \delta(x) \frac{d^n}{dx^n} \phi(x) = (-1)^n \frac{d^n}{dx^n} \phi(0). \quad (1.66)$$

This shall be enough for us about the theory of generalised functions. It is a vast field and we only grazed the surface of it. A more comprehensive overview can be found for example, in the books by Lighthill [50] or Bremermann [51]. This exceeds the original proposal by Glauber and Sudarshan and also breaks with the notion of a classical distribution to associate a number to each point  $\alpha$  as we stated earlier. A useful property of this P-representation is the way how expectation values of annihilation (creation) operators  $a(a^\dagger)$  are calculated through c-number integrals

$$\langle : a^{\dagger p} a^q : \rangle = \text{Tr} \left\{ \rho a^{\dagger p} a^q \right\} = \int d^2\alpha P(\alpha) \alpha^{*p} \alpha^q. \quad (1.67)$$

$\langle : a^{\dagger p} a^q : \rangle$  indicates a normal ordering of the operators, which also corresponds to measurements in an experiment. Normal ordering refers to having all creation operators on the left of all annihilation operators in the product. We will, later on, expand on the idea of the P-distribution in the context of the variational principle for bosonic fields.



## Wigner representation

The first attempt to represent quantum states as distributions in phase-space was by Wigner [52]. A good overview of the interesting properties of the Wigner distribution can be found in [53]. Here, we want to focus on its connection to the P-distribution through the introduction of the characteristic function  $\chi$ . This can be used as an alternative way to represent a given probability distribution and the differences in the calculation of expectation values. We already found such an expression in Eq. (1.64) with

$$\chi_N(z, z^*) = \text{Tr} \left\{ \rho e^{iz^* a^\dagger} e^{iza} \right\} \quad (1.68)$$

The function defines all normal-ordered operator averages as

$$\langle a^{\dagger p} a^q \rangle = \frac{\partial^{p+q}}{\partial (iz^*)^p \partial (iz)^q} \chi_N(z, z^*) \Big|_{z=z^*=0}. \quad (1.69)$$

The Wigner distribution can now be formulated as the fourier transformation of the characteristic function

$$\chi_S(z, z^*) = \text{Tr} \left\{ \rho e^{iz^* a^\dagger + iza} \right\}, \quad (1.70)$$

which yields

$$W(\alpha, \alpha^*) = \frac{1}{\pi^2} \int_{-\infty}^{+\infty} d\mu \int_{-\infty}^{+\infty} d\nu \chi_S(\mu + i\nu, \mu - i\nu) e^{-2i(\mu x - \nu y)}. \quad (1.71)$$

The original proposal by Wigner defined the function by the position  $x$  and momentum  $p$  to obtain a quantum analogue to the classical phase-space. However, in the context of quantum optics, the representation in terms of the eigenvalues of the annihilation/creation operators  $\alpha, \alpha^*$  is more relevant.

Like the P-distribution, the Wigner distribution is also only a quasi-probability distribution because some states can show negative values in the distribution. Contrary to the P-distribution, these negativities do not appear for all nonclassical states [54, 55]. In stark contrast to the representation by Glauber, the  $W$ -representation does not have singularities, which makes it an ideal candidate for the visual representation of quantum states [56]. Both distributions can be connected by

$$W(\alpha) = \frac{2}{\pi} \int d^2 \alpha' e^{-2|\alpha - \alpha'|^2} P(\alpha'). \quad (1.72)$$

## 1. Theoretical Background

The expectation values we obtain by calculating

$$\langle (a^\dagger{}^p a^q)_S \rangle = \frac{\partial^{p+q}}{\partial (iz^*) \partial (iz)} \chi_S(z, z^*) \Big|_{z=z^*=0} \quad (1.73)$$

are another important difference between the two distributions. With Eq. (1.70) we obtain expectation values in symmetric order instead of the normal order. The ordering involves the average of all  $\frac{(n+m)!}{n!m!}$  possible operator sequences of  $(a^\dagger{}^n a^m)_S$ , e.g.

$$(a^\dagger a)_S = \frac{1}{2}(a^\dagger a + a a^\dagger)$$

$$(a^\dagger a^2)_S = \frac{1}{3}(a^\dagger a^2 + a a^\dagger a + a^2 a^\dagger) \quad (1.74)$$

$$(a^{\dagger 2} a^2)_S = \frac{1}{3}(a^{\dagger 2} a + a^\dagger a a^\dagger + a a^{\dagger 2})$$

$$\vdots \quad (1.75)$$

This ordering scheme is not well suited for application in quantum optics because quantities are always measured in normal order at the detectors but it should be mentioned that all symmetric ordered operator can be brought into a normal ordered form like [49]

$$(a^\dagger{}^p a^q)_S = \sum_{k=0}^{\min(p,q)} \frac{1}{2^k} \frac{p!}{(p-k)!} \frac{q!}{(q-k)!} a^{\dagger p-k} a^{q-k}. \quad (1.76)$$

### Q-representation

At last, we want to briefly discuss the representation of antinormal-ordered averages like  $\langle \hat{a}^n \hat{a}^{\dagger m} \rangle$ . The characteristic function  $\chi$  for this ordering has to look like

$$\chi(z, z^*) = \text{Tr} \left\{ \rho e^{iza} e^{iz^* a^\dagger} \right\} \quad (1.77)$$

and like before when we can define the Fourier transform of Eq. (1.77) as a new representation

$$Q(\alpha) = \frac{1}{\pi^2} \int_{-\infty}^{\infty} d^2\beta e^{\alpha\beta^* - \alpha^*\beta} \chi(\beta). \quad (1.78)$$

This can be brought into a more understandable form of

$$Q(\alpha) = \frac{1}{\pi} \langle \alpha | \rho | \alpha \rangle \quad (1.79)$$

### 1.3. Quasiprobability distributions

which is the probability distribution for finding the coherent state  $\alpha$  in state  $\rho$ . We can immediately see from Eq. (1.79) that the Q-function is non-negative and normalized to unity based on the definitions of the density matrix  $\rho$  and the coherent states  $|\alpha\rangle$ .

Like the P-representation for normal ordered averages, the Q function turns expectation values for anti-normal order into c-number integrals like

$$\langle \hat{a}^n \hat{a}^{\dagger m} \rangle = \text{Tr} \{ \rho \hat{a}^n \hat{a}^{\dagger m} \} = \int_{-\infty}^{\infty} Q(\alpha) \alpha^n \alpha^{\dagger m}. \quad (1.80)$$

It can be related to the P-representation by

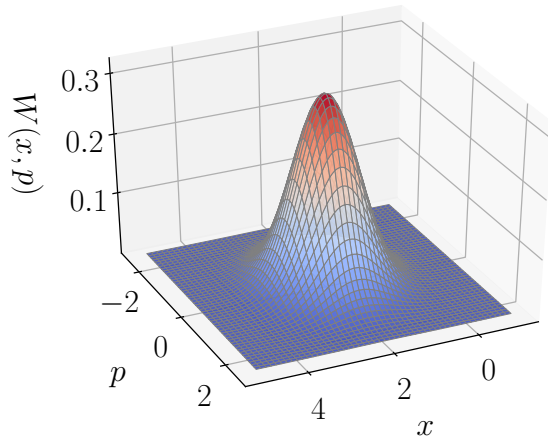
$$Q(\alpha) = \frac{1}{\pi} \int P(\beta) e^{-|\alpha-\beta|^2} d^2\beta \quad (1.81)$$

and the two examples in the form of coherent state  $|\beta\rangle$  and the Fock state  $|n\rangle$  that look like

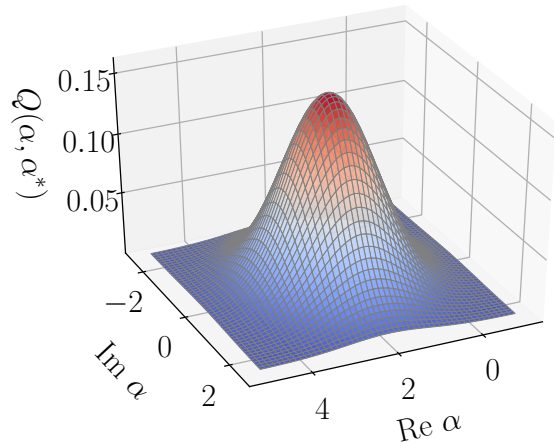
$$Q_{\text{coherent}}(\alpha) = \frac{1}{\pi} e^{-|\alpha-\beta|^2}, \quad Q_{\text{fock}}(\alpha) = \frac{|\alpha|^{2n}}{\pi n!} e^{-|\alpha|^2} \quad (1.82)$$

are shown next to their Wigner function in Fig. 1.5. Its clear advantage over the other two representations we showed is that the Q-function is always positive. It is still classified as a quasiprobability distribution because its definition over the non-orthogonal coherent states brakes the additivity axiom of normal probability distributions [57]. It is also not often used because the measurements in experiments are in normal order.

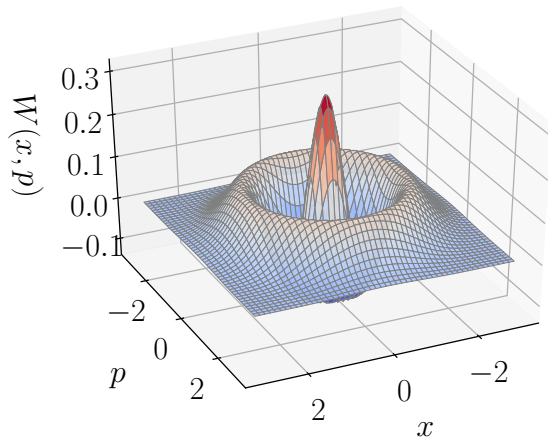
## 1. Theoretical Background



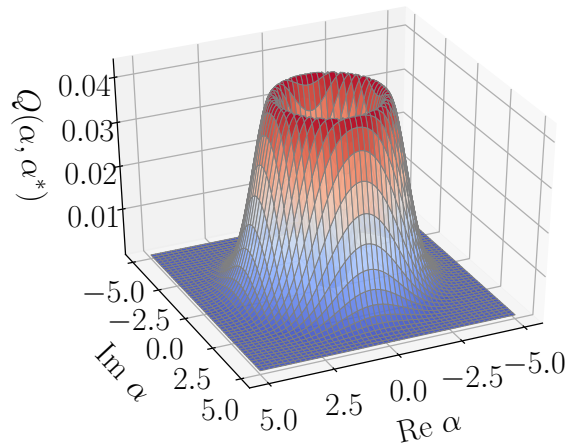
(a) coherent state, W-function



(b) coherent state, Q-function



(c) Fock state, W-function



(d) Fock state, Q-function

Figure 1.5.: Representation of a coherent state with  $\alpha = \sqrt{2}$  and a Fock state with  $n = 2$  in the W- and Q-representation. For the classical coherent state are the representations qualitatively similar but the non-classical Fock state shows a more drastic divergence between the two representations. Whereas the Q-function stays positive everywhere, the Wigner-function has negative values around its center which breaks the definition of classical distribution functions.

## 1.4. Light-Matter interaction

### Dark states and EIT

The ideas of electromagnetically induced transparency and dark states are both related to interference phenomena in atomic physics. We want to focus ourselves on atoms with a three-level structure for this section. The goal is to drive the system into a state in which it cannot absorb any photons of a specific frequency which results in the transparency to this light. We will later see that one transition between the different states has to be dipole-forbidden. This leads to the three possible configurations shown in Fig 1.6 but the mechanism is the same in all the setups. Because this thesis is focused on systems with Rydberg atoms, we will focus our attention on the ladder configuration in the middle of Fig. 1.6, which represents a possible excitation scheme to reach the Rydberg state in atoms. Furthermore, the state  $|1\rangle$  will be the ground state and  $|2\rangle$  and  $|3\rangle$  excited states of the atom.

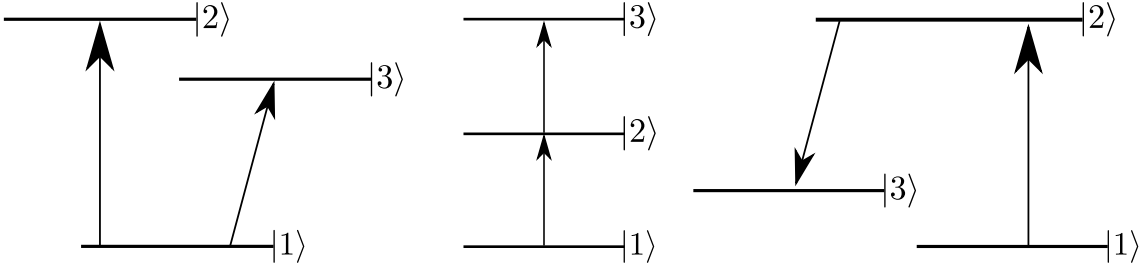


Figure 1.6.: Different settings to achieve EIT in a three-level system: (left) vee-, (middle) ladder- and (right) lambda-scheme. The pictures show all possible transitions which implies each setup has a dipole-forbidden transition which is necessary for EIT. Additionally, the states  $|1\rangle$  and  $|3\rangle$  need to be (meta-)stable states against dephasing to observe the effect.

We now drive the two transitions in the atom by a probe and a control laser. Within the dipole approximation, the interaction between the light and the atom is  $H_{\text{int}} = \mu E$  with  $\mu$  as the transition electronic dipole moment and  $E$  as the electric field. In the rotating frame approximation, we can rewrite it in terms of the Rabi frequency  $\Omega = \frac{\mu E_0}{\hbar}$  with the amplitude of the electric field  $E_0$ . The resulting Hamiltonian  $H = H_{\text{int}} + H_0$  where  $H_0$  describes the bare atom can then be written as

$$H = -\hbar \begin{pmatrix} 0 & \frac{\Omega_p}{2} & 0 \\ \frac{\Omega_p}{2} & \Delta & \frac{\Omega_c}{2} \\ 0 & \frac{\Omega_c}{2} & \delta \end{pmatrix}. \quad (1.83)$$

## 1. Theoretical Background

The two different Rabi frequencies are  $\Omega_p$  for the probe and  $\Omega_c$  for the control laser. The detuning  $\Delta = \omega_p - \omega_{12}$  is the single photon detuning of the probe laser from the transition frequency of the atom between states  $|1\rangle$  and  $|2\rangle$ . We need two photons to reach  $|3\rangle$  and thus we also get a two photon detuning  $\delta = \omega_{31} - \omega_p - (\omega_{32} - \omega_c)$ . Furthermore, we describe the spontaneous emission of a photon from the excited states by the decay rates  $\gamma_2$  and  $\gamma_3$  (see Fig. 1.7).

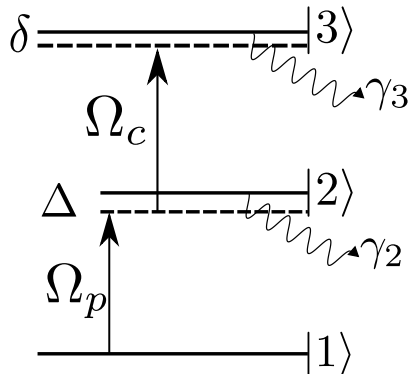


Figure 1.7.: Detailed three-level ladder system with  $\Delta/\delta$  being the one-/two-photon detunings,  $\Omega_p/\Omega_c$  the probe-/control-laser Rabi frequency and  $\gamma_2/\gamma_3$  as the decay rates of the intermediate ( $|2\rangle$ ) and the excited ( $|3\rangle$ ) state.

If we set the system to a two-photon resonance ( $\delta = 0$ ), we can find analytical expressions for the eigenstates of Eq. (1.83). If we define the two angles

$$\tan \Theta = \frac{\Omega_p}{\Omega_c} \quad (1.84)$$

$$\tan 2\phi = \frac{\sqrt{\Omega_p^2 + \Omega_c^2}}{\Delta} \quad (1.85)$$

we get the following three eigenstates

$$|a^+\rangle = \sin \theta \sin \phi |1\rangle + \cos \phi |2\rangle + \cos \theta \sin \phi |3\rangle \quad (1.86)$$

$$|a^0\rangle = \cos \theta |1\rangle - \sin \theta |3\rangle \quad (1.87)$$

$$|a^-\rangle = \sin \theta \cos \phi |1\rangle - \sin \phi |2\rangle + \cos \theta \cos \phi |3\rangle. \quad (1.88)$$

We can immediately see that  $|a^0\rangle$  is decoupled from the intermediate state  $|2\rangle$ . If we now choose a system in which only the state  $|2\rangle$  decays with a significant rate, the state  $|a^0\rangle$  is called a *dark state*. The system cannot absorb any more photons or exit this state in any other way, it is trapped in  $|a^0\rangle$ . That also means, that no matter what, if we wait long enough, the system will end up in this state. Hence, all further incoming photons pass through the medium and we reach a point of an electro-

magnetically induced transparency (EIT). Other explanations of the effect like the dressed states or the interference between different transition pathways rely both on the additional assumption that  $\Omega_c \gg \Omega_p$ . The dark state picture shows, that this is not a necessary condition for EIT. Besides the general structure our medium has to have, we need a two-photon resonance as an EIT condition and  $\gamma_3 \ll \gamma_2$ . We will later see that the last condition makes Rydberg systems ideal candidates to observe EIT.

## Polaritons

The description of light propagation through a Rydberg medium was simplified by the introduction of quasi-particle that corresponds to the superposition of an electromagnetic and an atomic excitation. These quasi-particle are called polaritons. We extend the Hamiltonian in Eq. (1.83) by a quantised probe field. The corresponding operator of the electric field reads as

$$\hat{E} = \sqrt{\frac{\hbar\omega_p}{2\epsilon_0}} \hat{\mathcal{E}} e^{-i(\omega_p t - k_p z)} + h.c. \quad (1.89)$$

with  $\hat{\mathcal{E}}^{(\dagger)} = \sum_k e^{ikz} a_k^{(\dagger)}$  as the slowly varying envelope operator of the field. Therewith, the system Hamiltonian is

$$H = \Delta\sigma_{ee} + \delta\sigma_{rr} - (\Omega_c\sigma_{re} + g\hat{\mathcal{E}}\sigma_{eg} + h.c.) \quad (1.90)$$

The operators  $\sigma_{ij} = |i\rangle\langle j|$  describe the transitions between the states of the atom. We obtain the polaritons of the system by transforming it into its eigenbasis. In Fig. 1.8 we show the eigenenergies of Eq. (1.90) and their scaling with the wavevector  $k$  of the probe light field. By additionally analysing the eigenvectors, we also obtain the contributions of the different fields to each eigenvalue. Each path of the eigenvalue represents a type of polariton. We can distinguish between the  $\pm$ - bright polaritons above and below the zero energy line and a third one around it. This so called dark-state polariton is of special interest because like in atomic picture before, its wave function does not contain any contribution of the intermediate atomic level

$$\Psi_{dp} = \frac{1}{\sqrt{\Omega_r^2 + \Omega_e^2}} (\Omega_r \hat{\mathcal{E}} - \Omega_e \sigma_{gr}) \quad (1.91)$$

## 1. Theoretical Background

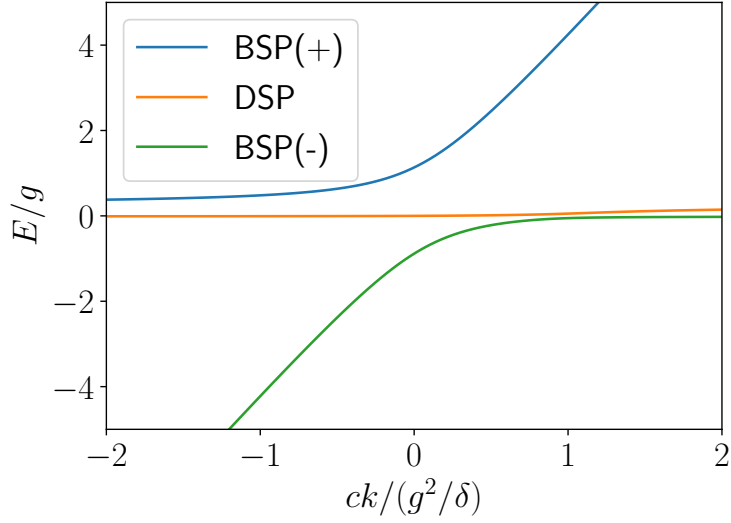


Figure 1.8.: Real part of the eigenenergies of a three-level system. The different branches belong to non-interacting polaritons. The group velocity  $v_g = \frac{d\epsilon}{dk}$  of the dark state polariton (DSP) is almost zero in comparison with the two bright polariton branches (BSP  $\pm$ ).

## 1.5. Rydberg atoms

In the 19th century, Johannes Robert Rydberg found a formula to describe the spectral lines of the valence electron of hydrogen. Nowadays, we know that atoms with large principle quantum numbers  $n > 30$  and a highly excited electron also behave hydrogen-like and are called Rydberg atoms. They are used in a wide variety of applications, e.g. quantum simulation, quantum computing, quantum optics and sensing [58, 59, 60, 61, 62, 13, 63, 64, 65, 66, 67, 68, 69, 70, 71, 72, 73, 74].

In this section, we want to discuss the properties of Rydberg atoms to understand why they are so useful and versatile. In this context, we will discuss some basic properties like their long lifetime and how it makes Rydberg states good candidates for the previously discussed EIT. We will also need to have a look at the van der Waals interaction and the blockade mechanism as important features.

### Properties of Rydberg atoms

The main difference between atoms in its Rydberg state and a hydrogen atom is that the core is not only the nucleus but can also include many electrons. A few adjustments helped in recovering the same scaling properties that were already known



for the hydrogen atom. By the usage of quantum defect theory, it was found that Rydberg atoms have the same scaling properties as hydrogen atoms if we use an effective principle quantum number like  $n^* = n - \delta_l$  with  $\delta_l$  as a quantum defect that depends on the angular momentum number  $l$  and the specie of atom. The defect arises from orbitals with low angular momentum numbers crossing and interacting with the core electrons and therefore changes the Coulomb potential experienced by the valence electron. In 1.1 we listed a few properties of Rydberg atoms and how they scale with  $n^*$ .

The long lifetime and the strong dipole moment are of special interest for us. The

Parameter	scaling
Bohr radius	$n^{*2}$
Dipole moment	$n^{*2}$
polarizability	$n^{*7}$
life-time	$n^{*3}$

Table 1.1.: Scaling of different Rydberg properties.

spontaneous emission from the Rydberg state has a strong influence on the lifetime of the state and can be calculated by the usage of Fermi's golden rule

$$\gamma = \frac{2\pi}{\hbar} |\langle i | V | f \rangle|^2 \rho(E_f) \quad (1.92)$$

that describes the transition probability  $\gamma$  of an initial to a final state  $|i\rangle \rightarrow |f\rangle$  under the influence of a perturbation operator  $V$ . It also depends on the density of states  $\rho$  at the energy level of the final state  $E_f$ . Normally we would need to sum over all possible final states but a closer analysis reveals that the probability for a transmission improves with higher frequencies and therefore favours transitions to the lowest allowed states. The overlap with these states and the Rydberg state, given by the matrix element in Eq. (1.92), is very low and which results in a long lifetime  $\tau = \frac{1}{\gamma}$ .

A second decay channel that we only want to mention is the black body radiation. Even though the gap to the ground state is large and out of range for thermal radiation, the same is not true for transitions between different Rydberg states. The large dipole matrix elements  $\langle i | \mu | f \rangle$  further enhance the dissipation from the original state to other energetically nearby states [75].

In modern experiments, the lifetime of Rydberg atoms reaches up to  $\tau \sim 100\mu s$ . Therefore, we consider Rydberg atoms as metastable and can use them in EIT systems as a medium.

Let us now see how Rydberg atoms interact with each other. We assume that the

## 1. Theoretical Background

interparticle separation is large enough to neglect the overlap of their wave functions [76]. An analysis of the multipole expansion for the overall neutral Rydberg atoms shows a dipole-dipole interaction as the first leading term like

$$V_{dd}(\mathbf{r}_1 - \mathbf{r}_2) = D(\phi) \frac{C_3}{|\mathbf{r}_1 - \mathbf{r}_2|^3} \quad (1.93)$$

where  $\mathbf{r}_1$  and  $\mathbf{r}_2$  denote the positions and the factor  $D(\phi)$  includes all angle-dependencies between the two atoms. We now want to know how Eq. (1.93) couples the two-atom state  $|\Psi\rangle = |nlj, nlj\rangle$  to other states which can differ in their principal quantum number  $n$  or azimuthal quantum number  $l$  but are limited by dipole selection rules. Fermi's golden rule for a dipole perturbation rules out many possible states. The matrix element cannot be too small for a significant transition and this strongly depends on the overlap of the wave functions. This reduces the possible coupling by the dipole-dipole interaction to only a few states that are energetically close to our original two-atom state.

The interaction Hamiltonian can be written as

$$H = \begin{pmatrix} \delta_F & \frac{C_3}{r^3} \sqrt{D(\phi)} \\ \frac{C_3}{r^3} \sqrt{D(\phi)} & 0 \end{pmatrix} \quad (1.94)$$

if we use a two-level approximation for the atoms and the FÄurster defect  $\delta_F$  to account for any energy differences between the two states.

The eigenvalues of Eq. (1.94) are

$$V_{\pm}(r) = \frac{\delta_F}{2} \pm \frac{1}{2} \sqrt{\delta_F^2 + 4 \frac{C_3^2 D(\phi)}{r^6}} \quad (1.95)$$

with  $r = |\mathbf{r}_1 - \mathbf{r}_2|$  as the distance between the two atoms. We can observe that for small distances between the atoms, we obtain an interaction with dipole character. For larger distances, on the other hand, we get

$$V_{\text{vdW}}(r) \approx -\frac{C_3^2 D(\phi)^2}{\delta_F r^6} = \frac{C_6}{r^6}, \quad (1.96)$$

which has a characteristic form of the van der Waals interaction. The van der Waals coefficient  $C_6$  for two rubidium atoms in an s-state can be calculated by the scaling law

$$C_6 = n^{11} (11.97 - 0.8486n + 3.385 \times 10^{-3} n^2) \quad (1.97)$$

in atomic units, which translates to a range of  $25\text{MHz}\mu\text{m}$  to up to  $3 \times 10^4\text{GHz}\mu\text{m}$  for  $30 < n < 95$  [74].

## Rydberg blockade

We want to dedicate an extra section for a specific phenomenon that results from the van der Waals interaction in Rydberg atoms: the Rydberg blockade. If we go back to the notation introduced in the EIT chapter and represent each atom by the ground state  $|g\rangle$ , the intermediate state  $|e\rangle$  or the Rydberg state  $|r\rangle$ , we can write the two-atom dipole-dipole interaction as

$$H_{\text{int}} = \frac{C_6}{r^6} |r, r\rangle \langle r, r|. \quad (1.98)$$

This can be understood as a (two-photon) detuning for the state in which both atoms are in the Rydberg state. For large  $\frac{C_6}{r^6}$ , this leads to a suppression of any Rydberg excitations around another atom in the Rydberg state. The blockade radius at which the detuning is too large depends on the concrete system and the purpose. We want to focus on its definition for the case of the EIT picture from the previous chapter. There, it is defined as

$$r_b = \sqrt[6]{\frac{C_6|\gamma_3 + i\Delta|}{\Omega^2}} \quad (1.99)$$

and indicates the radius at which the two-photon detuning of the interaction is equal to the EIT linewidth  $V_{\text{vdW}}(r_b) = \frac{\Omega^2}{|\Delta + \gamma_3|}$ . That means for the polaritons that all dark and bright polaritons are getting strongly mixed and the whole polariton picture breaks.

## 1. Theoretical Background

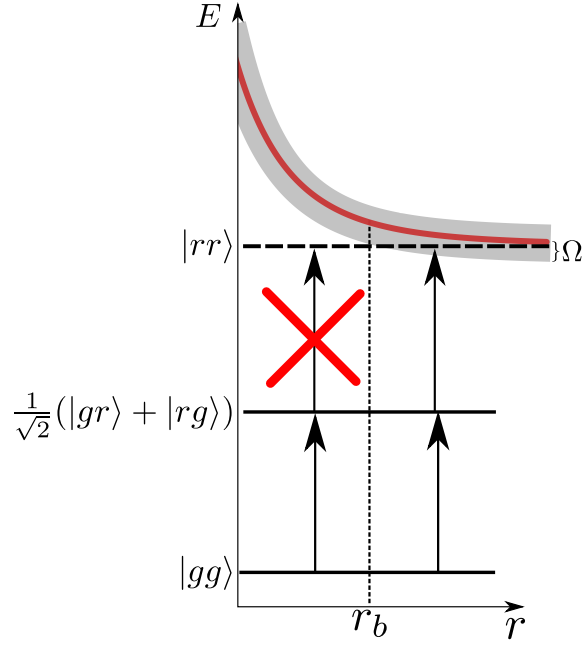


Figure 1.9.: Visualisation of the Rydberg blockade effect. The red line is the interaction potential between the two atoms. Under a distance of  $r_b$  the Rabi frequency  $\Omega$  is not sufficient to excite the system from a single excitation to a double excited state.

## 1.6. Optical lattices

We now want to present how light can confine cold atoms into an optical lattice. To trap an atom in a confined space, we need a force that holds it there. If we put atoms into an off-resonant light field, they will experience a ac Stark shift which changes in space. This leads to the formation of an external potential and with that a dipole force

$$\mathbf{F} = \frac{1}{2}\alpha(\omega_L)\nabla[|\mathbf{E}(\mathbf{r})|^2] \quad (1.100)$$

for the atoms [77]. We only use the time-average intensity  $|\mathbf{E}(\mathbf{r})|^2$  because the center-of-mass motion of the atoms is a lot slower than the time scale of the light which is given by the inverse laser frequency  $\frac{1}{\omega_L}$ . The polarizability  $\alpha(\omega_L)$  now dictates the direction of the force. If the light field is only slightly detuned from an atomic transition  $|g\rangle \rightarrow |e\rangle$  with frequency  $\omega_0$ , we can approximate the polarizability by

$$\alpha(\omega_L) \approx \frac{|\langle e|\hat{d}|g\rangle|^2}{\hbar(\omega_0 - \omega_L)} \quad (1.101)$$

with  $\hat{d}$  being the dipole operator. If we insert Eq. (1.101) into Eq. (1.100) we can see that the atoms are attracted to the nodes of the intensity of a blue-detuned

( $\omega_L > \omega_0$ ) laser light or to the peaks of it if it is red-detuned ( $\omega_L < \omega_0$ ).

The trapping of atoms with light can form lattices in different dimensions. If we use two counterpropagating laser beams to form a periodic potential, we can trap the atoms in place with an periodicity of  $\lambda/2$ . The period can further be changed by choosing a different angle at which the two beams interfere with each other [78, 79]. For laser beams with a Gaussian profile this results in a trapping potential of

$$V(r, z) = -V_0 e^{-2r^2/w^2(z)} \sin^2(kz) \quad (1.102)$$

with  $k = \frac{2\pi}{\lambda}$  as the wave vector of the light and  $V_0$  the maximum depth of the potential. With only two laser beams, we subtract a potential dimension of movement for the atoms which results in cigar-like figures in the medium.

To restrict the atoms to individual lattice sites we need to introduce another pair of light beams that usually acts in an orthogonal direction to the original pair.

For our purpose, it is enough if we focus the attention on the 1D case. Particles in such a lattice follow the time-independent Schrödinger equation

$$H\Psi = \left( -\frac{\hbar^2}{2m} \frac{\partial^2}{\partial x^2} + V(x) \right) \Psi = E\Psi. \quad (1.103)$$

The full wave function then simply reads as  $\Psi(x, t) = \Psi(x)e^{-iEt/\hbar}$  with  $\Psi(x)$  as the solution of Eq. (1.103).

The information about the lattice is contained in the periodic potential  $V(x)$ . The periodicity of a lattice is defined through a translation invariance under the transformation through a translation operator like

$$T_{\mathbf{R}_n} f(\mathbf{r}) = f(\mathbf{r} + \mathbf{R}_n). \quad (1.104)$$

$\mathbf{R}_n$  is the crystal translation vector consisting of the primitive translation vectors  $\mathbf{v}$  of the lattice and their  $n$ -th multiple. These vectors  $\mathbf{v}$  are noncoplanar and form the smallest possible vector under which the system is translationally invariant. In the case of a 1D lattice  $R_n = na\hat{\mathbf{e}}_x$  with  $a$  as the lattice constant and  $\hat{\mathbf{e}}_x$  the unit vector in  $x$  direction.

The potential  $V(x)$  has to have the same periodicity as the lattice

$$T_{R_n} V(x) = V(x + na) = V(x). \quad (1.105)$$

With that condition fulfilled we can see that the Hamiltonian in Eq. (1.103) commutes with the translation operator  $T_{R_n}$  and therefore must have a common set of

## 1. Theoretical Background

eigenstates. If the potential is periodic it should also be possible to write it as a Fourier series

$$V(x) = \sum_q c_q e^{iqx}. \quad (1.106)$$

Putting Eq. (1.106) in Eq. (1.105) results in the additional condition

$$e^{iqR_n} = e^{iqna} = 1 \quad (1.107)$$

which also leads to the definition of the one dimensional reciprocal wave vector

$$q = \frac{2\pi}{a}m \quad (1.108)$$

The periodic condition for the potential has a direct consequence for the wave function in the Schrödinger equation that is known as the Born-von Karman boundary condition

$$\Psi(x + Na) = \Psi(x) \quad (1.109)$$

for lattices with N sites.

A possible wave function that obeys Eq. (1.109) is a set of plane waves

$$\Psi(x) = \sum_k c_k e^{ikx}. \quad (1.110)$$

The boundary condition implies that

$$k = \frac{2\pi}{Na}n = \frac{2\pi}{L}n \quad (1.111)$$

with  $L = Na$  being the size of the lattice and  $n \in \mathcal{N}$ . Substituting Eq. (1.110) and Eq. (1.106) into Eq. (1.103) results in

$$\sum_k e^{ikx} \left[ \left( \frac{\hbar^2 k^2}{2m} - E \right) c_k + \sum_q V_q c_{k-q} \right] = 0. \quad (1.112)$$

Here, we used the fact that the Born-von Karman condition also applies to the reciprocal lattice vectors  $q$  which allowed us to rewrite

$$V(x)\Psi = \sum_{q,k} V_q c_k e^{i(G+k)x} \quad (1.113)$$

to

$$V(x)\Psi = \sum_{q,k} V_q c_{k-q} e^{ikx}. \quad (1.114)$$

The plane waves defined through the Born-von Karman boundary condition form an orthogonal set of function which implies that

$$\left[ \left( \frac{\hbar^2 k^2}{2m} - E \right) c_k + \sum_q V_q c_{k_q} \right] = 0. \quad (1.115)$$

for all  $k$ .

Finally, we can further simplify Eq. (1.115) by restricting  $k$  to lie in the first Brillouin zone. It is defined as the primitive cell of the lattice in the reciprocal space and contains all the necessary information. Therefore, if we use a new  $k'$  that lies in the Brillouin zone and rewrite  $k = k' - q'$  with  $q'$  being another reciprocal lattice vector, we get

$$\left[ \left( \frac{\hbar^2 (k' - q')^2}{2m} - E \right) c_{k'-q'} + \sum_q V_q c_{k'-q'-q} \right] = 0. \quad (1.116)$$

Another transformation of  $q'' = q + q'$  yields our final result

$$\left[ \left( \frac{\hbar^2 (k' - q')^2}{2m} - E \right) c_{k'-q'} + \sum_{q''} V_{q''-q'} c_{k'-q''} \right] = 0. \quad (1.117)$$

Our result in Eq. (1.117) is in general applicable to any kind of particles inside a lattice. Furthermore, we did not use any kind of assumption of the particular strength or form of the potential. We reduced the problem of solving a differential equation into a set of eigenvalue problems for each  $k$ . This way, we also derived the Bloch theorem that states that for any periodic potential the wave function can be written as

$$\Psi_k(x) = e^{ikx} u_k(x). \quad (1.118)$$

This statement directly follows if we substitute  $k = k' - q'$  into Eq. (1.110) like

$$\Psi_k(x) = \sum_q c_{k'-q'} e^{i(k'-q')x} = e^{ik'x} \sum_q c_{k'-q'} e^{-iq'x} = e^{ikx} u_k(x). \quad (1.119)$$

In the last step we redefined  $k' \rightarrow k$  to make it clearer and is anyway only a question of conventions. The Bloch function automatically inherits both conditions that  $\Psi(x + na) = \Psi(x)$  and  $\Psi_{k+k'}(x) = \Psi(x)$ .

The obtained wave functions are eigenfunctions of the Hamiltonian but are delocalized throughout the crystal. We can turn this around by performing a discrete Fourier transformation like

$$w_R(x) = \frac{1}{N} \sum_k e^{-ikR} \Psi_k(x). \quad (1.120)$$

## 1. Theoretical Background

This creates a located function at position  $R = an$ ,  $n \in \mathbb{N}$  which corresponds to the lattice site centers. These so constructed function are orthonormal and are called Wannier functions. The inverse transformation

$$\Psi_k(x) = \sum_R e^{ikR} w_R(x) \quad (1.121)$$

is also possible and allows the reconstruction of the Bloch functions from a linear superposition of Wannier functions  $w_R(x)$  with the appropriate phases  $e^{ikR}$ .



## 2. Quantum many-body dynamics of driven-dissipative Rydberg polaritons

Now that we covered the basics, we first want to look at the driven-dissipative quantum many-body dynamics of Rydberg polaritons in an optical lattice potential. We obtain the dispersion relations for the single-particle problem by using a Bloch wave ansatz. In combination with a transformation into the Wannier basis, we derive an effective Bose-Hubbard model for the dark state polaritons with long-range hopping. The van der Waals interaction of the Rydberg states also leads to additional long-range interaction terms in the model. We show that under experimentally realistic conditions, the dynamics is confined to a single dark state polariton band, even in the presence of dissipation from the decay of the Rydberg state and the possible conversion of dark-state polaritons into bright polaritons caused by the interaction. We provide a numerical analysis of this driven-dissipative many-body model using a variational approach, which we benchmark against wave function Monte-Carlo simulations for small system sizes. Finally, an additional calculation of the two-time correlation function shows that strongly correlated photons can be observed when the polaritons are leaving the system.

This chapter offers a more detailed insight into the results of [80].

### 2.1. Setup

For our model we want to confine multiple ensembles of rubidium atoms in an effective one-dimensional (1D) geometry with length  $L = Na$  with  $a$  being the spacing between the  $N$  lattice sites. We already discussed how to achieve this in Sec. 1.6. We assume a Gaussian distribution like

$$n(z) = n_0 \exp\left(\frac{1}{\sigma^2}(z - z_0)\right) \quad (2.1)$$

## 2. Quantum many-body dynamics of driven-dissipative Rydberg polaritons

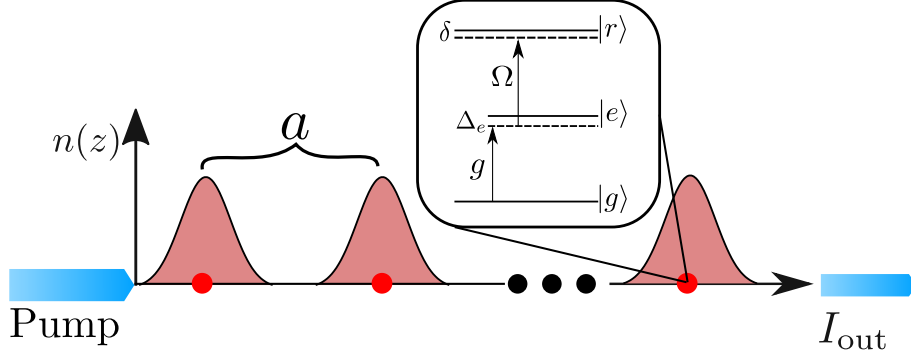


Figure 2.1.: Setup of the system for dark-state polariton propagation. A one-dimensional optical lattice potential creates lattice sites separated by a distance  $a$ , around which the atoms exhibit approximately Gaussian density profile. The system is being pumped from the left by a coherent light field, leading to an output intensity  $I_{\text{out}}$ . Each atoms is driven by a photon field with a space-dependent coupling  $g$  and a coherent laser field  $\Omega$  with a two-photon detuning  $\delta$ . The photon field is detuned by  $\Delta_e$  from the intermediate state.

for the atoms inside each lattice site with an average particle density  $n_0 = 10^{13} \text{ cm}^{-3}$  and a standard deviation of  $\sigma = 25 \text{ nm}$ .

There are multiple setups to achieve stationary polaritons in our system. The simplest setup works in the three-level ladder that we discussed in 1.4 but with the addition of counterpropagating light fields  $\Psi_{E_L}$  and  $\Psi_{E_R}$  that couple the ground state  $|g\rangle$  to the single excited state  $|e\rangle$  with a transition frequency of  $\omega_{ge}$ . The light fields can be detuned by  $\delta_e$  from the atomic transition which we combine with the linewidth  $\gamma_e$  of  $|e\rangle$  to a complex detuning  $\Delta = \delta_e - i\gamma_e$ . We further have a classical control field that is assumed to be constant in the areas it can interact with the excited atoms. The driving is then given by a Rabi frequency  $\Omega$ , which enables the transition to the Rydberg state  $|r\rangle$ . An in-depth analysis of the stationary light in this system is given by *I. Iakoupov et.al.* [81].

Now, if we are working on a two-photon resonance ( $\delta = 0$ ), our system enters the EIT regime. The collective, single-photon Rabi frequency  $g(z)$  in this regime is then given by

$$g(z) = \tilde{g} \sqrt{n(z)} \sum_l e^{ik_l a} \quad (2.2)$$

with  $\tilde{g} = [6\pi\gamma_e c^3 / \omega_{ge}^2]^{1/2}$  and  $c$  being the speed of light [27]. We split the phase factor up in two parts by setting  $\tilde{k} = k_0 + k$  which corresponds to the wave vector  $k_0 = \omega_{ge}/c$  and a deviation from the EIT condition  $k$ . This will help us to calculate the dispersion relation for our system. The transition processes within the atoms can then be described by the bosonic field operators  $\hat{\Psi}_p = |g\rangle \langle e|$  and  $\hat{\Psi}_r = |g\rangle \langle r|$

[26]. In the continuum, the non-interacting part of the Hamiltonian can then be written as

$$H_0 = \hbar \int dz \hat{\Psi}^\dagger \begin{pmatrix} -ic\partial_z & 0 & g(z) & 0 \\ 0 & ic\partial_z & g(z) & 0 \\ g(z) & g(z) & \Delta & \Omega \\ 0 & 0 & \Omega & \delta \end{pmatrix} \hat{\Psi}. \quad (2.3)$$

with  $\hat{\Psi} = \{\hat{\Psi}_{E_L}, \hat{\Psi}_{E_R}, \hat{\Psi}_e, \hat{\Psi}_r\}$ . The kinetic terms for the quantized light fields only account for the previously mentioned deviation from the two-photon resonance.

### 2.1.1. Dispersion relation

A periodic spatial modulation of the coupling constant already suggests the usage of localized Wannier function that we introduced in chapter 1.6. We follow the same steps and first find the single-particle solution of (2.3) by using a Bloch wave ansatz  $\phi_k(z) = e^{ikz} \mathbf{u}_k(z)$  in combination with a plane wave expansion for the periodic functions  $\mathbf{u}_k(z)$ .

The eigenstates of the resulting band structure are a composition of the previously defined bosonic fields. The structure of the composition in Fig. 2.2 shows clearly that the system, like in the case without a lattice, can be described by dark-state polariton and light state polaritons. The two states without any contribution from the  $|e\rangle$  state at around  $E = 0$  can be identified as the only two dark-state-polaritons. We can also see that states with large  $|E|$  show no contribution from the Rydberg state and form a pure two-level system between the ground and intermediate state. These eigenstates will dissipate into the environment because of the spontaneous emission that arises from any contribution of  $|e\rangle$ . Hence, we want to focus on the dark-state polaritons with their vanishing population  $\langle \hat{\Psi}_e^\dagger \hat{\Psi}_e \rangle$ .

Fig. 2.4 shows the dispersion relations  $E(k)$  of the two bands and the surrounding light polaritons. The parameters are chosen for a typical excitation scheme in  $^{87}\text{Rb}$  like  $5s \rightarrow 5p \rightarrow 34s_{1/2}$ . The states form two symmetrical bands around  $E = 0$ , which would not be the case if the forward and backward propagating light did not have the same polarization. This results in a similar situation as we discussed for different stationary light setups. Even though, we depict our three levels as a ladder in Fig. 2.1, this is essentially the same as the  $\lambda$ -configuration for three-level systems. The biggest difference here is that we deal with a discrete model enforced by the optical lattice. This has important consequences, especially around the EIT resonance  $k = 0$ . The solution there presents a superposition of both bands which results in an elimination of the Rydberg part in the polaritons and a crossing of the

## 2. Quantum many-body dynamics of driven-dissipative Rydberg polaritons

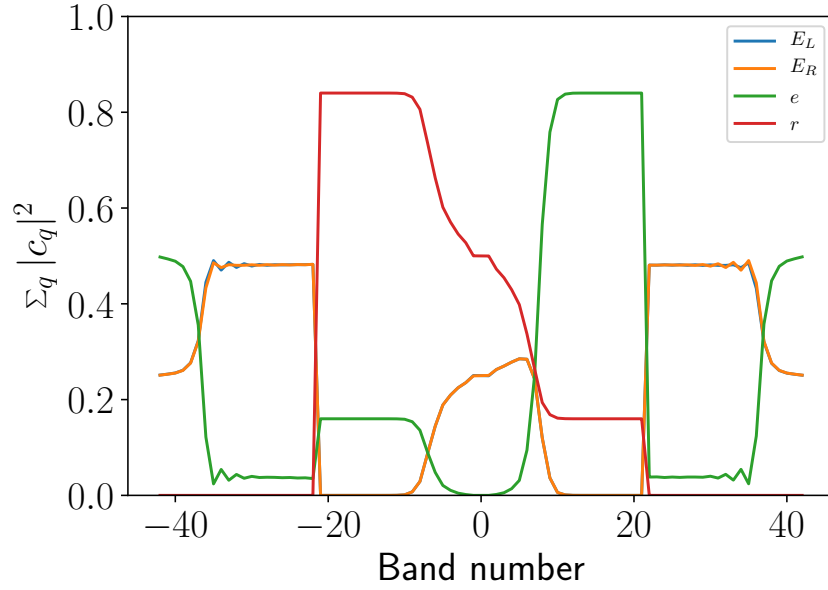


Figure 2.2.: The summation over the absolute squared coefficients  $\sum_q |c_q|^2$  for the different modes  $\hat{\Psi} = \{\hat{\Psi}_{E_L}, \hat{\Psi}_{E_R}, \hat{\Psi}_e, \hat{\Psi}_r\}$  at  $k = 0$  shows the distribution of each field to the Bloch wave of the corresponding band. In the lowest and highest energy bands are the Rydberg state occupation 0 which allows for a two-level description in that regime. The two energy bands around  $E = 0$  can be identified as the dark-state polariton because they have a vanishing amplitude in the intermediate atomic level but still occupy the Rydberg state  $|r\rangle$ . The rest are all light polariton states with different distributions in the modes.

bands at that point. Furthermore, the standing wave of the control field is assumed to be constant and not zero at each lattice site. All of this results in the linear dispersion we can see in Fig.2.4 and these are also the only two bands in the system with a linear dispersion relation. Additionally, Fig.2.4 also shows the dissipation of the two dark-state polaritons which is the imaginary part of  $E(k)$ . The dissipation like the dispersion at  $k = 0$  is also zero because of EIT but it is overall so small that we will not investigate it further because we will later see that a different dissipation channel has a way bigger impact on the dynamics of our dark-state polaritons.

The surrounding bands above and below the two dark-state polaritons can already be classified as bright state polaritons with a occupation probability of  $\approx 4\%$  in the intermediate state and a relatively small dissipation, respectively. The band gap between these states and the dark-state polaritons allows us to use a two-band approximation. We can neglect all bands besides the two dark-state bands if the mean energy value of the bands are lower than the energy to the next band [82]. In Fig. 2.3 the scaling of the band gap is shown in dependence of the control field frequency  $\Omega$ . It is important to note that the gap scales with an experimentally tunable parameter. The gap disappears for  $\Omega = 0$  because the bands involving the Rydberg state collapse because they are no longer coupled to the intermediate state.

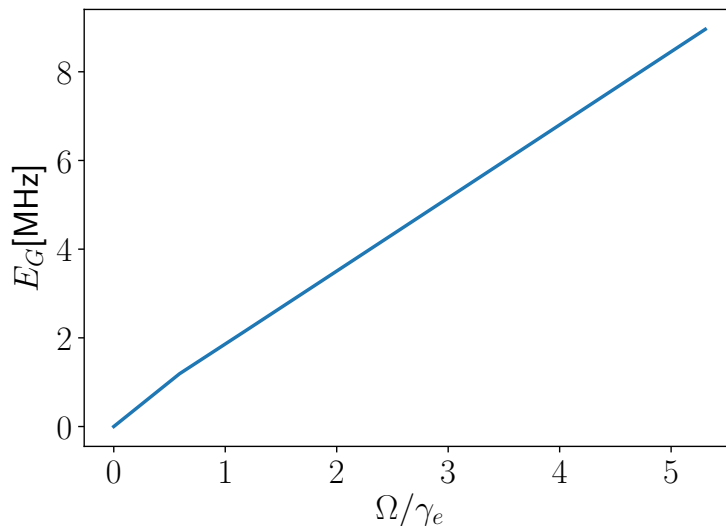


Figure 2.3.: Scaling of the energy gap  $E_G$  between the upper dark-state polariton band and the next band with the Rabi frequency of the control laser  $\Omega$ . The gap scales almost linearly with the strength of the control laser. When the atomic system changes from three to two levels for  $\Omega = 0$ , the gaps between the bands around  $E = 0$  also disappear because the system cannot form dark-states anymore.

## 2. Quantum many-body dynamics of driven-dissipative Rydberg polaritons

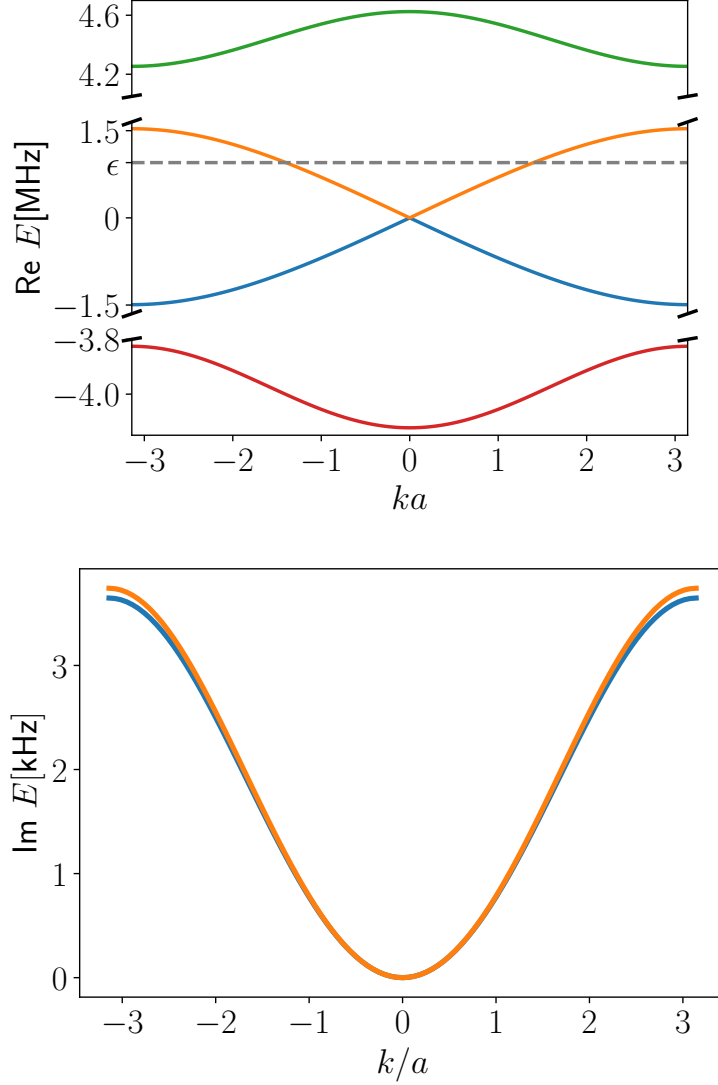


Figure 2.4.: (Upper) Dispersion relation for polaritons close to zero energy. We obtain two dark-state polariton bands and show the next bright state polariton bands. The dashed grey line indicates the average energy  $\epsilon$  of the upper dark-state polariton. (Lower) The dissipation of the two dark-state polaritons. For both dark-state bands are  $\frac{\text{Im}E}{\text{Re}E} \ll 1$  because of almost no contribution from the intermediate atomic level. The dissipation is by a factor of  $\approx 10$  smaller than the spontaneous decay from the Rydberg state  $\gamma_r = 25\text{kHz}$ . The parameters for the dissipation and dispersion are  $\Omega/2\pi = 18$  MHz,  $\delta_e/2\pi = 20$  MHz,  $\gamma_e/2\pi = 6$  MHz, and  $a = 532\text{nm}$ .

### 2.1.2. Hamiltonian

In the following, we transform the eigenstates of (2.3) into localized Wannier functions  $\mathbf{w}_j(z) = \frac{1}{\sqrt{N}} \sum_k e^{-ikaj} \phi_k(z)$  that we discussed in the first chapter of this thesis, resulting in bosonic creation operators  $a_i^\dagger = \int dz \mathbf{w}(z) \Psi(z)$  for the upper band and the analogous operators  $b_i$  for the lower band. Fig. 2.5 and Fig. show an exemplary Bloch wave and a Wannier function for our system and how we achieve strong localised functions by the transformation. The Hamiltonian

$$H_0 = - \sum_{i,j} J_{i,j} (\hat{a}_i^\dagger \hat{a}_j - \hat{b}_i^\dagger \hat{b}_j + h.c.) + (2\epsilon - \beta) \sum_i \hat{b}_i^\dagger \hat{b}_i + \beta \sum_i \hat{a}_i^\dagger \hat{a}_i \quad (2.4)$$

$$(2.5)$$

describes the non-interacting dynamics of the two bands. The first line in Eq. (2.4) describes hopping between the sites with a strength of  $J_{i,j}$ , which can be written in terms of the hopping length  $m$  as  $J_m$  with  $|i - j| = ma$ . This parameter arises from the operator transformation into the Wannier basis and describes the probability of a particle on site  $i$  with Wannier function  $w_i(z)$  to change to a particle on site  $j$  with Wannier function  $w_j(z)$

$$J_{i,j} = - \int_{-\infty}^{\infty} w_i^*(z) H w_j(z) \quad (2.6)$$

It is important to note that the scaling of  $J_{i,j}$  with the distance  $|i - j|$  does not follow an exponential decay but an asymptotic power law decay like  $|i - j|^{-2}$ , which arises from the linear dispersion of the bands at around  $k \approx 0$ . Fig. 2.7 shows the polynomial fit  $b \log x + a$  in an logarithmic scale with the parameters  $b = -2.4$  and  $a = 0.2\text{MHz}$ . Hence, we cannot approximate the system by a nearest neighbor-hopping  $J_1$ , which is the usual assumption considering other level schemes [83].

The following two terms are the on-site energy shifts where the factor  $\beta$  indicates the detuning from a resonant driving of the upper polariton branch. The explicit form of  $\epsilon$  is quite similar to  $J$  and is given by  $\epsilon = -J_{i,i}$ . The term can also be understood as hopping from site  $i$  to site  $i$  and can, therefore, decrease the chance that the particles moves through the system which we will later use to constrain ourselves to a single band model. Our goal is to have a description of an open system which means that additional dissipative channels will enter the system. To counteract the loss, we add a continuous, coherent light beam from the left side

## 2. Quantum many-body dynamics of driven-dissipative Rydberg polaritons

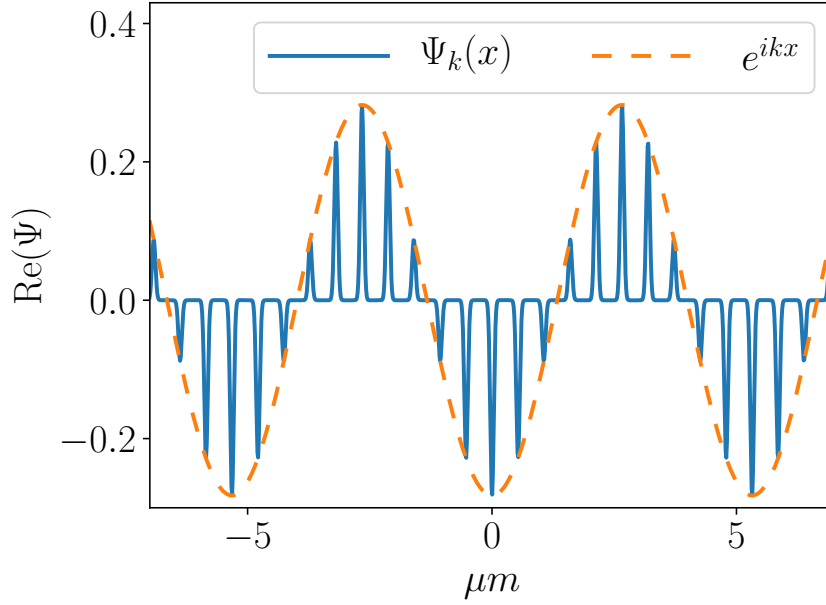


Figure 2.5.: The blue solid line shows the real part of the Bloch function  $\Psi_k(z)$  of the upper dark-state polariton band for  $k = \frac{2\pi}{L}n$  with  $n = 10$ . The orange dashed line shows only the  $e^{ikz}$  factor of the Bloch function.

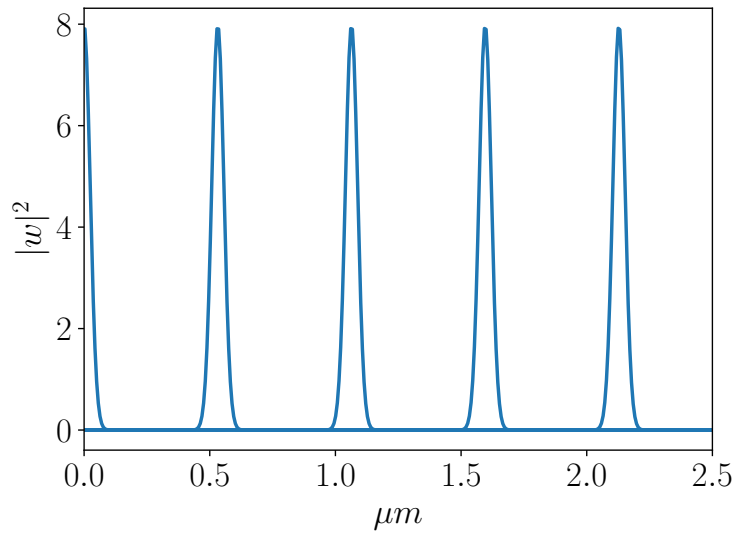


Figure 2.6.: The Wannier functions  $|w_i(z)|^2$  of the dark-state polariton of the upper branch for  $0\mu m \leq z \leq 2.5\mu m$ . We see the strong localization of each function around the site center.



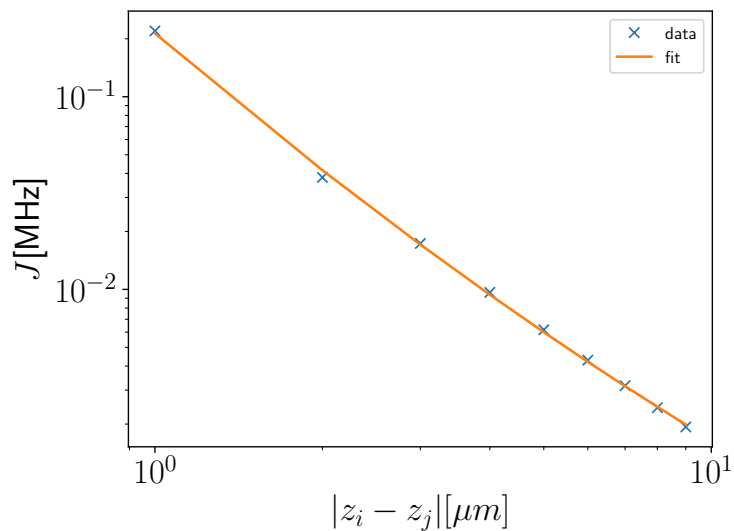


Figure 2.7.: Logarithmic scale of the hopping terms with a polynomial fitting function  $f(|z_i - z_j|) = a|z_i - z_j|^b$  with  $b = -2.4$  and  $a = 0.2\text{MHz}$

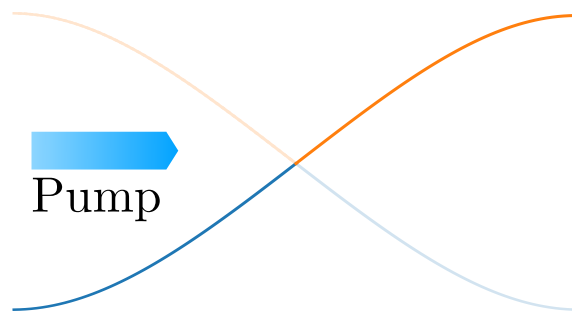


Figure 2.8.: Depiction of the parts of the dark-state polariton bands that are getting excited by a forward propagating wave as the pumping pulse.

of the system to act as a pump (see fig. 2.1). For the dark-state polaritons, the consequence is that we pump only half of the states of two bands instead of all states in one band, see Fig. 2.8. For  $J_1/(2\epsilon - \beta) \ll 1$  the lower band is far detuned and can be neglected.

### 2.1.3. Influences of the environment

Until here we described a closed system and obtained a Bose-Hubbard-model for two bands. We already described in section 1.1.1 how the Lindblad formalism allows us to describe an open quantum system. We want to use it to describe the system in an open environment. We will see that even though we do not have a band gap between the upper and lower dark-state polariton we still can neglect one band under the correct conditions.

## 2. Quantum many-body dynamics of driven-dissipative Rydberg polaritons

In section 1.5 about the properties of Rydberg atoms, we already discussed what can cause losses in these systems. The largest dissipation channel appears in the form of the decay from the intermediate atomic level. For most states in our system that would be the most significant contribution to any kind of loss but we already saw in the last section that this is not true for our dark-state polaritons.

Here, a second natural dissipation channel comes into play in the form of the spontaneous decay from the Rydberg state. We did not include it so far because the typical rates for it are only a few kHz which is neglectable to the intermediate decay rate with typically a few MHz. Now that we want to focus on the dynamics of the long-living dark-state polaritons, we are suddenly working in a time scale where these slow decay rates are becoming more important. A large part of the composition of the polaritons is the Rydberg state and we can express its effect on them by an effective decay rate  $\gamma_i = \int dz |w_r^{(i)}(z)|^2 \gamma_r = 12.5 \text{kHz}$  [84]. The jump operator that describes the process can then be written as  $c_i = \sqrt{\gamma_i} \sigma_-^{(i)}$  for each site  $i$ .

Another problem arises from the finite lattice we are working with. The dynamics of the polariton particle do not suddenly end at the edges of our system. Instead, the dynamical process of hopping which we discussed previously can also happen towards the surrounding environment. There are multiple problems we need to address with that description. Outside the lattice we do not have Rydberg atoms which destroys the polariton picture we were working in and with that it could have an impact on the probability of a jump occurring. We assume here that this is not the case with the simple argument that the dynamical process of hopping between the sites of the polaritons is mostly defined by the photonic part of the particles. Furthermore, photons are also not influenced by the optical lattice so that we can disregard it here. Altogether can we describe the emission of the photons into the environment as another dissipation channel with jump operators  $c_{1(N)} = \gamma_{\text{out}} \sigma_{1(N)}^-$  that only acts on the first and last sites of the lattice. Here, we consider the case where  $\gamma_{\text{out}} = J_1$ , i.e., the coupling to the outside has the same strength as the internal nearest-neighbour hopping. Similar processes can also be defined for the other sites but show an insignificant influence on the overall dynamics.

The output dissipation channel allows us to define an output photon intensity utilizing the internal dynamics of the polaritons in the system, providing a similar approach as the input-output formalism in for example cavity QED systems [85, 86]. The probability of emitting a photon in the opposite directions of the incoming photons depends on the polariton population of site  $N$ . Hence, we can define an output intensity as  $I_{\text{out}} = J_1 \langle \sigma_N^+ \sigma_N^- \rangle$  which describes the incoherent part of the master equation for  $\langle \sigma_N^+ \sigma_N^- \rangle$  without the Rydberg decay. The Rydberg decay is not included in

our definition because the process of spontaneous emission emits photons in random direction from the lattice site and hence adds very little to a photon detector at the end of the lattice. It should further be noted, that similar terms could also be defined for all previous sites with accordingly long-range hopping terms  $J_{2,3,\dots}$  but we found no significant change in the output signal by including these additional terms for larger systems because of the combination of the low population or low hopping strength.

To counteract the dissipation in our system we also want to pump the transition from the ground to the intermediate state. We are doing this through a forward propagating wave which enters at one edge of the system. In the description of the here established band model of the polariton, we always assumed a symmetric probe laser. Fig. 2.8 shows the parts of the two bands that would get excited from forward propagating wave. We also need to know how this translates into the real space.

We can write the upper branch as  $\sum_{k_n=0}^{k_{N/2}} a_k^\dagger$  and the lower part as  $\sum_{-k_{N/2}}^{k=0} b_k^\dagger$ . If we again use the Fourier transformation into the real space we get

$$\sum_{k_n=0}^{k_{N/2}} a_k^\dagger = \frac{N+1}{2\sqrt{N}} a_0^\dagger + \frac{1}{\sqrt{2N}} \sum_{j=1}^N a_j^\dagger \quad (2.7)$$

for the upper band and

$$\sum_{-k_{N/2}}^{k=0} b_k^\dagger = \frac{N+1}{2\sqrt{N}} b_0^\dagger + \frac{1}{\sqrt{2N}} \sum_{j=1}^N b_j^\dagger \quad (2.8)$$

for the lower part. The full calculation can be found in the Appendix A. Even though all sites are getting pumped, most of it ends up in the first lattice site. Especially for larger lattice sites with  $N \gg 1$ , the second part is neglectable compared to the first one. We will later show with the help of another argument that arises from the interaction of the polaritons on different site why we can drop the second part completely.

#### 2.1.4. Long-range interaction

An important point we neglected so far is the interaction between the Rydberg atoms and the effects it has on the different polariton states. The interaction between Rydberg atoms is dominated by the van der Waals interaction, which we discussed in Chapter 1. There, we already defined the interaction Hamiltonian between Rydberg

## 2. Quantum many-body dynamics of driven-dissipative Rydberg polaritons

atoms in a continuum. For a one dimensional model this reads as

$$H_{\text{int}} = \int dz \int dz' V(z - z') \sigma_{gr}^\dagger(z) \sigma_{gr}^\dagger(z') \sigma_{gr}(z') \sigma_{gr}(z). \quad (2.9)$$

In [87] we find an comprehensive summary how to obtain Eq. (2.9). They show that an effective description is possible if the beam waist of the probe laser is small compared to the EIT blockade radius  $r_B = \sqrt[6]{C_6 \Delta \Omega^2}$ . The correct choice of the radial dipole trap plays an important role to achieve this condition for Rydberg systems [88].

By also transforming the operators in Eq. (2.9) with the previous established Wannier functions, we obtain

$$\begin{aligned} H_{\text{int}} = \sum_{i,j} ( & V_{i,j}^{(1)} \hat{a}_i^\dagger \hat{a}_j^\dagger \hat{a}_i^- \hat{a}_j^- + V_{i,j}^{(2)} \hat{b}_i^\dagger \hat{b}_j^\dagger \hat{b}_i^- \hat{b}_j^- \\ & + V_{ij}^{(3)} a_i^\dagger a_i b_j^\dagger b_j + V_{ij}^{(4)} a_i^\dagger a_j^\dagger b_i b_j \\ & + V_{ij}^{(5)} a_i^\dagger b_j^\dagger a_i a_j + V_{ij}^{(6)} a_i^\dagger b_j^\dagger b_i b_j + h.c. ) \end{aligned} \quad (2.10)$$

for both bands. The coefficients  $V_{i,j}^{(i)}$  have the general form

$$V_{ij} = \frac{C_6}{2} \int dz dz' \frac{\mathbf{w}_i^*(z) \mathbf{w}_j^*(z') \mathbf{w}_j(z') \mathbf{w}_i(z)}{r_b^6 + |z - z'|^6} \quad (2.11)$$

with the Wannier function  $w$  that belongs to the site and band of the corresponding operator in the term and we chose  $r_b$  as a regularization constant for the calculation of the interaction strength.

The first line in Eq. (2.10) describes the two possible interband interactions. The other terms are the possible intraband interactions in the system. We also need to consider the interaction between dark and light polariton states. The blockade mechanism allows to greatly reduce the complexity of the system. We already mentioned the EIT radius  $r_b = \sqrt[6]{\frac{C_6 |\Delta|}{\Omega^2}}$  and how the EIT brakes for atoms inside of it. That means the description of dark-state polaritons are not valid anymore and incoming photons can get absorbed into the intermediate state of the atoms. Without the possibility to form a dark state or reaching the Rydberg level, the fast decay of the intermediate state causes an undirected scattering of the photons into the environment. This enforces a minimal distance  $r_b$  between the creation of two polariton states and is the reason why it is our choice for the regularization in Eq. (2.11). The blockade mechanism has more consequences for our model but we need to change the radius to take into account that we are in a lattice and only can create polaritons by hopping between the sites. Like we said earlier the strength of this process is

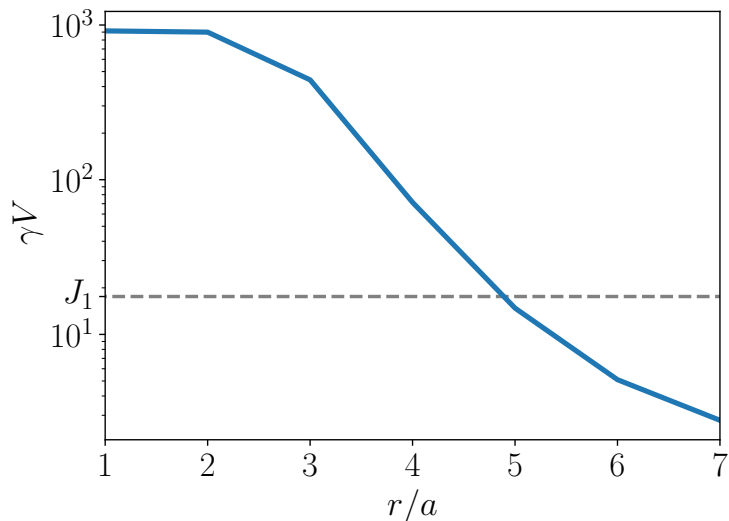


Figure 2.9.: Interaction strength of two interacting polaritons for different distances between the two particles in a semi-logarithmic scale. The crossing of the grey line at hopping strength  $J_1$  with the interaction strength  $V$  indicates the the Rydberg blockade radius  $r_b$ . Hopping of the polaritons closer to each cannot happen below this radius because the energy is not sufficient enough to overcome the interaction barrier.

mostly defined by the nearest-neighbour hopping  $J_1$ . For a jump to occur we need to weigh its strength against repulsive van der Waals interaction which leads to a different blockade radius  $\tilde{r}_b = \sqrt[6]{\frac{C_6}{J_1}}$ . Fig 2.9 shows how the interaction strength falls off over the distance  $r$  between two polaritons and also when it crosses blockade radius we defined through the hopping strength  $J_1$ . For  $r \leq r_b \approx 2a$  is the interaction strength almost constant because of our choice of the regularization and  $\tilde{r}_b \approx 5a$  for the chosen parameters. We note that  $\tilde{r}_b > r_b$  is always the case because  $J_1 \propto \Omega, 1/|\Delta|$ . The relationship between the different radii can only change if the intermediate state is decoupled from the ground state by a large detuning which leaves the system in the trivial ground state.

We now know that a second polariton cannot jump into the radius  $\tilde{r}_b$  around another polariton or can be created otherwise inside  $r_b$ . Therefore, we can neglect the scattering process from one dark state to the other for small distances and in combination with the low population of the detuned band, we can also ignore the terms in our calculations. Also, the energy scale of  $V_{ij}$  outside  $\tilde{r}_b$  is very small and cannot couple to the surrounding light polariton bands, which keeps our single-band

## 2. Quantum many-body dynamics of driven-dissipative Rydberg polaritons

approximation intact. Hence, we can rewrite Eq. (2.11) as

$$H_{\text{int}} = \sum_{i,j} V_{i,j} \hat{a}_i^\dagger \hat{a}_j^\dagger \hat{a}_i^- \hat{a}_j^-. \quad (2.12)$$

Furthermore, with  $r_b > a$  the formation of more than one dark-state polariton per site is not possible. Therefore, we have either a single polariton or none on any lattice site. In the case of a single band we express that as a kind of spin-1/2 particle lattice which can be either in the up  $|\uparrow\rangle$  or down state  $|\downarrow\rangle$ . We use the convention that the up state corresponds to having a polariton on that site and the down state if we do not find one. Instead of having an infinite subspace, we now can express it with the Pauli matrices  $\sigma_x, \sigma_y, \sigma_z$  which are the generators of the SU(2)-group to which spin-1/2 systems belong. The density matrix for one site is then

$$\rho_i = \frac{1}{2}(\mathcal{I} + \alpha_x \sigma_x + \alpha_y \sigma_y + \alpha_z \sigma_z). \quad (2.13)$$

The annihilation operator  $a$  changes accordingly to  $\sigma^- = \frac{1}{2}(\sigma_x - i\sigma_y)$ , similarly  $\sigma^+ = \frac{1}{2}(\sigma_x + i\sigma_y)$  for the creation operator  $a^\dagger$ .

For the dynamics of both dark-state polariton bands the situation is different. It does not matter if we are in the lower or upper dark-state band, the interaction between the Rydberg states blocks an additional excitation for both bands. This leads to three possible states on each site: it can be in the lower or upper dark-state band or in neither of them. This kind of triplet state belongs to the SU(3)-group and is also used to describe spin-1 particles. As an analogue to the Pauli matrices we can use the Gell-Mann matrices  $\lambda_i$  to span the Hilbert space of a single spin-1 particle, which corresponds to a single site of our lattice. From the 9 matrices (including the unitary matrix) we can again define new annihilation (creation) operators

$$\lambda_a^{-(+)} = \begin{pmatrix} 0 & 0 & 0 \\ 1 & 0 & 0 \\ 0 & 0 & 0 \end{pmatrix}^{(\dagger)}, \quad \lambda_b^{-(+)} = \begin{pmatrix} 0 & 0 & 0 \\ 0 & 0 & 1 \\ 0 & 0 & 0 \end{pmatrix}^{(\dagger)} \quad (2.14)$$

for the dark-state polaritons in the upper (a) and the lower (b) dispersion branch in 2.4.

Putting everything together gives us an extended Bose-Hubbard Hamiltonian for

interacting dark-state polaritons

$$\begin{aligned}
H = & - \sum_{i,j} J_{i,j} \lambda_{a,i}^+ \lambda_{a,j}^- + p(\lambda_{a,1}^+ + \lambda_{a,1}^-) + \beta \sum_i \lambda_{a,i}^+ \lambda_{a,i}^- \\
& - \sum_{i,j} J_{i,j} \lambda_{b,i}^+ \lambda_{b,j}^- + p(\lambda_{b,1}^+ + \lambda_{b,1}^-) + (2\epsilon - \beta) \sum_i \lambda_{b,i}^+ \lambda_{b,i}^- \\
& + H_{\text{int}}.
\end{aligned} \tag{2.15}$$

for two interacting dark-state polaritons in a lattice with  $H_{\text{int}}$  being Eq. (2.10). This simplifies further to

$$\begin{aligned}
H = & - \sum_{i,j} J_{i,j} \sigma_i^+ \sigma_j^- + p(\sigma_1^+ + \sigma_1^-) \\
& + \beta \sum_i \sigma_i^+ \sigma_i^- + \sum_{i,j} V_{ij} \sigma_i^+ \sigma_j^+ \sigma_i^- \sigma_j^-
\end{aligned} \tag{2.16}$$

for the upper dark-state polariton if the other one is far detuned.

Eq. (2.16) will be our end result and we will focus on that in the next section but before we do that we want to have a brief look at the dynamics of Eq. (2.15) which we will do with the QuTiP module in Python [89, 90] and the quantum Monte Carlo wave function method. Fig. 2.10 shows the expectation value of finding a dark polariton on a site  $\langle P_{\text{dp}} \rangle_i$  for a lattice of size  $N = 3$ . Here, we use the coherent pump we introduced before and if the detuning of both bands are equal we also observe a similar behavior of them. In the second part we far detune one band and set the other on resonance which result in an almost complete suppression of one band after the first site, which is not influenced by the detuning because it is the site that we directly pump. In Fig. 2.11 we additionally look at a slightly different situation where we exchange the coherent pumping by an incoherent pump which can be implemented by the two jump operators  $c_{a,b} = \sqrt{p} \lambda_{1,a}^+, \sqrt{p} \lambda_{1,b}^+$ . We observe a different dynamics overall but especially also if we change the detuning. Even though the detuning still reduces the population on each site for one of the bands, neither of them vanish completely. The coherent pumping populates virtual states at the off-resonant energy level and even though hopping can occur there are no processes on the other sites that the depopulate these virtual states except on the first site.

2. Quantum many-body dynamics of driven-dissipative Rydberg polaritons

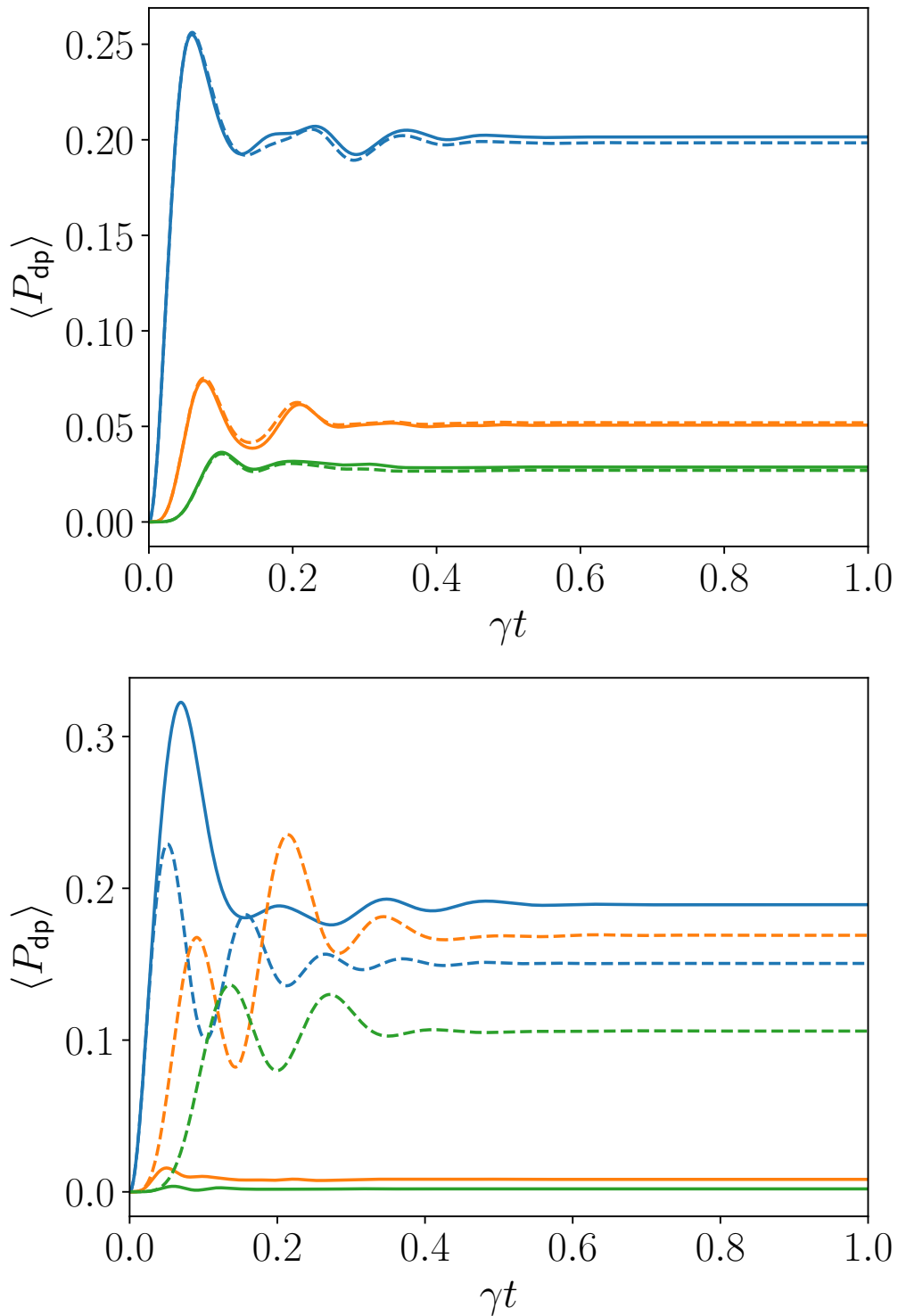


Figure 2.10.: Time evolution of a small system ( $N = 3$ ) to see the effect of the detuning between the two dark-state polaritons if we have a coherent pump. (Upper) For  $\epsilon = 1$  the detuning for both bands is the same which results in very similar dynamics between the two. (Lower) For  $\epsilon = 0$  the lower band vanishes almost completely. The occupation numbers are also higher for the single band than the two bands for  $\epsilon = 1$  together because of no additional detuning through the interaction between the two bands. The results are calculated by WFMC.



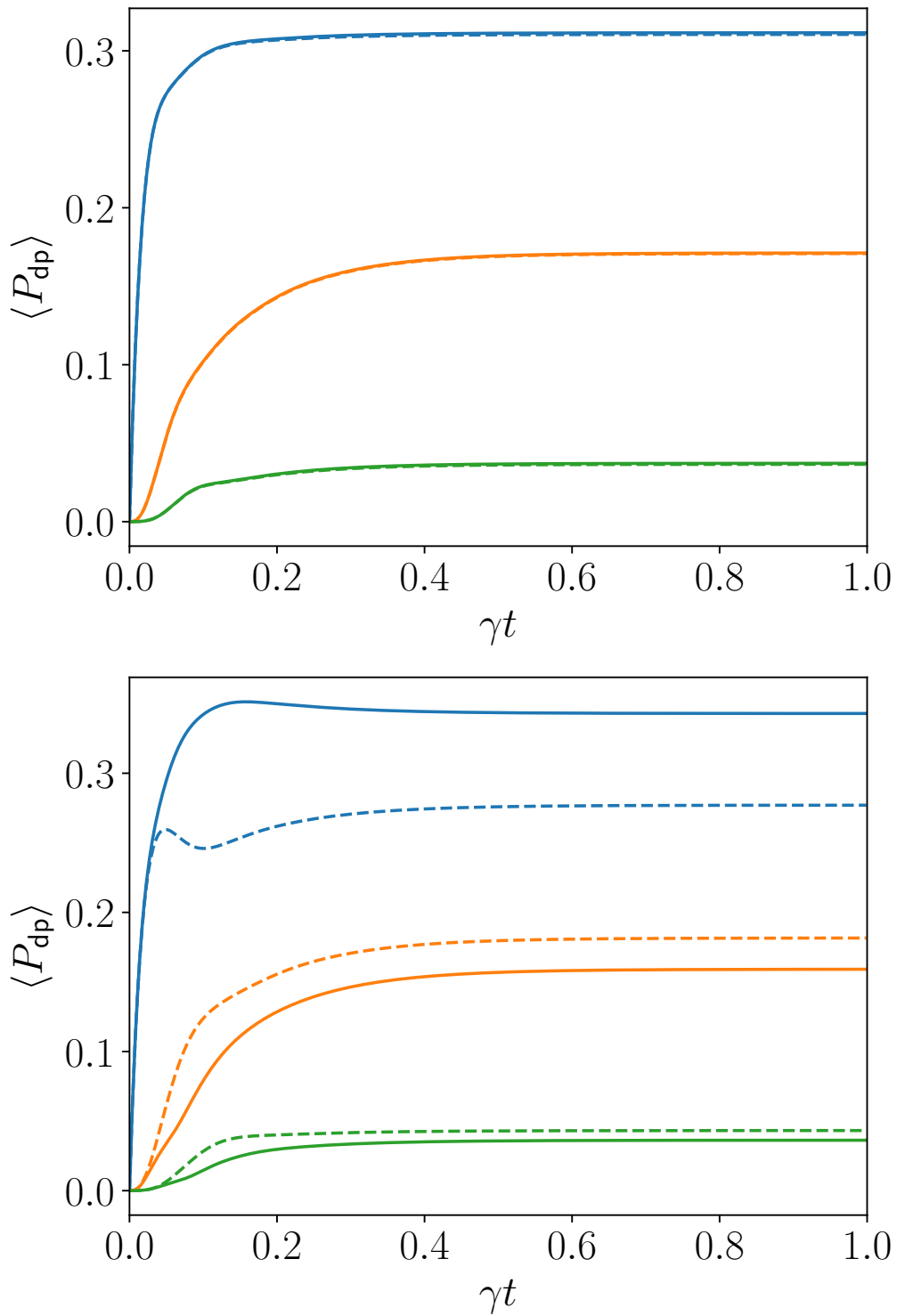


Figure 2.11.: Time evolution of the two dark-state polaritons with an incoherent pump. In comparison to the coherent pump in 2.10 the effect of the detuning of the two bands is much smaller because the virtual processes that capture the polariton on the first site only appear in with coherent pump processes.

## 2.2. Time evolution

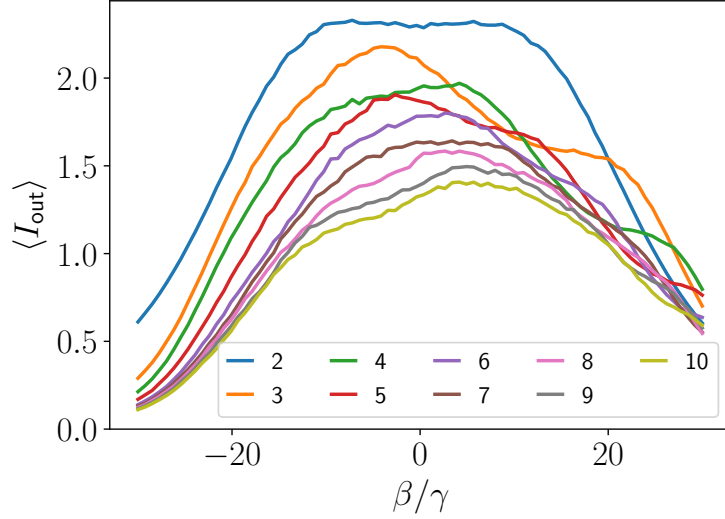


Figure 2.12.: Scaling of the intensity output  $\langle I_{\text{out}} \rangle$  for different detunings  $\beta$  under coherent pumping. For  $N = 2$  a symmetrical behaviour is visible but does not last for larger system sizes.

Now that we have fully described our model we want to investigate its dynamics. We perform exact numerical simulations of the system for site numbers up to  $N = 10$  with the Monte-Carlo wave function method using the QuTiP library [90, 91], which amounts to an average of about two polaritons inside the system. In all our simulations, we choose the initial state to have no polaritons in the system. To analyse the output for larger lattices, we use a variational approach [40, 92] starting with a product ansatz for the density matrix

$$\rho = \prod_{i=1}^N \rho_i = \frac{1}{2} \prod_{i=1}^N \left( 1 + \sum_{\mu \in \{x,y,z\}} \alpha_{\mu} \sigma_{\mu}^i \right) \quad (2.17)$$

with  $\rho_i$  as the density matrix for each lattice site and  $\alpha_{\mu}$  as our variational parameters.

A product state ansatz is insufficient to describe the blockade phenomena associated with the van der Waals interaction in Rydberg system but we can solve this problem by adding a constraint to the minimization process regarding the pair-correlation function

$$g_2(z_i - z_j) = \frac{\langle P_r^i P_r^j \rangle}{\langle P_r \rangle^i \langle P_r \rangle^j}. \quad (2.18)$$

In a strongly correlated regime, which in our case is given by the area inside the

blockade radius  $\tilde{r}_b$ , the pair-correlation function vanishes and the correlations are neglectable outside of it which corresponds to  $g_2 = 1$ . We can assume a very sharp transition from one regime to the other which allows us to describe the correlation function as a step function

$$g_2(|z|) = \Theta(|z| - r_b). \quad (2.19)$$

In combination with an adaptive version of the normalisation condition for  $g_2(|z|)$  for dissipative systems

$$\frac{1}{2r_b} \sum_{ix_0 \leq r_b} \langle P_r \rangle_i \int dz [1 - g_2(z)] \leq 1, \quad (2.20)$$

we can derive a blockade constraint for the polaritons, which restricts the summed probabilities inside a 1d-sphere with radius  $r_b$  to a single polariton, i.e.,

$$\sum_{i-r_b < j < i+r_b} \langle \sigma_+^{(i)} \sigma_-^{(i)} \rangle \leq 1 \quad (2.21)$$

for all sites  $i$ . A similar approach was already successfully implemented in the equilibrium analysis of Rydberg gases [93]. For the variational integration of the quantum master equation, we use an implicit midpoint method [92]. To reduce the number of variational parameters in a single optimization, we evolve the system from  $t$  to  $t + \Delta t$  by minimizing the parameters for one site while holding every other site constant [31]. This procedure is repeated for all sites before moving on to the next time step. For the variational optimization we use the norm  $D_i$  for each site  $i$  given by

$$D_i = \sum_{j \neq i} \left\| -\frac{\tau}{2} \mathcal{L}[\rho_i(t + \tau)\rho_j(t) + \rho_{ij}(t)] \right. \\ \left. + \rho_i(t + \tau)\rho_j(t) - \rho_{ij}(t) \right\|_1 \rightarrow \min, \quad (2.22)$$

where  $\|\cdot\|_1$  denotes the trace norm  $\text{Tr}\{|\cdot|\}$ . Additionally, we add constraints to the minimization to enforce the positivity of the density matrix  $\rho_i \geq 0$  and to enforce the blockade of the polaritons.

Fig. 2.13 shows the intensity output  $I_{\text{out}}$  for different lattices sizes  $N$ . Additionally, we benchmark the variational results against wave function Monte-Carlo simulations. The product states in combination with the hard-sphere constraint are both not suitable for small system sizes because they do not depict the influences of the strong correlations in the system if the particle number is below 1 at all

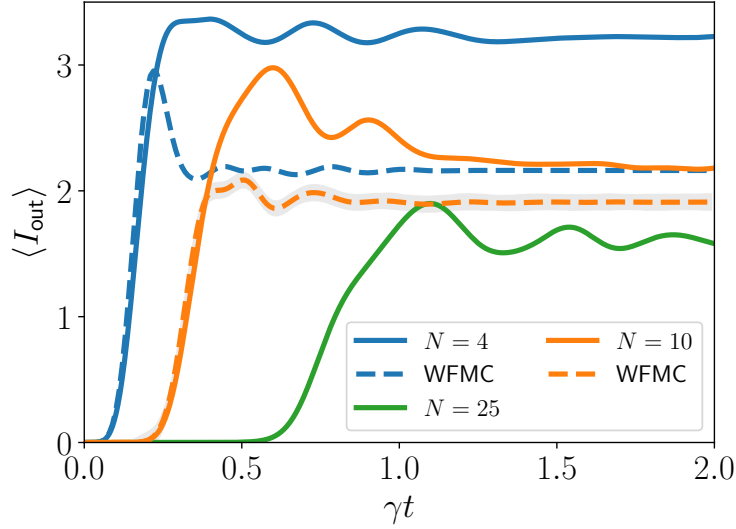


Figure 2.13.: Intensity output  $\langle I_{\text{out}} \rangle$  for different system sizes for a pump strength of  $P = 10 \gamma$ . For smaller system size ( $N = 4, 10$ ) the variational approach (solid) is compared to Monte Carlo wave function (MCWF) simulations (dashed). The shaded region shows the statistical error of the WFMC simulations for 500 trajectories.

times. This is visible in Fig. 2.13 for the  $N = 4$  where the variational solution is larger than the expected one from WFMC. The difference decreases substantially for  $N = 10$  with the remaining difference being caused by short-range correlation between the ends. The product state ansatz is not well suited to capture those. On the other hand, it allows us to also investigate larger system sizes that are way out of reach for other methods. For the wave function Monte Carlo simulation one of the highest reported numbers is a system of up to 20 particles [94]. In Fig. 2.13 we already showed the intensity output for  $N = 25$  which already seems hard to achieve otherwise. After having demonstrated the viability of the variational approach, we now want to go one step further in the system size.

Fig. 2.15 displays the dynamics of the polariton population on each site for a lattice size of  $N = 40$ . We observe that a significant portion of the polariton density remains confined to the initial pump site, with the rest of the population spreading throughout the system similar to a light cone, which is a consequence of the linear dispersion relation. We see an oscillation pattern that also appears if we look at the scaling of the error between the Monte Carlo simulation and the variational solution in Fig. 2.14. The repeating pattern comes from the hard-sphere blockade, where we used the Rydberg blockade radius of  $\approx 5$  sites.

We can get a better understanding of the blockade effect onto our system by looking

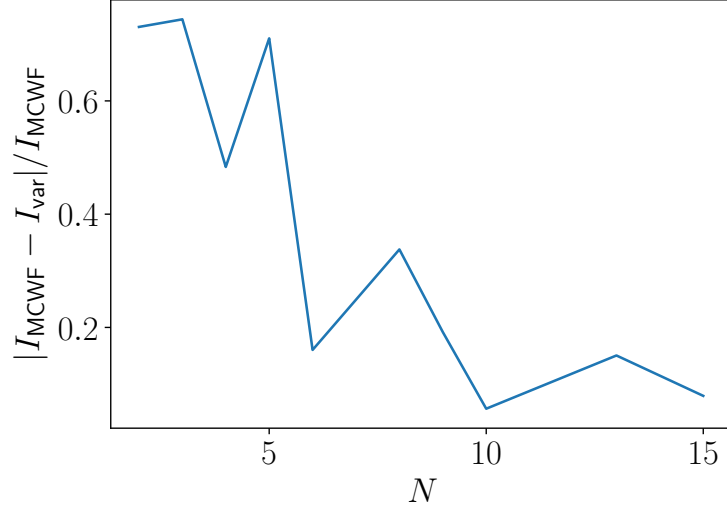


Figure 2.14.: Scaling of the difference between the variational and the Monte-Carlo wave function (MCWF) solution with system size  $N$ . Overall, we see a decrease in the differences between the two methods with increased system sizes. The fluctuations arise from the fact that the constraint for the Rydberg blockade in the variational approach is not always active. That is also the reason why the methods are the closest at system sizes that are around a multiple of the Rydberg blockade radius  $r_b = 5x_0$ .

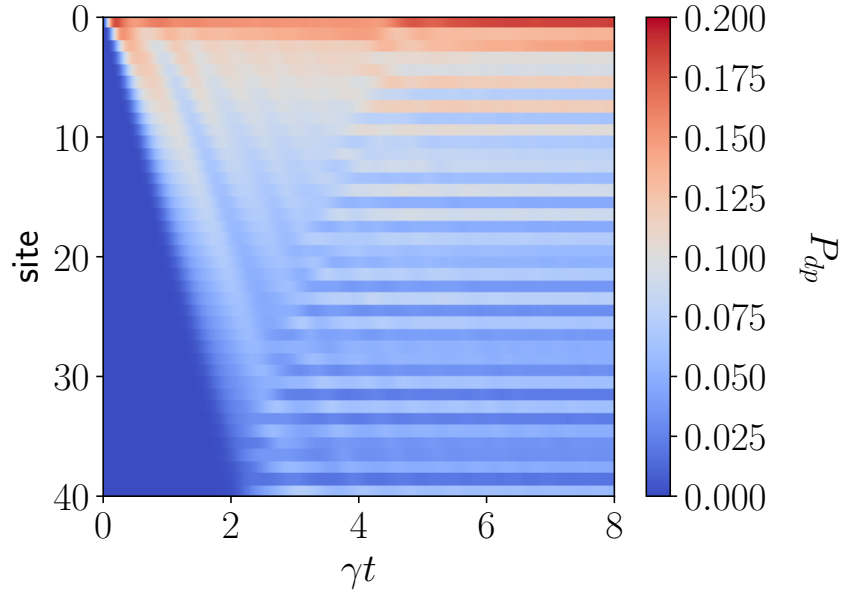


Figure 2.15.: Time evolution of the polariton population  $P_{dp}^{(i)} = \langle \sigma_+^{(i)} \sigma_-^{(i)} \rangle$  of each site  $i$  in a lattice of size  $N = 40$  for a pumping strength of  $P = 10\gamma$ .

## 2. Quantum many-body dynamics of driven-dissipative Rydberg polaritons

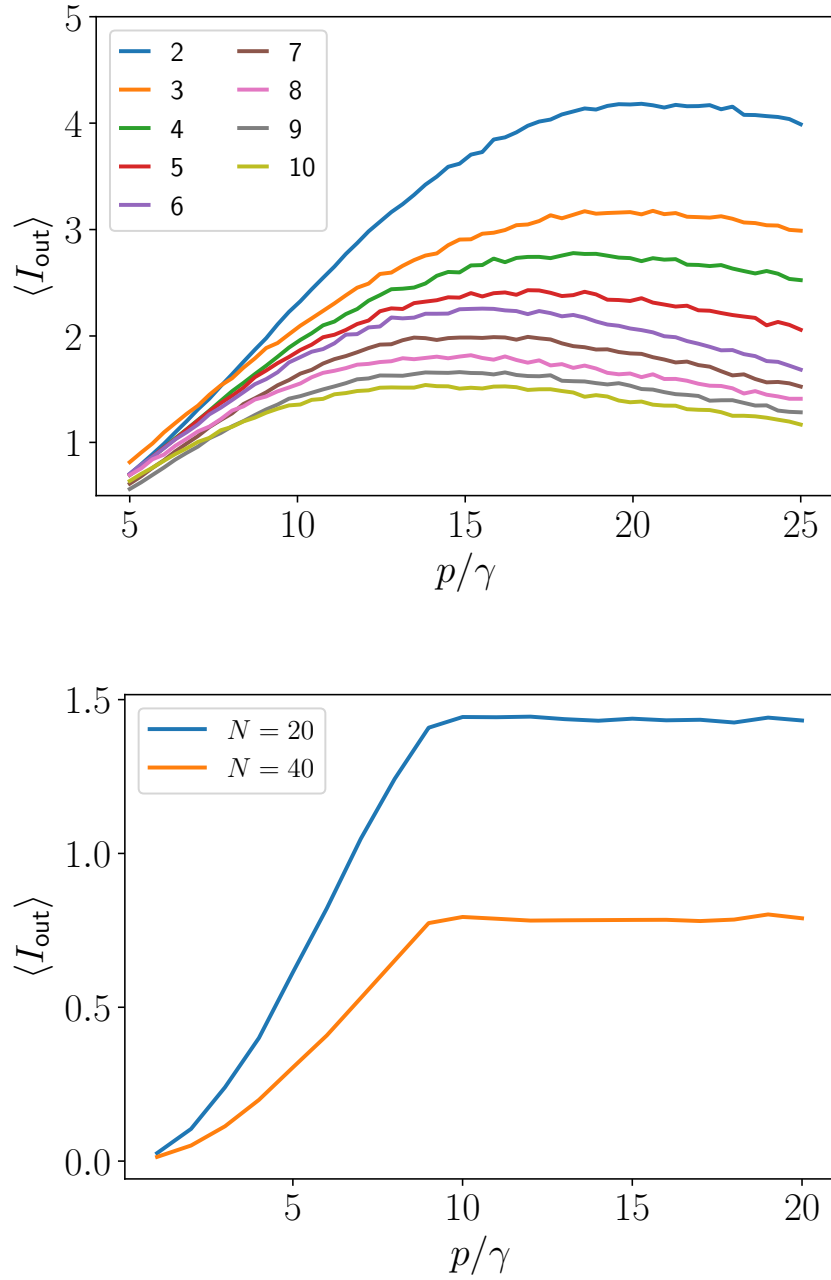


Figure 2.16.: The upper plot shows the scaling of the intensity output  $\langle I_{\text{out}} \rangle$  with the pumping strength for system sizes up to  $N = 10$ . The curves are getting flatter with larger system sizes. The lower plot then shows the same but for system sizes  $N = 20$  and  $N = 40$ . Above a pumping strength of  $p \approx 9.5$  the curve does not change significantly. The reason are the blockade phenomenon and that the system reaches an optical depth of 1 for system sizes above  $2r_b$  which means that no further photon can be absorbed.

at the scaling of the intensity output  $\langle I_{\text{out}} \rangle$  for different pumping strength and system sizes. Fig. 2.16 shows the scaling for different system sizes and especially for large system sizes ( $N = 20, 40$ ) leads the blockade phenomenon to a limitation of the possible output of the system and further increase of the pumping strength shows no further impact. This is also shown by the comparison of the time evolutions of system sizes  $N = 6$  and  $N = 40$  for two different pumping strengths  $P = 10$  and  $P = 15$  in Fig. 2.17. For  $N = 40$  is the steady state the same and we can only observe small difference in the time evolution towards the steady state whereas  $N = 6$  a substantial difference between the two pumping strengths shows.

Before we move on to the temporal correlations in the system, we want to utilize the time evolution of the chosen variational method more by changing from a continuous pump to a pulse. The result in Fig. 2.18 shows the evolution of multiple sites with  $N = 40$  sites. In addition to the effects, we observed for the continuous pumping, we see another interesting phenomenon in the shape of the polariton pulse that moves through the lattice. The pulse broadens slightly during the time evolution whereas the free-space polaritons form a form-stable solution of the corresponding wave equation [95]. This also comes from the Rydberg blockade because the limitation of only one possible Rydberg excitation in the Rydberg radius around an excited site causes a necessary delay in the transport to fulfil this constraint. Another detail we can see through the pumping pulse is a small backpropagation of polaritons visible by smaller oscillations after the main pulse. The fact that forward and backwards propagating probe fields couple to the same intermediate level and the resulting Bose-Hubbard-like Hamiltonian already implied that but was not clearly visible in the search for the steady state of the system.

## 2. Quantum many-body dynamics of driven-dissipative Rydberg polaritons

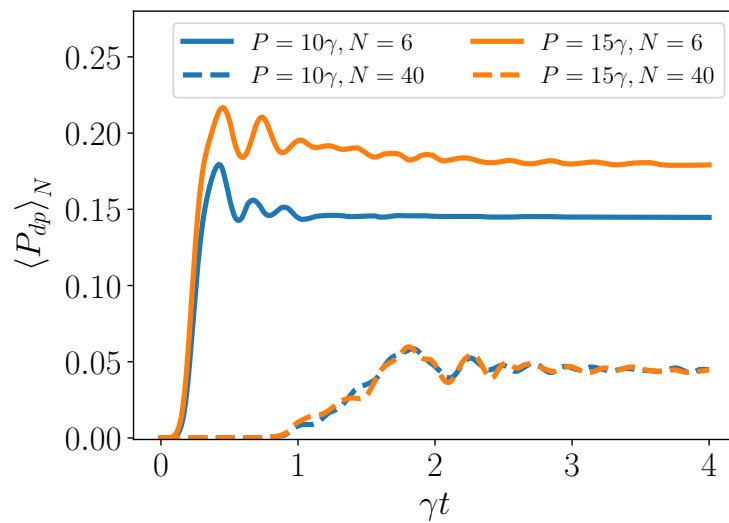


Figure 2.17.: Difference between pumping strengths  $P = 10\gamma$  and  $P = 15\gamma$  for system sizes  $N = 6, 40$ . The difference between the pumping strengths for the smaller system size vanishes almost completely for  $N = 40$  because the blockade mechanism creates a bottle neck for the polariton population in the system.



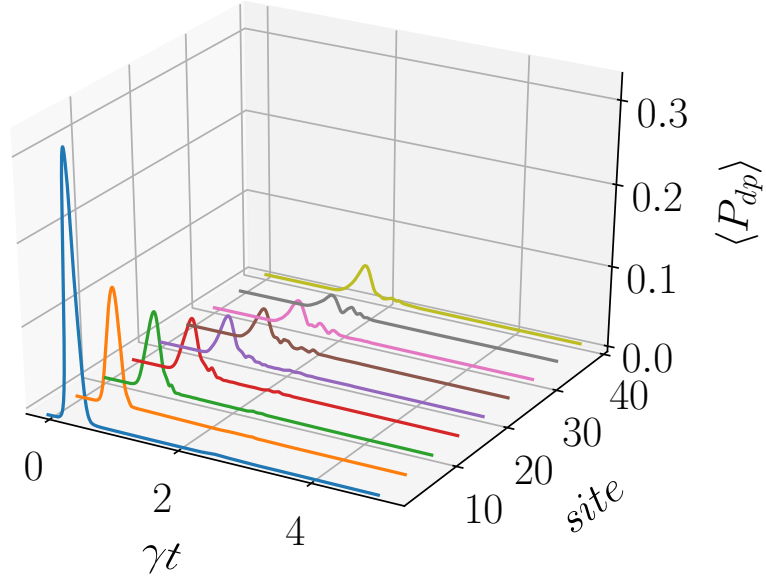


Figure 2.18.: Time evolution of  $\langle P_{dp} \rangle$  of every fifth site out of  $N = 40$  with a Gaussian pump pulse on the first site with a peak of  $P = 15\gamma$  and a standard deviation of  $\sigma = 0.1$ . The drop-off after the first site is a consequence of the hard-sphere blockade. It also slightly alters the form of the pulse on the first site (see Fig. 2.19). Later sites show the back propagation of the pulse through the lattice but because of the size of the system it does not have any impact on the output.

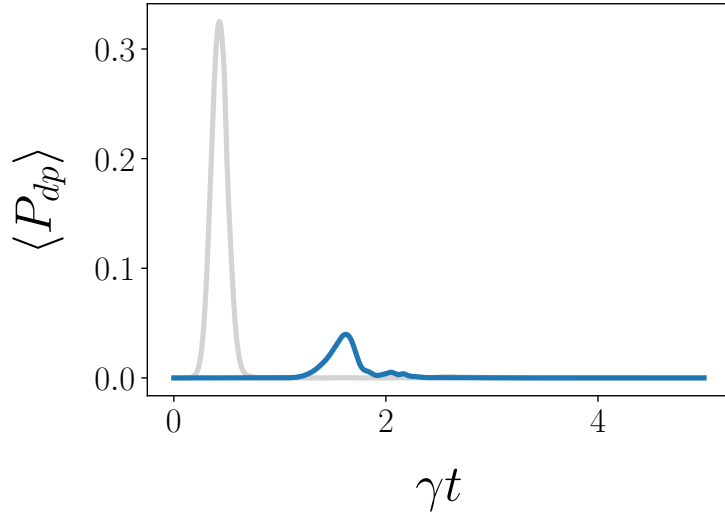


Figure 2.19.: Probability to find a dark-state polariton  $\langle P_{dp} \rangle$  on the first (grey) and last site (blue) of a lattice with size  $N = 40$  if it is getting pumped by a Gaussian pulse with a peak of  $P = 15\gamma$  and a standard deviation of  $\sigma = 0.1$ . After the travel trough the lattice, the last site shows a clear distortion from the original Gaussian shape which comes from the hard-sphere blockade and the fact that our level scheme allows for back and forward propagation in the lattice.

### 2.2.1. Temporal correlations

Finally, we also want to look at the temporal correlations in the output intensity. To obtain the temporal function, we let the system evolve until it reaches a steady state at time  $t_{ss}$ . At this time, we consider the effect of a quantum jump corresponding to measuring a photon at the detector, after which we let the system evolve for an additional time  $\tau$ . Then, the probability to observe a second photon is described by the two-time intensity-intensity correlation function

$$g^{(2)}(\tau) \propto \langle \hat{O}_1(t_1) \hat{O}_2^+(t_2) \hat{O}_3(t_1) \rangle \quad (2.23)$$

$$= \langle \sigma_N^+(t_1) \sigma_N^+(t_2) \sigma_N^-(t_2) \sigma_N^-(t_1) \rangle \quad (2.24)$$

with  $\hat{O}_1 = \sigma_N^+$ ,  $\hat{O}_2 = \sigma_N^+ \sigma_N^-$ ,  $\hat{O}_3 = \sigma_N^-$  and  $t_2 > t_1 > 0$ . The subscript  $N$  of the operators denotes their acting on the last site of the lattice. The *quantum regression theorem* allows us to reduce this problem to the calculation of a single-time correlation function [96, 97, 49]. The theorem relied originally on the Markov approximation which we introduced in the derivation of the quantum master equation in Sec. 1.1.1. If we neglect any memory effects of the environment, we also assume that noise operators are uncorrelated with system observables that are measured at earlier times. With the theorem in play we can calculate (2.24) by

$$\langle \hat{O}_1(t_1) \hat{O}_2^+(t_2) \hat{O}_3(t_1) \rangle = \text{Tr} \left\{ \hat{O}_2 e^{\mathcal{L}\tau} [\hat{O}_3 \rho(t) \hat{O}_1] \right\}. \quad (2.25)$$

For a similar situation as in experiments we are interested in the dynamics after the system reached a steady state by the time  $t_{ss}$ . The linearity and trace preserving properties of the master equation also imply that the function will go back to the steady state. Therefore, we use the normalization that is often used in the field of quantum optics by normalizing the correlation function by the steady state mean values  $\langle \hat{O}_2 \rangle_{SS} \langle \hat{O}_1 \hat{O}_3 \rangle_{SS}$ . Finally, we obtain for our system the correlation function

$$\begin{aligned} g^{(2)}(\tau) &= \frac{\langle \sigma_N^+(t_{ss}) \sigma_N^+(t_{ss} + \tau) \sigma_N^-(t_{ss} + \tau) \sigma_N^-(t_{ss}) \rangle}{\langle \sigma_N^+ \sigma_N^- \rangle_{t_{ss}}^2} \\ &= \frac{1}{\langle \sigma_N^+ \sigma_N^- \rangle_{ss}^2} \text{Tr} \left\{ \sigma_N^- e^{\mathcal{L}\tau} \left[ \sigma_N^- \rho(t_{ss}) \sigma_N^+ \right] \sigma_N^+ \right\}, \end{aligned} \quad (2.26)$$

where we have used the cyclicity of the trace [98]. The quantum jump from the first measurement also affects the other sites because of the long-range Rydberg-Rydberg interactions. In our hard-sphere model, we use a self-consistent approach to identify the affected sites by adding the excitation probabilities of the sites beginning from

site  $N - 1$  until  $\sum_{i=N-1} \langle \sigma_i^+ \sigma_i^- \rangle = 1$ . To see the effect of the interaction on the other sites in terms of the product states we use for the density matrix, we calculate the full density matrix for smaller system sizes and only look at the partial trace for one of the affected sites. We observe that they are also set back to the ground state when measuring a photon leaving the system which is expected because this corresponds to the blockade phenomena associated with the strong interactions in our system. The blockaded region defined in that way is for smaller system sizes identical to our previous definition of the blockade radius. For larger system sizes, the radius is slightly extended because the self-consistent method to determine the blockade radius also includes the decay from the Rydberg state which we could not include in the hard sphere approximation.

We can use the correlation function to determine how long it takes for the system to emit a second photon after the first one and also when the system is back in the steady state. If  $g^{(2)}(\tau) \approx 0$  we get photon antibunching because the system will not emit a second photon in this time. This is also what we are looking for if we want to use the polariton lattice system to mediate Rydberg-Rydberg correlation onto the photons. On the other hand, if  $g^{(2)}(\tau) \geq 1$  it is called bunching because there is an increased probability that the system emits a second photon in comparison to the steady state. Fig. 2.20 illustrates the differences between bunched, coherent and anti-bunched light.

Fig. 2.21 shows an extended anti-bunched region  $g^{(2)}(\tau) \approx 0$  resulting from the blockade, we discussed previously. Furthermore, we also observe bunching before the system recovers its steady state  $g^{(2)}(\tau) = 1$ . The oscillations depend on the lifetime of the polaritons but also on the internal dynamics of the system given by the Hamiltonian. Our chosen product state ansatz is often accompanied by longer oscillation patterns in comparison to calculations with the full density matrix. We already saw this in the time evolution of our system in Fig. 2.13 between our solution and the Monte-Carlo simulations. The same effect results in long relaxation times in the temporal correlation function.

Even though we also observe bunching in the Monte-Carlo simulation, it is unclear if the scaling of the strength and duration of the bunching with system size is correct or also a consequence of the product states. These findings underline the possibility of using Rydberg polariton systems to generate strongly correlated photon streams, similar to some free-space systems [99].

2. Quantum many-body dynamics of driven-dissipative Rydberg polaritons

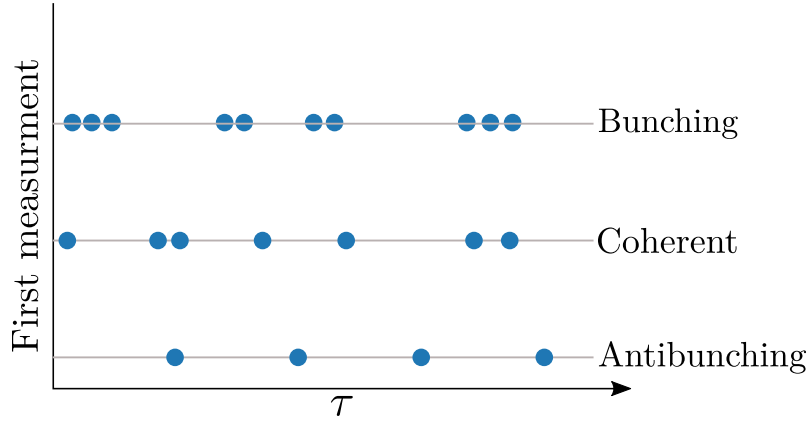


Figure 2.20.: Difference of the structure in emitted photons. Each circle indicates the emission of a photon from the system. Bunched light has multiple photons leaving the system together. Coherent light sources emit photons independently from each other. Antibunching is a quantum mechanical effect that forbids the emission of a another photon for some time.

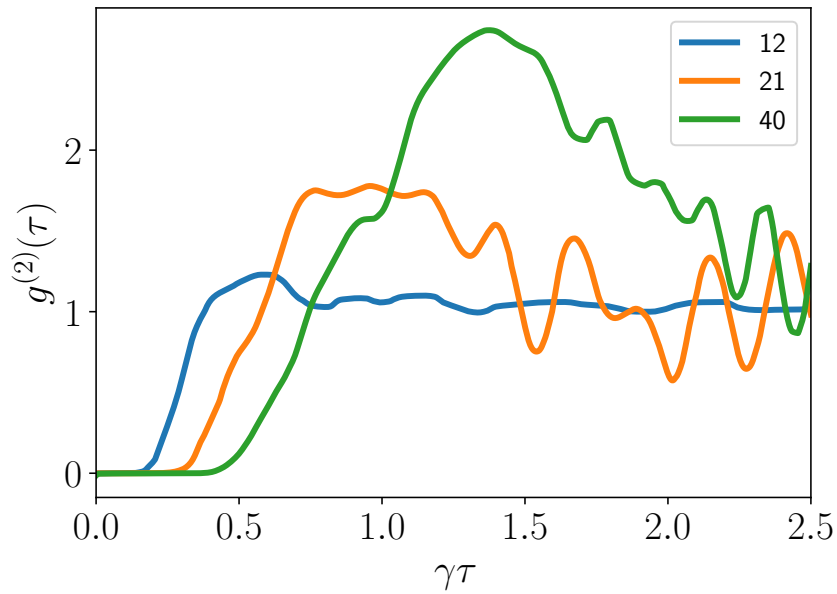


Figure 2.21.: Two time correlation function  $g^{(2)}(\tau)$  of the output signal from the last site of the lattice for different system sizes  $N$ .

### 3. The variational method for bosonic fields

The previous chapter revealed the complexity one faces in many-body systems. We used various techniques to reduce the dimensionality of the Hilbert space of the system and thereby brought the computational effort to a manageable level. In this chapter, we want to discuss how we can treat an infinite Hilbert space or more specific bosonic fields with light as the most important example. They can be used to describe spin-0 and spin-1 particles but also gauge and scalar fields. The description of such fields is a difficult task because there is no natural limitation in the Hilbert space dimension describing these fields. This is especially a problem in an open quantum system where the particle number is not fixed but can be changed through incoherent processes like pumping or dissipation.

Here, we use the phase-space representation of the density matrix to formulate a variational approach for the Fokker-Planck equation and the generalised Ehrenfest equations. The convolution theory of P-distribution will help us to cover a wide range of possible quantum states with our density matrix. We also give an overview of how different state distributions interact with each other.

We then test the method with the Jaynes-Cummings model [100]. The model consists of an atom interacting with a light field trapped inside a cavity and therefore forms one of the simplest systems to investigate atom-light interaction. The light mode will be represented by a density matrix in its P-representation. The mean-field treatment of this model has an area of bistability, which we will also investigate with the new approach and compare it with the Monte-Carlo simulation of the full model. We also use the P-distribution to examine the model for nonclassicality.

At last, we will look at another model that focuses around Rydberg atoms in a cavity. A polariton picture for the model is established and then analysed by the variational approach. To cover the strong correlations between the different modes in this model, we expand our method by introducing correlation functions as variational parameters. We then look at the intensity and the squeezing of the different modes and see how they scale with increased cavity pumping. The necessity of the

### 3. The variational method for bosonic fields

additional parameters in the form of the correlation function will be made clear and also how this variational approach can easily handle large particle numbers in the system.

We end this chapter by giving an outlook on which states are possible candidates to further expand this method and possible advantages of adapting the method to other phase-space representations than the P-distribution.

## 3.1. P-representation of the density matrix in the variational approach

Finding the right representation of the density matrix is a cornerstone of the variational approach. Previously, we used product states in combination with generalized Pauli matrices to construct a Hilbert space of multiple two- or three-level particles. Here, we make use of the phase-space representation of the density matrix which we introduced in 1.3.

We focus our attention on the P-representation by Glauber and Sudarshan [47, 48] but it should be noted that the general concept can be transferred to the other phase-space representations as well because they are connected via the characteristic function  $\chi$ , as we mention in Section 1.3. The convenience of our particular choice will be seen later.

At first, we need to discuss how we can expand the P-representation to also represent superpositions of multiple independent fields that are still emitting into the same mode. The construction of the corresponding P-distribution is done by a convolution

$$P(\alpha) = (P_i * P_j)(\alpha) = \int d\alpha d\alpha' P_i(\alpha') P_j(\alpha - \alpha') \quad (3.1)$$

of the original distributions  $P_i$  and  $P_j$  [101] If we insert (3.1) into (1.67) we obtain

$$\langle a^\dagger{}^p a^q \rangle = \sum_n^p \sum_m^q \xi_{p,q} \langle (a^\dagger)^n a^m \rangle_{P_i} \langle (a^\dagger)^{p-n} a^{q-m} \rangle_{P_j} \quad (3.2)$$

as a formula to calculate expectation values of a convoluted P-distribution with  $\xi_{n,m}$  as the number of possible combinations of the given expectation values from  $\langle a^\dagger{}^p a^q \rangle$ . If we assume one distribution is the one for a thermal state we regain the same result as in [102]. We see that the calculation depends on all expectation values up to the orders  $p, q$  of  $a, a^\dagger$  of the original expectation value but are calculated for the single P-distributions  $P_i$  and  $P_j$ . This process can then be repeated multiple times

### 3.1. P-representation of the density matrix in the variational approach

to combine multiple distributions.

Table 3.1 shows different convolutions  $P_1 * P_2$  between coherent, squeezed, thermal and Fock states to give a better understanding of the concept. Whereas the convolution between a coherent state  $\alpha_1 = i$  and a second coherent state  $\alpha_2 = 1$  results in another coherent state with  $\alpha = \alpha_1 + \alpha_2$ , leads the convolution with a thermal state to a broadening of  $P_2$  and can even destroy important aspects of the distribution, for example, the negativity in the Fock states. Especially the convolutions between  $P_{\text{Fock}}$  and  $P_{\text{squeezed}}$  result in interesting states that we would not be able to obtain without the convolution. One should further note, that we restricted ourselves to the convolutions of only two P-distributions as an overview but in our final variational approach we will have a convolution of multiple P-distributions which allows for even more possible combinations.

Now we have everything we need to combine the concepts of the variational principle and the P-distribution. There are two possible ways that we can take to derive a variational norm. Both are shown in the overview in Fig. 3.1.

Let us explore the upper approach first, which is in closer relation to our approach in the previous chapter. Our starting point is again the Lindblad master equation  $\frac{\partial}{\partial t}\rho = \mathcal{L}\rho$ . Here, we can directly insert the P-distribution  $P(\alpha)$  into Eq. (1.15). The action of the operators on  $|\alpha\rangle\langle\alpha|$  can now be transformed to  $\alpha$  and  $\alpha^*$  and the partial derivatives of these variables. After the transformation we often end up with a Fokker-Planck equation which originally described Brownian motion with classical probability distributions [103, 49]. The equation we end up with is of the form

$$\frac{\partial}{\partial t}P(\alpha) = \left[ \frac{\partial}{\partial\alpha}f(\alpha, \alpha^*) + \frac{\partial}{\partial\alpha^*}g(\alpha) + \frac{\partial^2}{\partial\alpha\partial\alpha^*}h(\alpha) \right] P(\alpha). \quad (3.3)$$

An example in the form of the damped harmonic oscillator is given in Appendix B. A more general form of 3.3 would be the Kolmogorov equation which can include higher-order derivatives in  $\alpha, \alpha^*$  but the Fokker-Planck equation is enough for our purpose. We can use Eq. (3.3) in a similar fashion in the variational approach as the master equation. We would need to find a test distribution  $P^{\text{var}}(\alpha)$  insert it in Eq. (3.3) and minimize an appropriate norm of the resulting equation which in this case would be Euclidean norm for complex numbers.

This approach leads to two major problems which ultimately makes this approach not feasible for most relevant problems. The first problem is the necessity to have an explicit expression of  $P(\alpha)$ . The variational test distribution needs to be as general as possible to be able to find an optimal solution through minimization. Generic functions for  $P(\alpha)$ , e.g. a sum of Gaussian functions, do not lead to a

### 3. The variational method for bosonic fields

valid density matrix. That is why we introduced the concept of convoluted P-distributions, but their exact calculations can be hard, especially if we want to include nonclassical states. This leads us to the second problem with Fokker-Planck approach: The equation makes it necessary to calculate different orders of derivatives of  $P(\alpha)$  in combination with the functions  $f, g$  and  $h$ . For many nonclassical states are the P-distribution highly singular which includes derivatives of the complex delta distribution  $\delta^{(2)}(\alpha)$  with  $\alpha = x + iy$ . To use these in the variational context, we would need to approximate the distribution by classical functions and even that does not guarantee that we can calculate the full derivative. Therefore, we take the other path in Fig. 3.1 and move into the Heisenberg picture of the master equation.

Here, we already saw that the equations of motion created by Eq. (1.25) for the expectation value  $\hat{A}$  depends only on expectation values like

$$\frac{d}{dt} \langle \hat{A} \rangle (t) = F(\{\langle a^{\dagger p} a^q \rangle\}_{p,q}). \quad (3.4)$$

We can formulate a variational norm for the equations of motion as

$$\sum_n \left| \frac{d}{dt} \langle \hat{A} \rangle_n^{\text{var}} (t) \right| = \sum_n |\mathcal{L}(\langle \hat{A} \rangle_n^{\text{var}})| \rightarrow \min \quad (3.5)$$

with  $\langle \hat{A} \rangle_n^{\text{var}}$  being the n-th variational expectation value  $\text{Tr} \{ \rho_{\text{var}} \hat{A} \} = \langle \hat{A} \rangle^{\text{var}}$ . If  $n \rightarrow \infty$ , the norm in Eq. (3.5) is equivalent to  $\|\dot{\rho}\|$  and a finite number of expectation values corresponds to an upper bound for the density matrix norm. If we insert (3.4) into (3.5) we obtain

$$D = \sum_i |F_i(\{\langle a^{\dagger p} a^q \rangle_{p,q}\})| \rightarrow \min. \quad (3.6)$$

with  $F_i$  describing the right hand side of Eq. (1.25) which depends on the set of expectation values  $\{\langle a^{\dagger p} a^q \rangle\}_{p,q}$ . Instead of using the expectation values as our variational parameters to reduce the equation, we want to use the previously introduced P-representation. To understand how it can be used, we first need to look at some P-functions of commonly known states. For the thermal state we obtain

$$P(\alpha) = \frac{1}{\pi n_0} e^{-|\alpha|^2/n_0} \quad (3.7)$$

with the average photon numbers  $n_0 = \langle n \rangle$ . The coherent state density matrix



### 3.1. P-representation of the density matrix in the variational approach

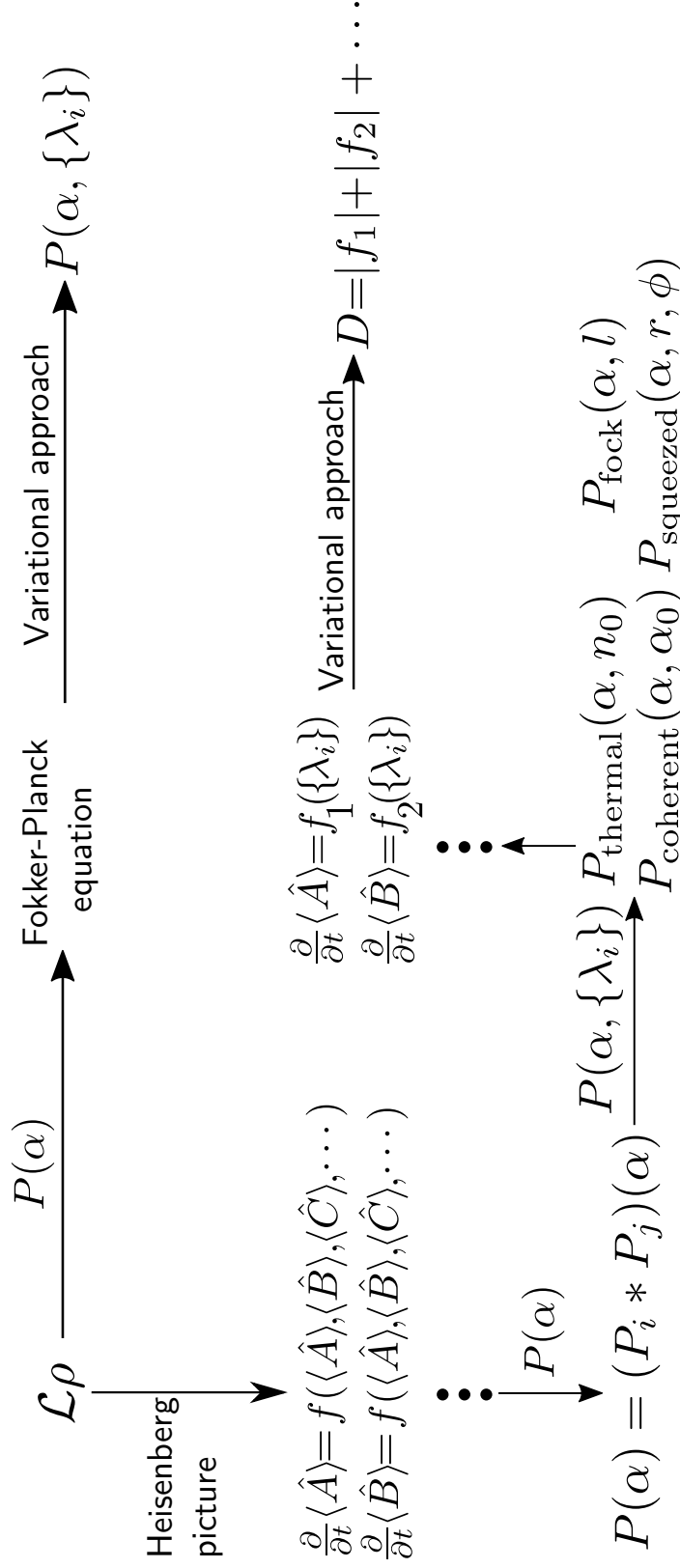


Figure 3.1.: Scheme on how to implement the P-representation into the variational method. Directly putting it in the Lindblad master equation results in a Fokker-Planck equation which allows us to formulate a classical analogon to the variational approach for the density matrix. Another way transforms the master equation into the Heisenberg picture and formulates a different variational norm based on the expectation values of the system.

### 3. The variational method for bosonic fields

$\rho = |\alpha_0\rangle \langle \alpha_0|$  can be expressed as

$$P(\alpha) = \delta^{(2)}(\alpha - \alpha_0) = \delta(x - x_0)\delta(y - y_0). \quad (3.8)$$

with the complex delta distribution  $\delta^{(2)}(\alpha)$  and the complex numbers  $\alpha = x + iy$  and  $\alpha_0 = x_0 + iy_0$ . As previously discussed, other nonclassical states are even more singular than  $\delta^{(2)}(\alpha)$  which referred to derivatives of that function. The Fock state is given by

$$P_{\text{fock}} = \frac{1}{l!} e^{|\alpha|^2} \frac{\partial^{2l}}{\partial \alpha^l \partial \alpha^{*l}} \delta^{(2)}(\alpha) \quad (3.9)$$

and the vacuum squeezed state by [104]

$$P(\alpha) = \exp \left[ -\frac{\delta_x^2 - \delta_p^2}{8} \left( \frac{\partial^2}{\partial \alpha^2} + \frac{\partial^2}{\partial \alpha^{*2}} - 2 \frac{\delta_x^2 - \delta_p^2 - 2}{\delta_x^2 - \delta_p^2} \frac{\partial}{\partial \alpha} \frac{\partial}{\partial \alpha^*} \right) \right] \delta(\alpha). \quad (3.10)$$

We can also look at a convoluted P-distribution. The convolution of coherent and thermal state can be done quite easily and yields

$$P(\alpha) = \frac{1}{\pi \langle n \rangle} e^{-\frac{|\alpha - \alpha_0|^2}{\langle n \rangle}} \quad (3.11)$$

We can obtain the two original distributions for the edge cases  $\langle n \rangle \rightarrow 0$  and  $\alpha_0 \rightarrow 0$ .

We can immediately see that each of these distributions has at least one defining parameter like  $\alpha_0 \in \mathbb{C}$ ,  $n_0 \in \mathbb{R}$  or  $l \in \mathbb{N}$ . The convoluted distributions depend on the set of the parameters of the original distributions like  $\{\beta\} = \alpha_0, n_0$ .

This allows us to formulate Eq. (3.6) as

$$D = \sum_i |F_i(\{\beta\})| \rightarrow \min \quad (3.12)$$

In consideration of Eq. (3.2) we can also see that we do not need to know the complete form of the P-distribution that corresponds to a specific state. Instead, it is enough to know how all expectation values depend on the state-specific parameters.

### 3.1. $P$ -representation of the density matrix in the variational approach

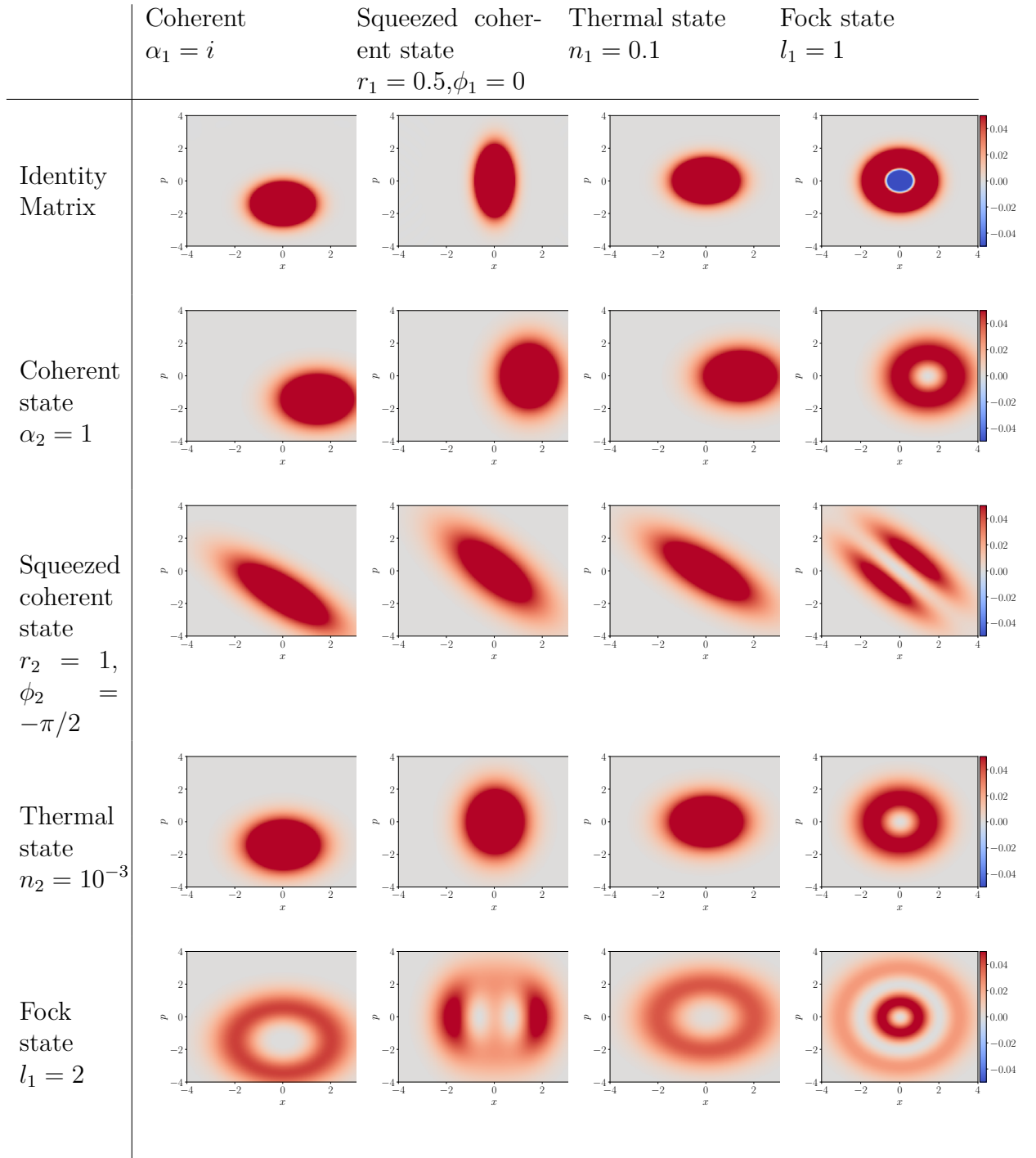


Table 3.1.: Convoluted Wigner functions of the coherent, squeezed coherent, thermal and Fock state with different parameters.

## 3.2. Jaynes-Cummings Model

We now want to look at the Jaynes-Cummings model [100] to see how our method performs in comparison to a Monte-Carlo simulation which we will do with the QuTIP module in Python [89, 90]. The Jaynes-Cummings model describes an atom interacting with a light field that is trapped inside a cavity, see Fig. 3.2. The Hamiltonian reads as

$$H = \Delta_c a^\dagger a + \Delta_a \sigma^+ \sigma^- + g(a\sigma^+ + a^\dagger \sigma^-) + p(a^\dagger + a). \quad (3.13)$$

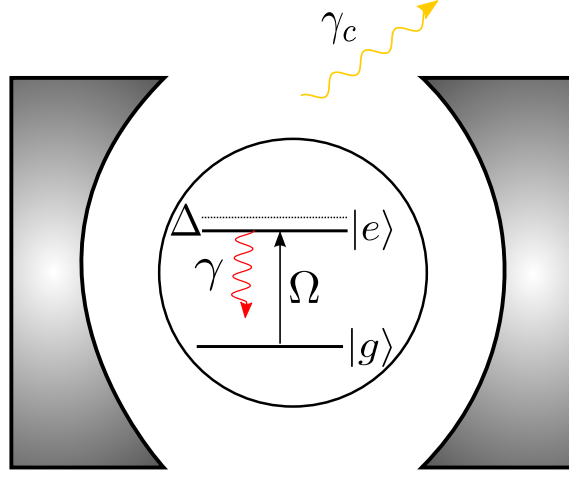


Figure 3.2.: Scheme of the open Jaynes-Cummings model with dissipative processes. An two level-system with Rabi-frequency  $\Omega$ , a detuning from the cavity light mode  $\Delta$  and decay rate  $\gamma$  is trapped inside a cavity which also has a decay rate of  $\gamma_c$ .

The first two terms describe the detunings  $\Delta_c$ ,  $\Delta_a$  for the cavity and the atom respectively. The atom and the cavity are coupled with a strength of  $g$  and the driving amplitude which corresponds to the driving strength  $p$ . Additionally, we include dissipation from the cavity to account for any imperfections and add a second dissipation channel for the atoms that accounts for any photon emission that does not go back into the cavity mode through the second part of Eq. (1.19) via jumping operators  $c_c = \sqrt{\gamma_c}a$  and  $c_a = \sqrt{\gamma}\sigma^-$  with decay rate  $\gamma_c$  for the cavity and  $\gamma$  for the atom.

We use a product ansatz for the atom and the cavity

$$\rho = \rho_{\text{cavity}} \otimes \rho_{\text{atom}} \quad (3.14)$$

### 3.2. Jaynes-Cummings Model

in the variational approach and use the variational parameter  $\alpha_i$  in  $\sum_{i=0,x,y,z} \alpha_i \sigma_i$  to describe the atomic part and for the cavity we use the P-representation. As our variational parameter set we use a convolution of coherent, thermal, Fock and squeezed states. To show an imminent advantage of the variational approach, we also want to analyse the Maxwell-Bloch equations of the Jaynes-Cummings model [105, 106]. This set of equations describes the time evolution of the lowest order of expectation values. The atom and cavity decouples in a similar fashion like in Eq. 3.14 but it also decouples the equation from higher order terms of the cavity field through the neglect of any correlation terms of the second or higher order [107]. The Maxwell-Bloch equation for the Jaynes-Cummings model then reads as

$$\frac{d}{dt} \langle a \rangle = -(\kappa + i\delta_c) \langle a \rangle - ig \langle \sigma^- \rangle - ip \quad (3.15)$$

$$\frac{d}{dt} \langle \sigma^- \rangle = -\left(\frac{\gamma}{2} - i\Delta_a\right) \langle \sigma^- \rangle + ig \langle a \rangle \langle \sigma^z \rangle \quad (3.16)$$

$$\frac{d}{dt} \langle \sigma^z \rangle = -\gamma(\langle \sigma^z \rangle + 1) + 2ig(\langle a^\dagger \rangle \langle \sigma^- \rangle - \langle a \rangle \langle \sigma^+ \rangle) \quad (3.17)$$

Fig. 3.3 shows a comparison between the solution of the Maxwell-Bloch equations, the Monte-Carlo wave function solution and the variational approach for the expectation value of the cavity field  $\langle a^\dagger a \rangle$ . The mean-field solution (orange) shows a large area of bistability between two solutions of Eq. (3.17). A variational treatment on the same level solves the problem by a clear transition between the solutions at the grey line. In comparison to the Monte-Carlo simulation is the point at which the transition appears still not correct. The third line (blue) now indicates the solution if we go one order higher in the equations of motion in the variational approach and the comparison clearly shows a strong improvement in a qualitative sense. Fig. 3.4 shows a reconstructed P-distribution from the variational expectation values through the usage of the characteristic function

$$\chi(z) = \sum_{k,l=0}^{\infty} \frac{z^k}{k!} \frac{(-z^*)^l}{l!} \langle a^{\dagger k} a^l \rangle \quad (3.18)$$

and

$$P(\alpha, \alpha^*) = \frac{1}{\pi^2} \int_{-\infty}^{\infty} d^2 z \chi(z) e^{-iz^* \alpha^\dagger} e^{-iza}. \quad (3.19)$$

The result is comparable to the solution through Monte-Carlo simulation and confirms an agreement between the methods to higher orders even though we only used a very limited amount of convoluted P-distributions. It also shows the non-

### 3. The variational method for bosonic fields

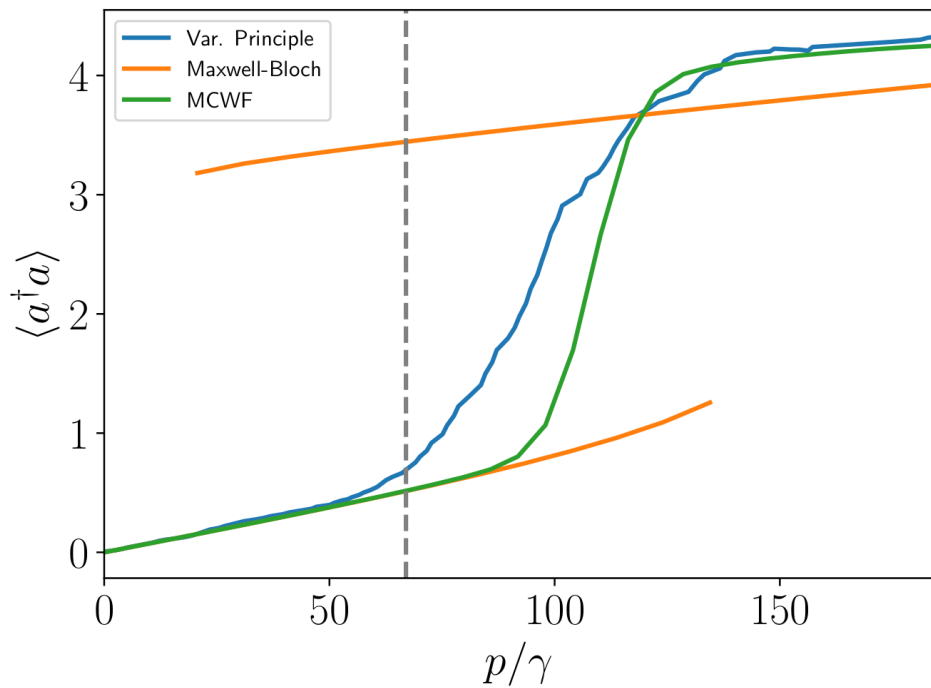


Figure 3.3.: Results of the Maxwell-Bloch equations, the variational approach and the Monte-Carlo wavefunction method (MCWF) for the Jaynes-Cummings model with  $g = 3347\gamma$ ,  $\gamma_c = 6\gamma$ ,  $\Delta_c = 340\gamma$ ,  $\Delta_a = 23.5 \times 10^3\gamma$ . The Maxwell-Bloch equations (orange) show a region of bistability which can be solved by a variational treatment of the equations which yields a prediction for the transition between the two solution at the grey line. For higher orders of the variational approach (blue) the transition shifts towards the MCWF solution.

classicality of the steady state for the given parameters which is indicated by the negative values of  $P(\alpha)$  in Fig. 3.4 [108, 104, 109].

Before we move on, we look at the cavity intensity  $\langle a^\dagger a \rangle$  and the atom population measured by  $\langle \sigma_z \rangle$  which is depending on the detuning  $\Delta_c$ . The effect we observe in the cavity intensity  $\langle a^\dagger a \rangle$  in the upper part of Fig. 3.5 is known as Rabi splitting and only occurs if the cavity field interacts with an atom [110, 111, 112, 113, 114]. The comparison with the Monte-Carlo wave-function method shows a good agreement between the solutions again. Therefore, we want to focus on the lower part of Fig. 3.5 which shows the difference between the two methods for the atomic part of the Jaynes-Cummings model measured by  $\langle \sigma_z \rangle$ . We see a large deviation between the two solutions around  $\Delta_c = 0$ . The same figure also shows the normalized correlation between the atom and the cavity  $\frac{\langle \sigma_z a \rangle}{\langle \sigma_z \rangle \langle a \rangle}$ , which gives us a good understanding of the deviation: the variational method we applied uses a product ansatz between the atom and the cavity and even though we saw before in Fig. 3.3 that the variational method exceeds mean-field treatments, we still neglect the correlation terms between the two subsystems. In the next section, we want to look at a different model where the correlation is more important but we also provide two approaches on how to overcome this problem.

### 3. The variational method for bosonic fields

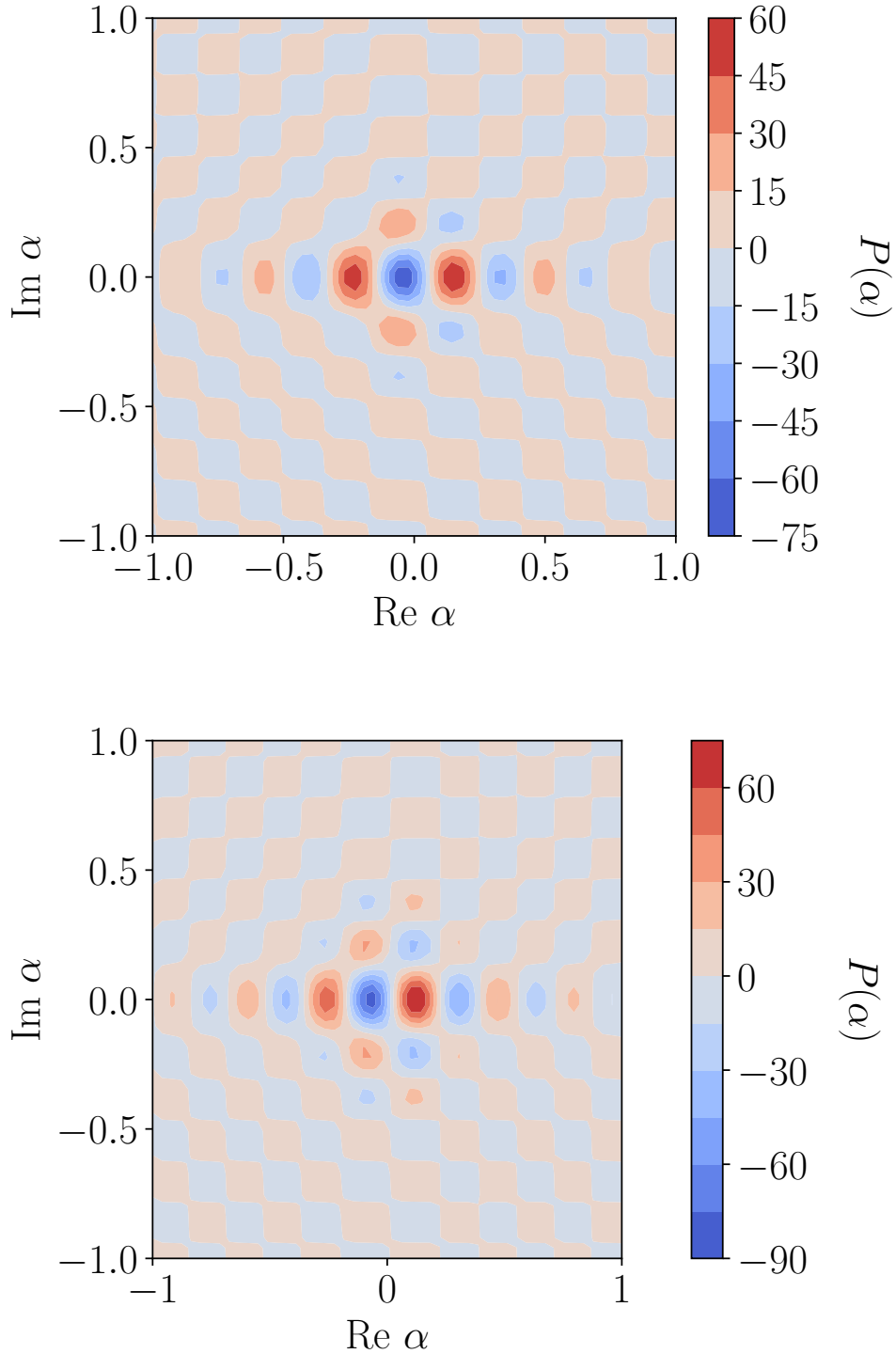


Figure 3.4.: P-distribution of the Jaynes-Cummings model for  $g/\gamma = 3347$ ,  $\kappa/\gamma = 6$ ,  $\Delta_c/\gamma = 340$ ,  $\Delta_a/\gamma = 23.5 \times 10^3$  and  $p/\gamma = 50$  calculated by the variational approach (upper) and the Monte-Carlo wavefunction method (lower). The comparison between the two shows a good agreement of the general structures of the P-distributions but also reveals small deviations in the exact values. The colormap is chosen to empathies the negative region in the P-distribution. Both plots show regions of strong negativity which indicates a non-classical behavior of the model for the given parameters.



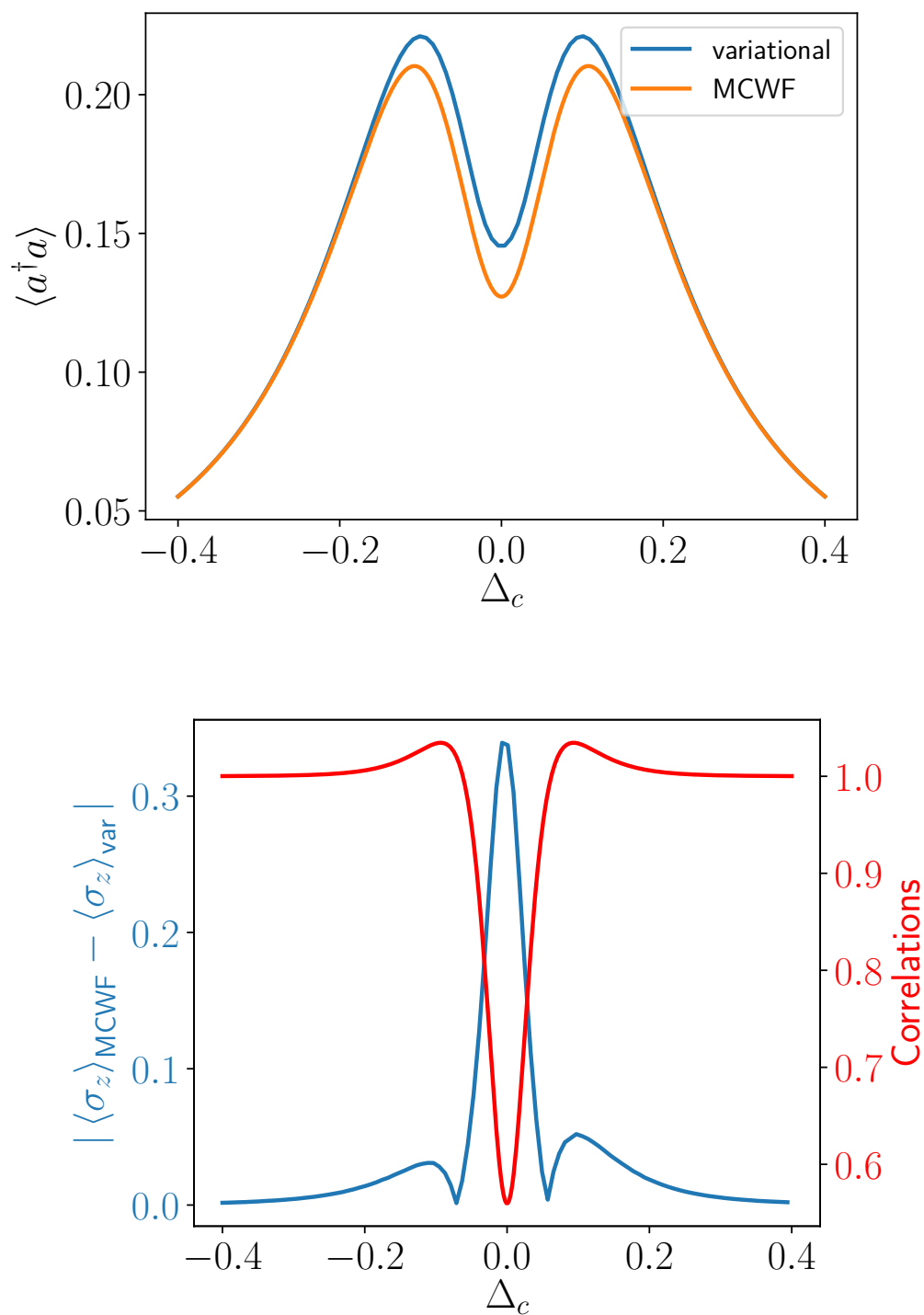


Figure 3.5.: Comparison of the cavity intensity  $\langle a^\dagger a \rangle$  (upper) and  $\langle \sigma_z \rangle$  of the atom between the variational solution and the Monte Carlo wavefunction (MCWF). Especially the lower plot show that the used product state is not capable to correctly reproduce the physics around the resonance ( $\Delta_c \approx 0$ ). This is also shown by the normalized correlation function  $\langle \sigma_z a \rangle / \langle \sigma_z \rangle \langle \sigma_a \rangle$  in the same plot which is equal to 1 for all  $\Delta_c$  in the variational approach.

### 3.3. Rydberg atoms in a cavity

We now want to have a look at the proposed effective three-boson model by *Grankin et al.* [115, 116] to describe non-linear effects that arise from the interaction of Rydberg atoms inside a cavity. At first, we want to briefly recapture the keynotes of the model. Consider a cavity filled with  $N$  three-level atoms with energy level  $g, e, r$  as the ground state  $|g\rangle$ , the intermediate state  $|e\rangle$  and a highly excited state which we denote as the Rydberg state  $|r\rangle$ . The atomic model we consider to describe Rydberg atoms inside a cavity is the same as in the previous chapter. The  $|g\rangle \leftrightarrow |r\rangle$  transition is dipole forbidden. Here, we introduce two additional parameters with the detuning of the Rydberg state  $\Delta_r = \omega_p + \omega_c - \omega_r$  (which we set to zero before) and a detuning of the cavity photon field to the probe field  $\Delta_e = \omega_p - \omega_c$ .

The system is described by a the general Hamiltonian (without the inclusion of environmental influences)

$$H_{\text{at}} = -\Delta_e \sum_{n=1}^N \sigma_{ee}^{(n)} + \sum_{m < n=1}^N \frac{C_6}{|r_m - r_n|^6} \sigma_{rr}^m \sigma_{rr}^n - \Delta_r \sum_{n=1}^N \sigma_{rr}^{(n)} + \frac{\Omega}{2} \sum_{n=1}^N (\sigma_{re}^{(n)} + \sigma_{er}^{(n)}) \quad (3.20)$$

$$H_{\text{cav}} = -\Delta_c a^\dagger a \quad (3.21)$$

where  $a(a^\dagger)$  is a bosonic field operator to destroy(create) a photon in the cavity mode and  $\sigma_{\alpha\beta} \equiv |\alpha\rangle \langle\beta|$  are operators to describe the transition from state  $\beta$  to state  $\alpha$ .

The ground state of this system consists of a collective atomic state which is symmetric in respect to permutations of the atoms. If the number of atomic excitations is small in comparison to the overall number of atoms  $N$ , we can focus our attention to the subspace of collective states with the same symmetrical behaviour [116]. We then can describe the system in terms of collective bosonic field operators describing with  $b = \frac{1}{\sqrt{N}} \sum_{n=1}^N \sigma_{ge}$  and  $c = \frac{1}{\sqrt{N}} \sum_{n=1}^N \sigma_{gr}$  as the collective operators for the atomic modes  $\sigma_{ge}$  and  $\sigma_{gr}$ . We are following the steps of [116] and rewrite our Hamiltonian with the collective operators to the following effective Hamiltonian

$$H = \Delta_c a^\dagger a - \Delta_e b^\dagger b - \Delta_r c^\dagger c + g\sqrt{N}(ab^\dagger + b^\dagger a) + \frac{\Omega}{2}(bc^\dagger + b^\dagger c) + \frac{\kappa_r}{2} c^\dagger c^\dagger c c \quad (3.22)$$

with the additional dissipation terms  $D_e = \gamma_e b$ ,  $D_r = \gamma_r c$  and  $D_{nl} = \kappa_i c c$ . The last term in the Hamiltonian  $\frac{\kappa_r}{2} c^\dagger c^\dagger c c$  expresses the dipole-dipole interaction of the Rydberg atoms but it also couples the symmetric subspace to the non-symmetric

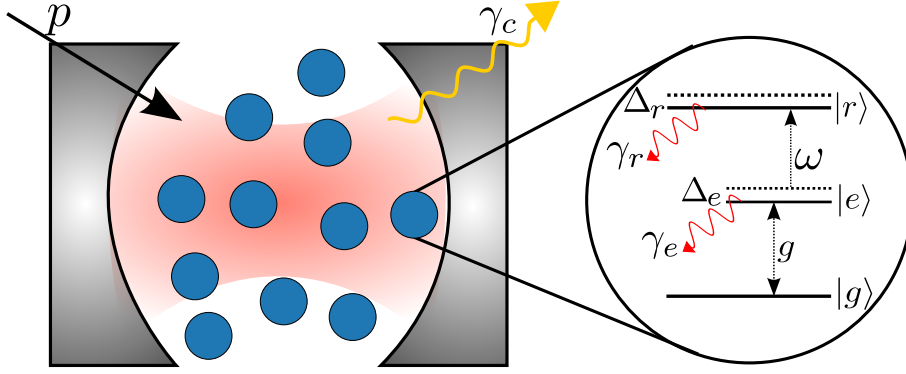


Figure 3.6.: Scheme of multiple Rydberg atoms trapped inside a cavity. The atoms are described by a three-level ladder scheme with  $g$  as the coupling constant between the cavity light field and the transition between the ground state  $|g\rangle$  and the intermediate state  $|e\rangle$ . A control laser then couples the intermediate to the Rydberg state  $|r\rangle$  with a strength of  $\omega$ . The one- and two-photon detunings of the atoms are given by  $\Delta_e$  and  $\Delta_r$ . The rates  $\gamma_c$ ,  $\gamma_e$  and  $\gamma_r$  describe decay processes of the cavity, the intermediate atomic state and the Rydberg state.

subspace which we express by the additional dissipation channel  $D_{nl}$ .

With that the Hamiltonian reads as

$$\begin{aligned}
 H = & -\Delta_c a^\dagger a + p(a + a^\dagger) - \Delta_e b^\dagger b - \Delta_r c^\dagger c \\
 & + g\sqrt{N}(ab^\dagger + a^\dagger b) + \frac{\Omega_{cf}}{2}(bc^\dagger + b^\dagger c) + \frac{\kappa_r}{2}c^\dagger c^\dagger cc
 \end{aligned} \tag{3.23}$$

and the the jump operators are given by  $c_e = \sqrt{\gamma_e}b$ ,  $c_r = \sqrt{\gamma_r}c$  for the intermediate and Rydberg state and also for the cavity. The nonlinear terms in the Hamiltonian arise from the van-der-Waals-force between atoms in the Rydberg state. The interaction also couples the symmetric subspace to the antisymmetric subspace which leads to an additional nonlinear dissipation term  $c_{nl} = \sqrt{\kappa_i}cc$ .

We now extend the mode by working the eigenbasis of the Hamiltonian. The diagonalisation of Eq.(3.23) results in  $H = \sum_{p \in +, 0, -} c_p \Psi_p^\dagger \Psi_p$ . The new states  $\Psi_p$  form polariton states. They are defined as a quasi particle consisting of both light and matter. For a three level atomic system we get 2 different types of polaritons with  $\pm$  indicating light polaritons and 0 being the dark state polariton. The dark state polariton is of special interest because this eigenstate is decoupled from the intermediate atomic level which leads to long lifetimes in the cavity. The interaction between the polariton leads to a strongly correlated many-body system which provides a difficult task for numerical calculation especially for larger system sizes and therefore large particle numbers [80].

### 3. The variational method for bosonic fields

To also be able to capture correlations between the modes we need additional variational parameters. If we look at the lowest order expectation values between different modes we get

$$\langle ab \rangle = \langle a \rangle \langle b \rangle + \delta(ab) \quad (3.24)$$

with  $\delta(ab)$  being the correlation function between mode  $a$  and  $b$ . These kind of factorizations for expectation values can be done for all orders and it provides us with the needed variational parameter in the form of the correlation functions  $\delta(a^n b^m)$  [117, 118, 119].

Fig. 3.7 shows the occupation number of the different modes and the squeezing strength. We see that the bright state polaritons are populated unevenly because of the detuning in the intermediate atomic state. Furthermore, the dark state shows squeezing in its mode evoked by the nonlinear terms in the Hamiltonian and the dissipation terms. The strength of the squeezing depends on the feeding parameter  $p$  but reaches a saturation for  $p \approx 5\gamma_e$  just like the intensity. The two bright polariton states show no sign of squeezing. The correlations and therewith the squeezing are closely related to the lifetime of the particles in the Rydberg state because the nonlinearity in the Hamiltonian arise from the Rydberg-Rydberg interaction. Like we already discussed in previous chapters the lifetime of the dark state polariton is significantly longer to the light state polariton because of its missing component from the intermediate atomic level and the associated dissipation channel.

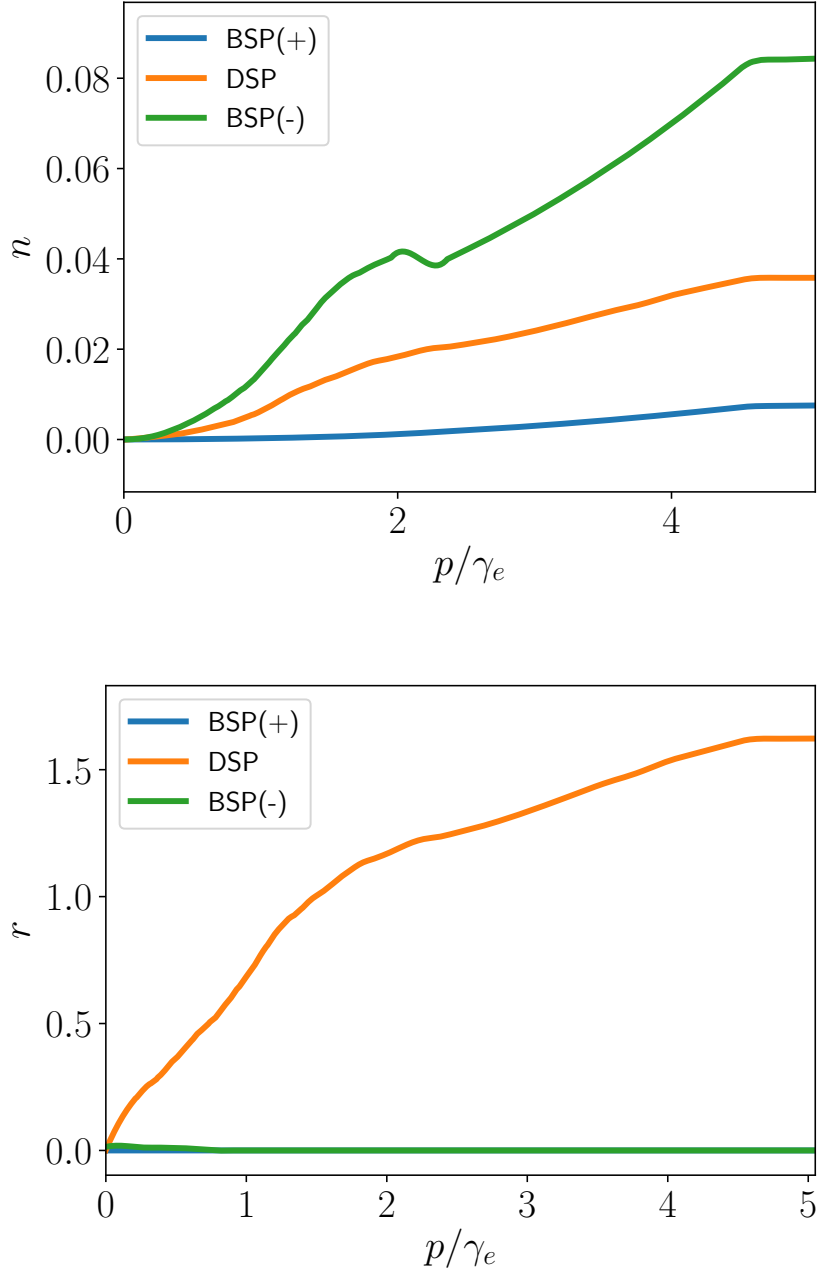


Figure 3.7.: Intensity (upper) and squeezing parameter  $r$  (lower) of the effective three boson model in the polariton picture. We observe a saturation of the bright and dark state polariton populations because of the van der Waals interaction. The effects of squeezing are only visible in the dark state polariton because of its longer lifetime compared to the bright-states. The parameters are:  $\gamma_r = 0.1 \gamma_e$ ,  $\gamma_c = 0.3 \gamma_e$ ,  $\Delta_c = 0$ ,  $\Delta_e = -10 \gamma_e$ ,  $\Delta_r = 0$ ,  $\kappa_r = -1.2 \gamma_e$ ,  $\kappa_i = 0.42 \gamma_e$ ,  $g = 4.2 \gamma_e$ ,  $N = 10^4$

### 3.4. Outlook

Throughout this chapter, we worked with only a handful of different convoluted states to construct our variational manifold. Before we come to a conclusion we want to show that our approach is not restricted to these few well-known states. Like we mentioned before it is not necessary to know the full P-distribution and that it is sufficient to know the expectation values of the given state which gives us access to a great variety of nonclassical states.

In the previous chapters we already discussed the coherent squeezed states as the most prominent candidate for squeezing but there are similar definitions for squeezed Fock state  $|l\rangle_{sf}$  and thermal states  $|n\rangle_{sth}$  [120, 121, 122]

$$|l\rangle_{sf} = S(r, \phi) |l\rangle \quad (3.25)$$

$$|n\rangle_{sth} = S(r, \phi) |n\rangle. \quad (3.26)$$

Both states were already studied before and it was shown that we can find an explicit expression for expectation values of all orders [123, 102]. Another state we want to mention is the cat state defined as

$$|\psi\rangle = A(|\alpha_1\rangle + \Theta |\alpha_2\rangle) \quad (3.27)$$

with  $|\alpha_1\rangle$  and  $|\alpha_2\rangle$  being two different coherent states. The expectation values for this state can be calculated via the explicit P-distribution [124].

Fig. 3.8 shows the Wigner distribution of all four states. We also want to make a clear distinction between the squeezed thermal (Fock) state and the convoluted distribution of a squeezed coherent state with a thermal (Fock) state. Tabular 3.1 shows the possible combinations of two states via convolution for all states we used for our calculations, i.e. thermal, Fock, squeezed coherent and coherent state. Especially in the case of the thermal state, it is not straight forward to see that the two results are actually different. That is why we want to look at a lower order expectation value like the intensity  $\langle a^\dagger a \rangle$  for the squeezed thermal state  $|n, r\rangle_{sth}$  and the convoluted case  $|n, r\rangle_{s+th}$ . The difference between the two results reads as  $\langle a^\dagger a \rangle_{sth} - \langle a^\dagger a \rangle_{s+th} = 2n_0 \sinh^2 r$ . The difference is enhanced for higher orders of expectation values which can significantly change the result of the minimization in (3.12).

In case of the cat state, the situation is reversed. Although the visual representation in 3.8 is clearly distinguishable from a simple coherent state, they are hard to distinguish in terms of expectation because the first order of the cat state reads

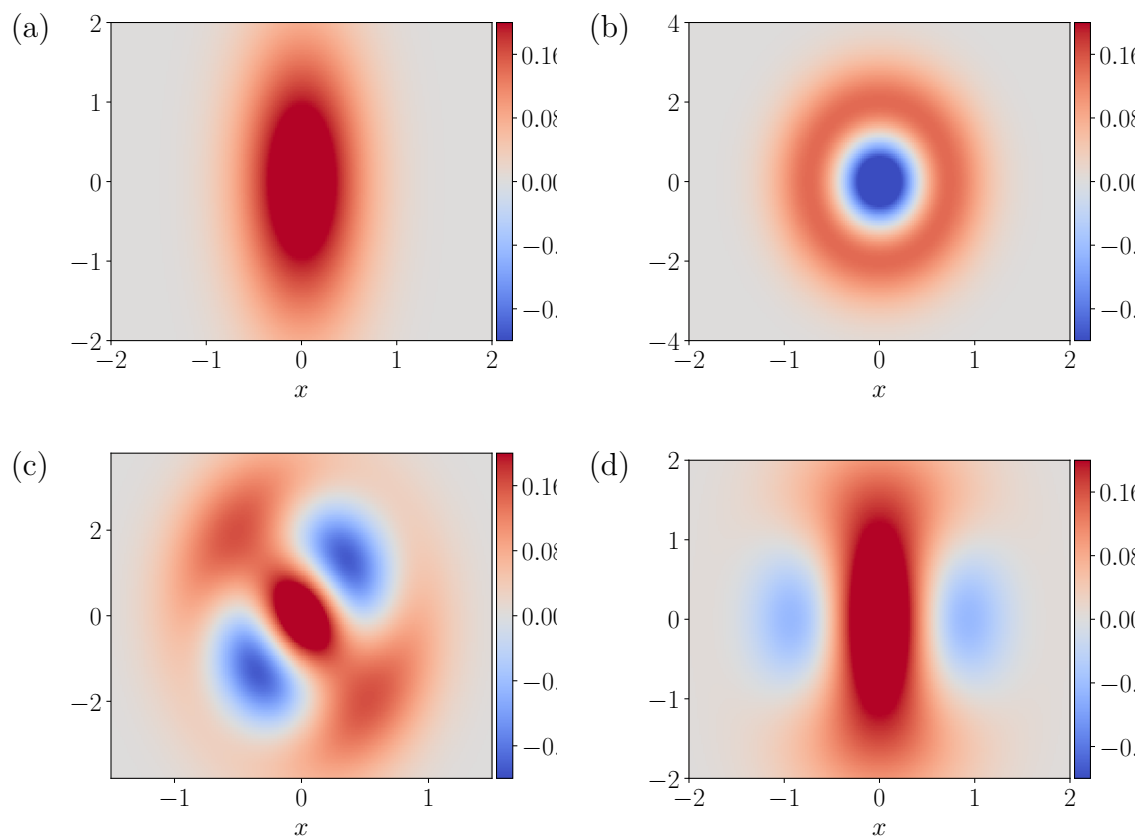


Figure 3.8.: Wigner function for different nonclassical states.(a) squeezed thermal state and (b) squeezed Fock state (c) Hermite polynomial states and (d) cat state .

$\langle a \rangle_{\text{cat}} = \alpha_1 + \alpha_2 = \tilde{\alpha}$ . Only the scaling with higher order expectation values can reveal the true nature of this state and shows the importance of incorporating as many orders as possible for the equations of motion.

Before we come to a conclusion we want to mention two more states with complex properties which exceed the scope of this work. We think that both the single-variable Hermite polynomial states [125, 126, 127, 128] and the photon-added (subtracted) coherent states [129, 130] good candidates to expand our method further.

### 3.5. Summary

In conclusion, we expanded the variational principle for open quantum systems through the usage of the P-distribution of the density matrix operator. We gave an example of its usage with the Jaynes-Cummings model. We then used the method

### *3. The variational method for bosonic fields*

to analyse the squeezing of the dark-state polariton in an effective three-bosonic field model for Rydberg atoms in a cavity by also implanting additional terms to cover the correlations between different modes. At the end, we gave an outlook on how the method can be expanded to other possible states of the quantum field. The zoo of possible states that can be implemented through the usage of convolution could allow for an interesting new perspective on different systems. Our method opens up the possibilities for the variational principle and we hope to find more application for it in the future.



## 4. Dynamical decoupling in the dissipative Ising model

In the last chapter of the thesis, we want to turn our attention to another kind of Rydberg systems. The problems and systems we encountered so far were focused around the interaction of Rydberg atoms with each other and also with light which led to the description in the polariton picture. In the optical lattice, we derived a Bose-Hubbard-like model to describe the dynamics in these systems. The Ising chain is another spin model with an important role in the theoretical and experimental description of strongly correlated many-body systems [32]. Here, we want to complement the work by V. Overbeck *et al.* [31] which focused on the multicritical behaviour of the Ising chain in the thermodynamical limit. In experiments, the numbers of realisable spins are far less than necessary to be comparable to this limit. Hence, we take a different approach and look at only two interacting sites to see if we find any traces of the predicted phase transitions in the system. We also take this occasion to deepen our understanding of the variational principle by inserting the analytical mean-field solutions of the Ising model into our variational norm to see if this changes the phase diagram in a similar way of what we saw in Section 3.2.

The Ising model is an experimental cornerstone and still important today in the context of quantum gates and quantum simulations. A rapid progress in experiments allows for tunable dissipation channels in these models which can lead to interesting many-body states [131, 132, 133, 134, 135, 136]. Quantum gates like the Mølmer-Sørensen gate are built upon Ising-like interactions between the different spins [137, 138, 139, 140]. Imperfection in the traps can add additional detuning in the system which would disturb the phase diagram. That is why we also propose a measurement protocol to overcome these unwanted detuning on the sites.

## 4.1. Phase transitions in the dissipative Ising model

An important finding of the work by V. Overbeck *et al.* [141] was how the phase diagram differs between the open model and in the equilibrium case. Besides the second-order transition, the dissipative Ising model also shows a first-order transition in combination with a tricritical point. We want to see how the magnetisation for a system of just two lattice sites behaves and we investigate if there are still signs of the different phase transitions that appear in the thermodynamical limit. At last, we will use the mean-field solution in combination with the variational method to analyse the system.

Quantum phase transitions are different from their classical counterparts by the absence of thermal fluctuations. Even at 0K temperature, we observe changes in the properties of matters by varying other parameters other than the temperature. The Ising model in equilibrium is often used to study the transition between a ferromagnetic (FM) and a paramagnetic (PM) phase. In classical thermodynamical system a non-analytic behaviour of the free energy is a sign of a phase transition. In the quantum case, we can replace this with a non-analytical ground state energy. This goes hand in hand with the crossing of eigenenergies of the Hamiltonian. A general Hamiltonian like

$$H = H_0 + gH_1 \tag{4.1}$$

with a coupling constant  $g$  can have level crossing if  $[H_0, H_1] = 0$ . In most cases, this condition is not fulfilled and a gap separates the two lowest eigenenergies, see Fig. 4.1. If the system size goes to infinite, which corresponds to the thermodynamical system, the gap closes and we can recover a non-analytical function for the ground state energy [33].

Before we look at the case of only two sites, we will need a better understanding of the results in [141] to know what to look out for in the finite system. The Ising Hamiltonian for a system with a translational invariance can be written as

$$H = \Delta \sum_i \sigma_i^z - J \sum_{\langle ij \rangle} \sigma_i^x \sigma_j^x. \tag{4.2}$$

The corresponding Lindbladian we get from (1.19) with the jump operators  $c_i = \sqrt{\gamma} \sigma_i^-$  has a  $Z_2$  symmetry because the dissipation channel is in the same eigenbasis as the transverse field. Symmetry in the system is necessary to observe a phase transition when it breaks and it allows us to distinguish between a ferromagnetic and paramagnetic phase in terms of the order in the system. The magnetization

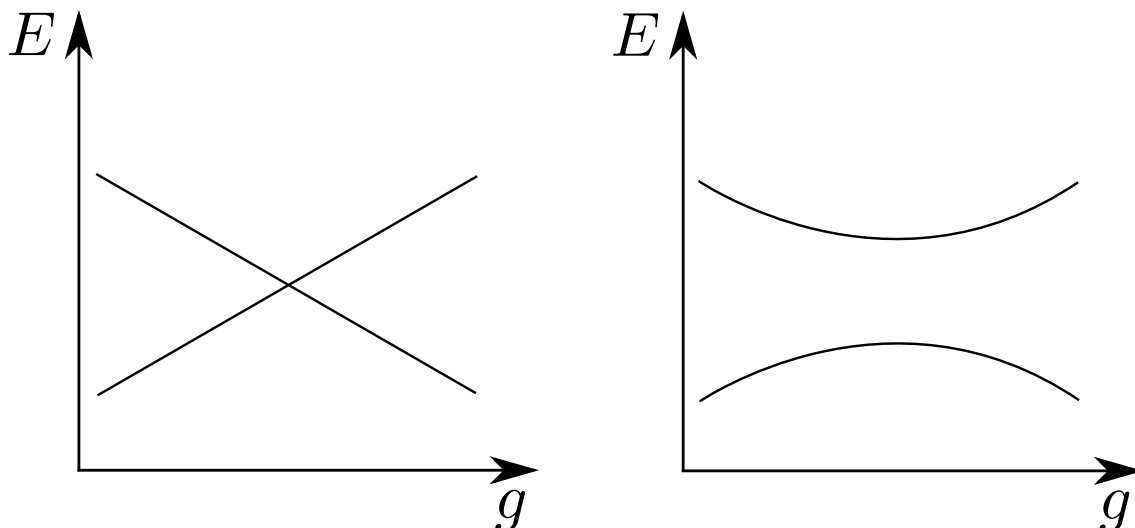


Figure 4.1.: Crossing(left) and anti-crossing(right) of two eigenenergies of the Hamiltonian  $H = H_0 + gH_1$ . The non-analytical behaviour caused by the crossing of the two disappears for finite system if  $[H_0, H_1] \neq 0$ .

will serve as the order parameter. The system can go from a completely ordered phase (ferromagnet) to a disordered phase (paramagnet). The order parameter can also be used to classify the phase transitions present in the system because of its connection to the free energy [142]. We will follow the modern approach in the classification of phase transitions by distinguishing between a discontinuous jump in the order parameter as a first-order transition and a discontinuity of its derivative as a second-order transition [143, 141, 144].

If we now turn our attention to only two lattice site, we find the ground states of(4.2) to be

$$\frac{\Delta}{J} \gg 1 : |g\rangle = |\downarrow\downarrow\rangle \quad (4.3)$$

and

$$\frac{\Delta}{J} \ll 1 : |g\rangle = |\rightarrow\rightarrow\rangle \text{ or} \quad (4.4)$$

$$|g\rangle = |\leftarrow\leftarrow\rangle. \quad (4.5)$$

The first state represents the paramagnetic phase and the other two the ferromagnetic phase. The quantity  $\langle\sigma_x\sigma_x\rangle$ , therefore, gives information about the magnetization in the system and also will be used as the order parameter. The susceptibility of the system is given by  $\frac{d\langle\sigma_x\sigma_x\rangle}{d\Delta}$ .

V. Overbeck *et al.* showed that there is a first-order transition if  $\gamma \gg \Delta$ . In Fig. 4.2 shows a map of the order parameter  $\langle\sigma_x\sigma_x\rangle$  over  $\gamma$  and  $\Delta$  with no additional dephasing terms. We see that there could be a transition between the ferromagnetic and

#### 4. Dynamical decoupling in the dissipative Ising model

the paramagnetic field for low dissipation rates. The thermodynamical limit would be needed to see a "real" phase transition because for finite particles the partition function is an analytic function everywhere. To see an indication of a transition for  $\gamma \ll 1$ , we also need to see the susceptibility. If we look at Fig. 4.3, we can see that for  $\gamma \rightarrow 0$  the susceptibility becomes large. We, therefore, can actually use even the smallest possible system size to find traces of the predicted phase transition in the dissipative Ising model.

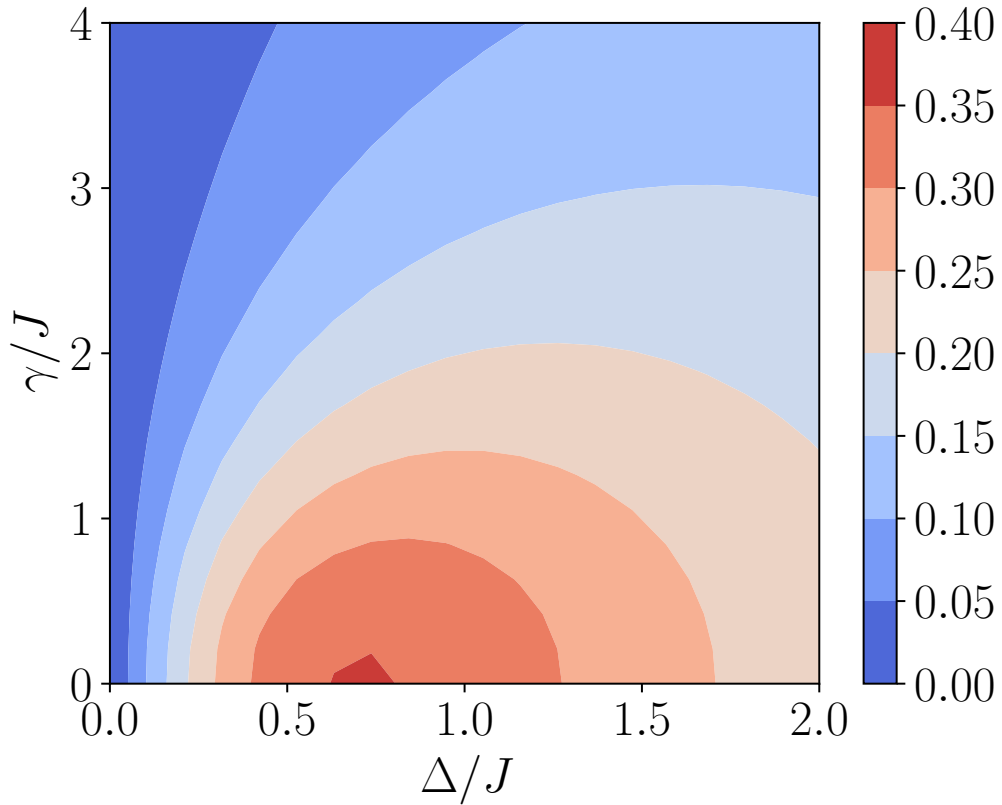


Figure 4.2.: Map of  $\langle \sigma_x \sigma_x \rangle$  for different  $\gamma$  and  $\Delta$ .

4.1. Phase transitions in the dissipative Ising model

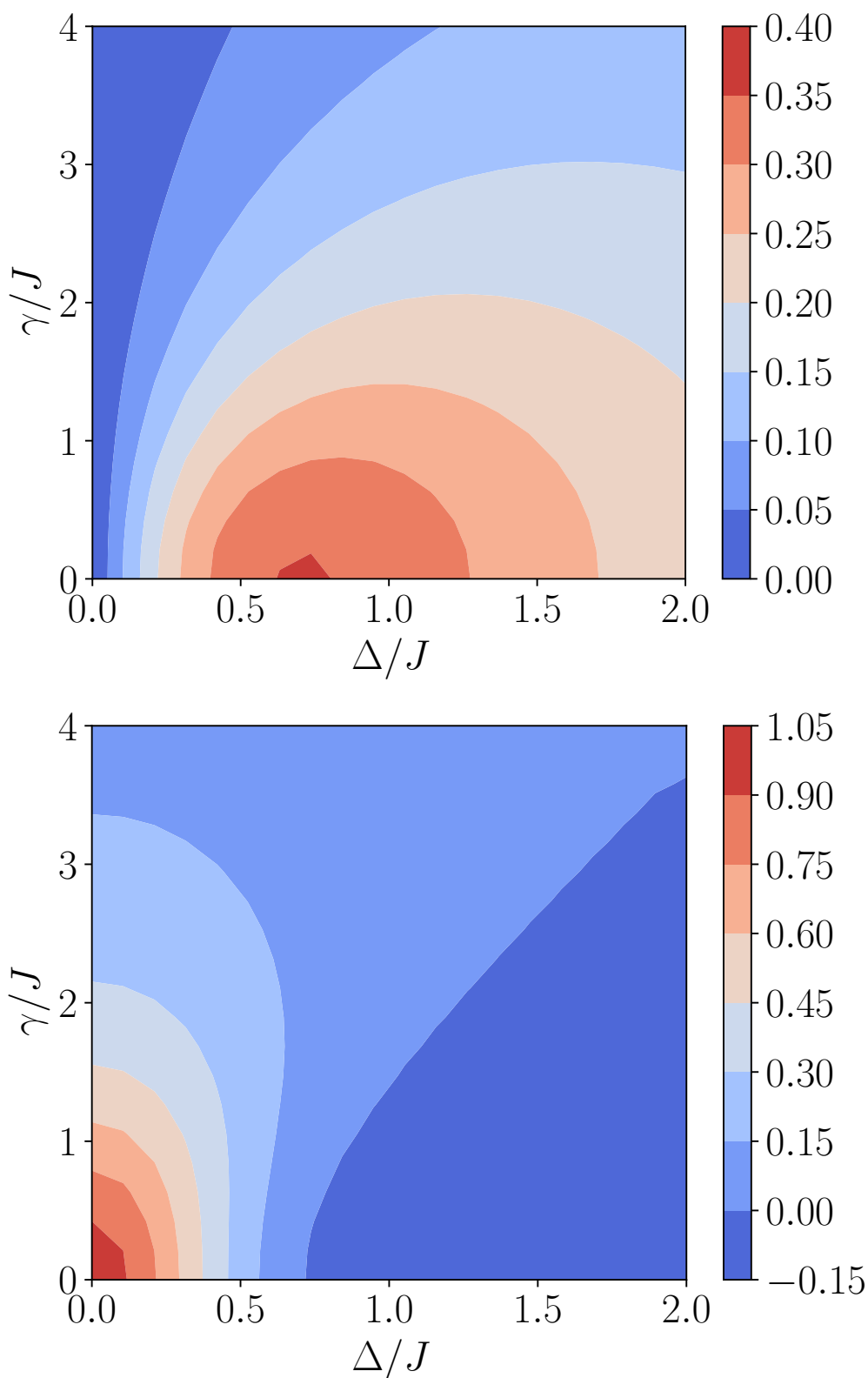


Figure 4.3.: (Upper) Map of  $\langle \sigma_x \sigma_x \rangle$  and (lower) map of  $\frac{d}{d\Delta} \langle \sigma_x \sigma_x \rangle$  for different  $\gamma$  and  $\Delta$  for an Ising chain with system size  $N = 2$ . The phase diagram does not show a clear transition line between the ferromagnetic and the paramagnetic phase. The derivative, on the other hand, indicates a divergence for  $\gamma, \delta \rightarrow 0$  and , therefore, a possible phase transition.

4. Dynamical decoupling in the dissipative Ising model

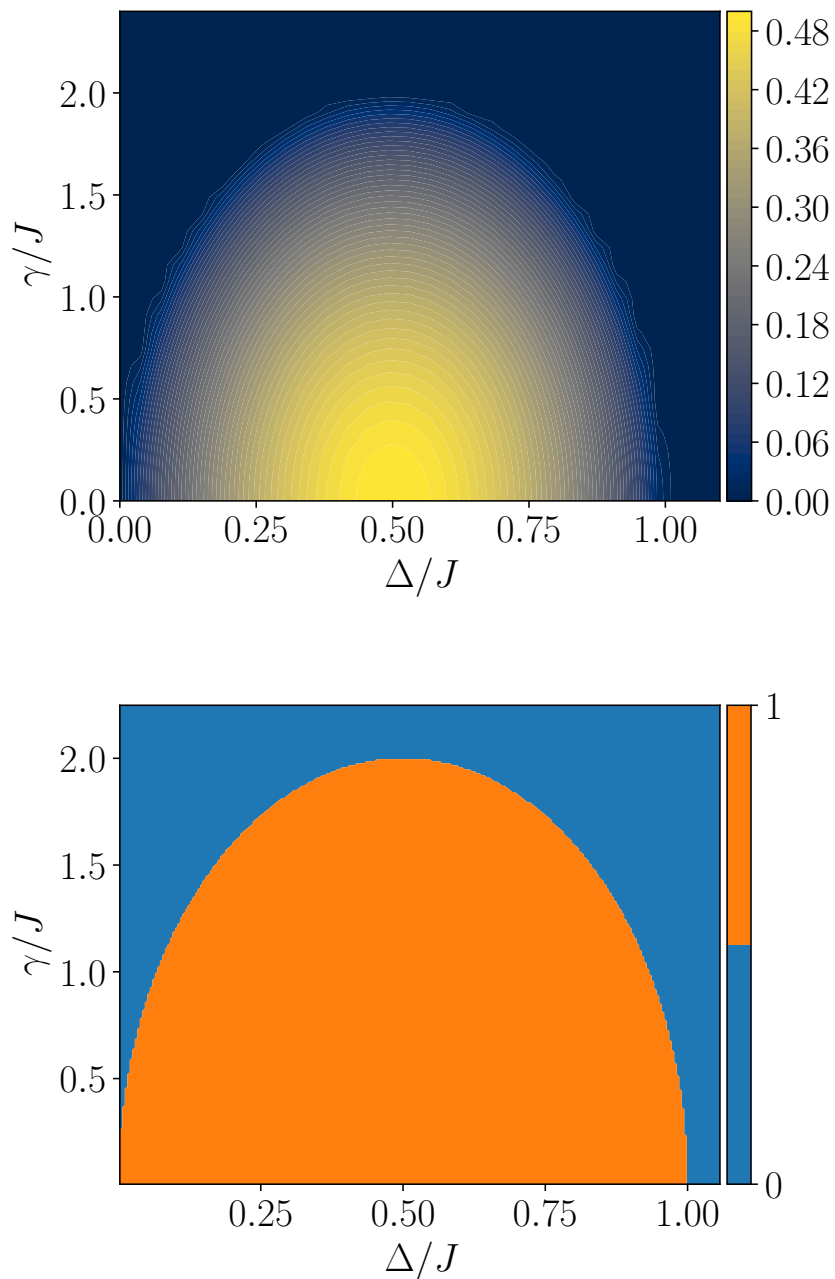


Figure 4.4.: (Upper) The phase diagram of the three dimensional Ising chain calculated by the combination of the mean-field solution with the variational principle. (Lower) The map of the used mean-field solution that gave the lowest norm for the given  $\Delta$  and  $\gamma$ . The trivial solution is marked with 0 whereas the other two solutions in (4.7) are distinguished by their sign  $+1, -1$ . In comparison to a full variational treatment like in [141], there are no indications for a first order transition.

## 4.2. Mean-field solution and the phase diagram

The phase diagram of the dissipative Ising model is significantly different from the one in equilibrium as it was shown in the work by Vincent R. Overbeck [141].

$$\begin{aligned}\frac{d}{dt} \langle \sigma_x \rangle &= -\frac{\gamma}{2} \langle \sigma_x \rangle - 2\Delta \langle \sigma_y \rangle \\ \frac{d}{dt} \langle \sigma_y \rangle &= -\frac{\gamma}{2} \langle \sigma_y \rangle + 2\Delta \langle \sigma_x \rangle + 2Jz \langle \sigma_x \rangle \langle \sigma_z \rangle \\ \frac{d}{dt} \langle \sigma_z \rangle &= -\gamma(1 + \langle \sigma_z \rangle) - Jz\Delta \langle \sigma_x \rangle \langle \sigma_y \rangle\end{aligned}\quad (4.6)$$

The equations in Eq. (4.6) result in three different solutions for the steady state  $\frac{d}{dt} \langle \sigma_x \rangle = \frac{d}{dt} \langle \sigma_y \rangle = \frac{d}{dt} \langle \sigma_z \rangle = 0$  and result from the mean-field approximation of the Ising model [34]. The trivial solution with  $\langle \sigma_x \rangle = \langle \sigma_y \rangle = \langle \sigma_z \rangle = 0$  and the two other solutions

$$\begin{aligned}\langle \sigma_x \rangle &= \pm \frac{1}{\sqrt{8J}} \sqrt{16\Delta J - 16\Delta^2 + \gamma^2} \\ \langle \sigma_y \rangle &= \pm \frac{\gamma}{8\sqrt{2}\Delta J} \sqrt{16\Delta J - 16\Delta^2 + \gamma^2} \\ \langle \sigma_z \rangle &= \pm \frac{1}{\sqrt{2}\gamma} \sqrt{16J\Delta^2 - \gamma^2\Delta - 16\Delta^3}.\end{aligned}\quad (4.7)$$

## 4.3. Measurement protocol

When it comes to the implementation of the Ising model in an experiment, we want to focus on the Mølmer-Sorensen gate and its realisation with trapped ions [145, 146]. The gate is realised by confining ions in a linear trap. The ions are coupled with each other by a collective quantized motion. The internal states of the particles represent the qubits of the gate and the interaction allows for multi-qubit operations. We will neither discuss the advantages of the setup nor how the Mølmer-Sorensen creates entangled states through the collective vibrational modes as this would far exceed the scope of this chapter but instead focus on experimental problems and how to overcome them by implementing a measurement protocol.

At first, we want to look at a brief summary of the theoretical description of the gate in the context of trapped ions. The full system is described by  $H = H_{\text{MS}} + H_m + H_z$ . The first part is the Mølmer-Sorensen gate which is given by

$$H_{\text{MS}} = \frac{\Omega}{2} \sum_{j=1}^2 (\sigma_j^+ + \sigma_j^-) \cdot (ae^{i\delta t} + a^\dagger e^{i\delta t}). \quad (4.8)$$

#### 4. Dynamical decoupling in the dissipative Ising model

The Pauli matrices  $\sigma_{i,j}$  are used to describe the ions and  $a^{(\dagger)}$  are the ladder operators of a harmonic oscillator which is used to represent the center-of-mass vibrational energy of the two ions. We focus on an idealised version by neglecting a possible time-dependence of the gate Rabi frequency  $\Omega$ . With  $\delta$  being the gate detuning from the high-frequency rocking mode of two ions, we can also choose the gate time to be  $t = \frac{2\pi}{\delta}$  which leads to an effective Hamiltonian of  $H_{\text{MS}} \propto \sigma_x \otimes \sigma_x$ . Therefore, we can use the Mølmer-Sørensen gate as a possible realisation of the Ising interaction. We apply a magnetic field to the particles that causes a shift in the energy level based on their magnetic momentum. The Hamiltonian of this Zeeman shift reads as

$$H_z = \frac{\Delta_\epsilon}{2}(\sigma_1^z + \sigma_2^z), \quad (4.9)$$

where we assume that both sites experience the same shift. We will later see how deviations from that adulterated the results and how to restore it.

This is enough to fully represent the Ising model for two particles. We ignored any instability in the rocking mode frequencies of the ions and also off-resonant coupling to other motional modes. We allow for tuneable dissipation channels in the atoms that are represented by  $c_i = \gamma_i \sigma_i^-$  and the rates  $\gamma_i$  are set to be equal for both sites.

Now, we want to propose a scheme to reduce the influence of possible errors in the AC-Zeeman shift. We can express them by the additional Hamiltonian  $H_{\text{err}} = \delta_1 \sigma_z + \delta_2 \sigma_z$ . Errors like that can appear through the inhomogeneity of the magnetic field or by displacements of the ions in the traps. By applying spin-flip operations on both sites we can average the unwanted  $\delta_i$ -terms out. Its functionality is based on already proven methods like the spin-echo or the dynamical decoupling in open quantum systems [147, 148, 149]. Both methods apply additional unitary transformations to the system to obtain an averaged Hamiltonian that is freed from unwanted decoherences. Fig. 4.5 shows our implementation of a similar approach to these two methods. The MS-gate stays on throughout the full measurement and because  $\sigma_x^1 \sigma_x^2$  is invariant under spin-flip operators the interaction term of the Hamiltonian is not affected throughout the measurement. We evolve the system for a time  $\tau$  before applying  $U_{\text{flip}} = \sigma_x^1 \otimes \sigma_x^2$  and let it evolve again for the same time  $\tau$ . The procedure is then repeated for the duration of the measurement. The time  $\tau$  determines the effectiveness of the scheme as it is also the case in the dynamical decoupling process. This covers the coherent part of the dynamics. The controllable dissipation channel for each ion has to be turned off with the spin-flip because the jump operators do not commute with it. If we still want to be in the same time scale as without the error correction, we need to double the dissipation rate while



it is on.

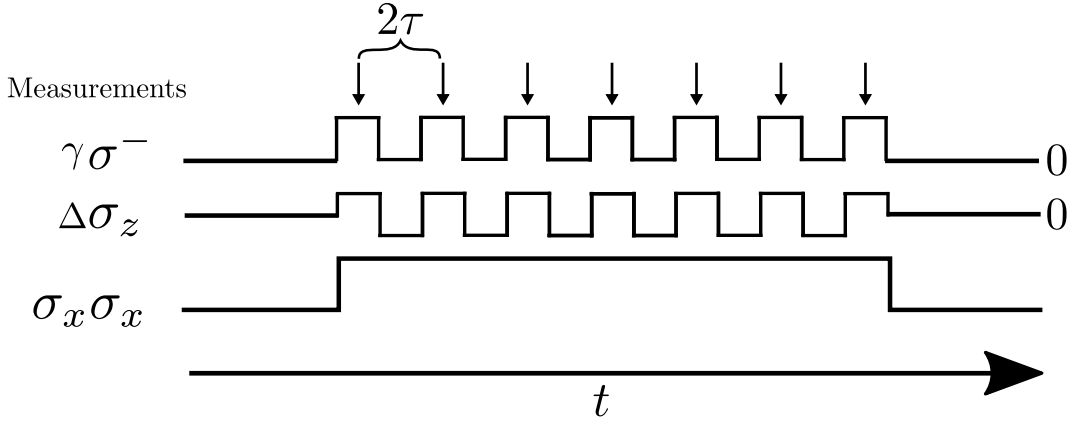


Figure 4.5.: Scheme to compensate unwanted detuning. The idea is to apply the flip operator  $U_{\text{flip}} = \sigma_x^1 \otimes \sigma_x^2$  multiple times during the measurement to average out the unwanted detuning. The dissipation ( $\gamma\sigma^-$ ) and the wanted detuning ( $\Delta\sigma_z$ ) must change in such a way that they are not affected by the operations. The Ising interaction ( $\sigma_x\sigma_x$ ) does not have to change over the duration of the measurement because it is unaffected by the flip operation.

The procedure for a full cycle of  $2\tau$  then can be written as

$$|\psi_1\rangle = e^{\mathcal{L}_1\tau} |\psi\rangle \quad (4.10)$$

$$|\psi_2\rangle = e^{\mathcal{L}_2\tau} U_{\text{flip}} |\psi_1\rangle. \quad (4.11)$$

We keep the wanted AC-Zeeman shift  $\Delta$  by changing its sign after each flip which keeps its impact on the dynamics of  $|\Psi_2\rangle$  the same as for  $|\Psi_1\rangle$ .

Each cycle consists of two flips and the measurements always have to happen at the same time in the cycle with the same conditions. There is still an arbitrary choice of when exactly in this interval of  $\tau$  the measurement can take place. Therefore, we compare the three scenarios of measuring at the beginning, in the middle and at the end of the interval in Fig. 4.6. The figure shows the steady state expectation value of the projection operator of the double excited state  $P_{ee} = |ee\rangle\langle ee|$  over different numbers of flips that occur during the full measurement procedure, thereby reducing the time span between each flip. The fastest approach to the solution without error terms is achieved by measuring in the middle of the interval at  $\tau/2$  (see also 4.5). At the beginning or at the end of the interval leads to a larger undershooting or overshooting respectively, with respect to the solution we aim at. We also see that if we approach  $N_{\text{flips}} \rightarrow 100$  the differences between the three measurement methods decrease. Hence, we can make a choice based on the experimental restriction that

#### 4. Dynamical decoupling in the dissipative Ising model

slower switching times are easier to achieve, which again leaves us with the choice of measuring at  $\tau/2$ .

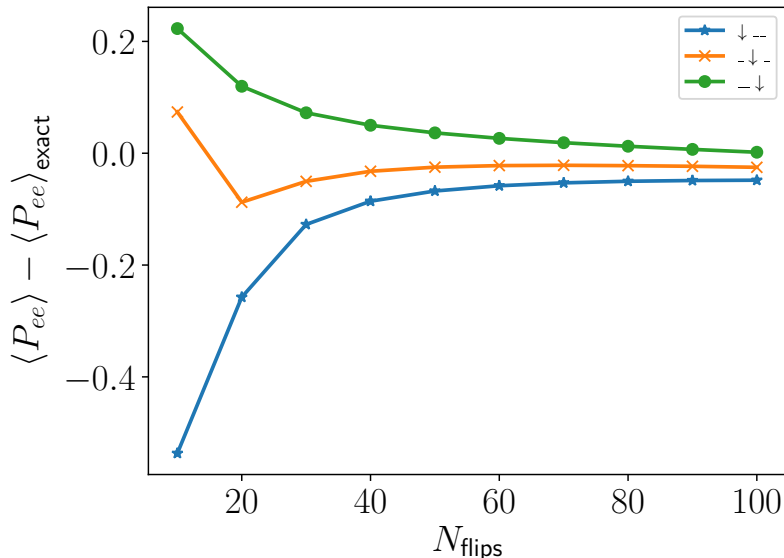


Figure 4.6.: Comparison between the system with  $\langle P_{ee} \rangle$  and without error  $\langle P_{ee} \rangle_{\text{exact}}$  and how the improvement scales with numbers of applied flips  $N_{\text{flips}}$  during the measurement. It also shows the difference between a measuring at the beginning, in the middle and at the end of the time interval. The parameters are:  $J/2\pi = 54\text{Hz}$ ,  $\Delta/2\pi = 54\text{Hz}$ ,  $\delta_1/2\pi = -50\text{Hz}$ ,  $\delta_2/2\pi = 100\text{Hz}$ ,  $\gamma/2\pi = 54\text{Hz}$

Next, we also want to check if and how the system parameters change the effectiveness of the scheme. Fig. 4.7 shows the results for different detunings  $\Delta$  and different errors  $\delta_1, \delta_2$ . For the correction scheme it does not matter how the error is split up between the sites but the overall error  $\delta_1 + \delta_2$ . Like in Fig. 4.6 is the deviation of the results  $< 0.1$  in most cases, which should be good enough for most experimental setups. The same is true if we change the decay rate  $\gamma$  of the system on both sides. There, the difference between different  $\gamma$  values is small in comparison to the detuning  $\Delta$ .

Our proposed scheme does not only work for finding the steady state but also produces good results for the dynamics of the system. In Fig. 4.9, we show the dynamics of the occupation numbers that cover the full system. Whereas previously we only looked at  $P_{ee}$ , we added in Fig 4.9 the probability to find both qubits in the ground state with  $P_{gg}$  and the combined probability to find them in the mixed states  $P_{ge}$  and  $P_{eg}$ .

Overall, Fig. 4.6-4.9 show that the scheme should be applicable to a wide variety

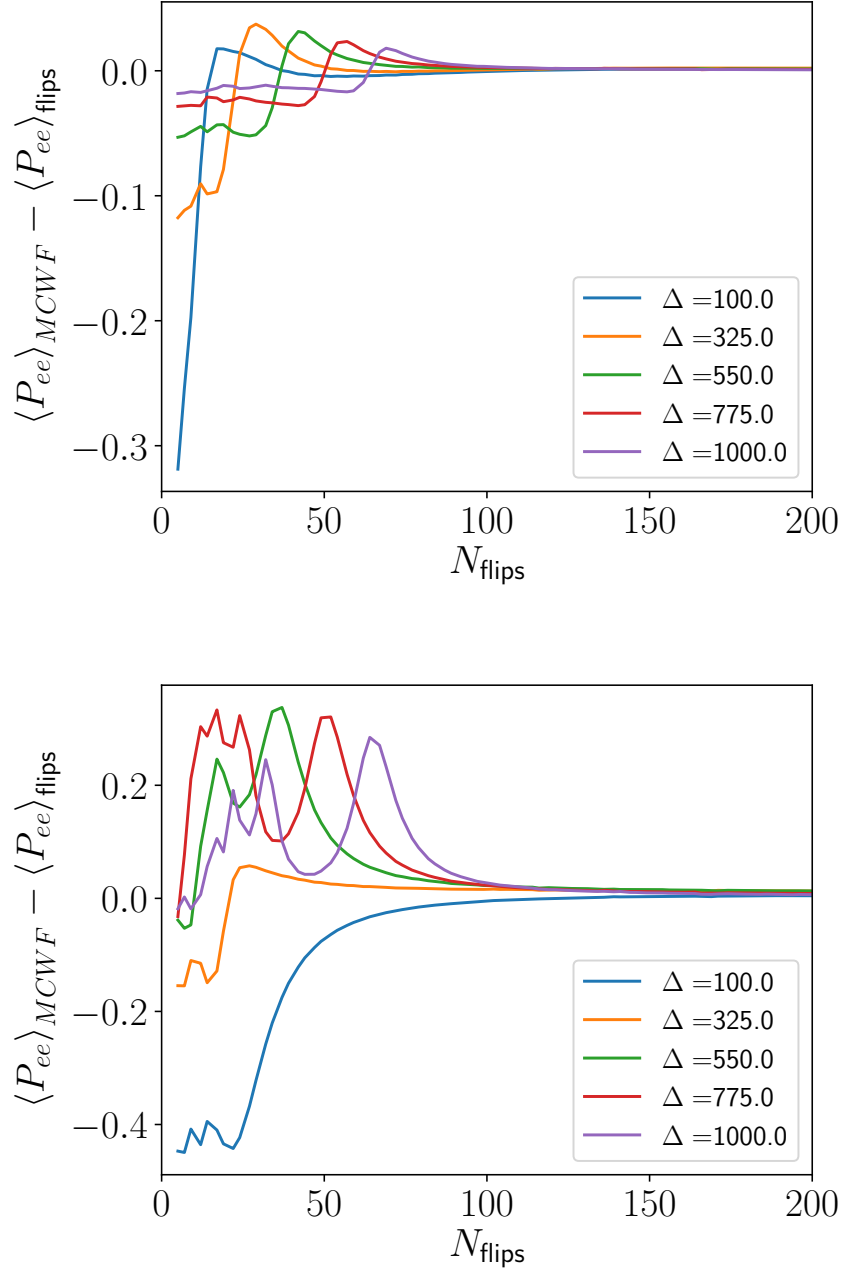


Figure 4.7.: Difference between the error correcting scheme and the solution without error over different number of flips  $N_{flips}$  for different detunings  $\Delta$ . The upper graph has errors on the two sites of  $\delta_1 = 0Hz$  and  $\delta_2/2\pi = 40Hz$  whereas the lower one has higher errors of  $\delta_1/2\pi = 80Hz$   $\delta_2/2\pi = 160Hz$ .

#### 4. Dynamical decoupling in the dissipative Ising model

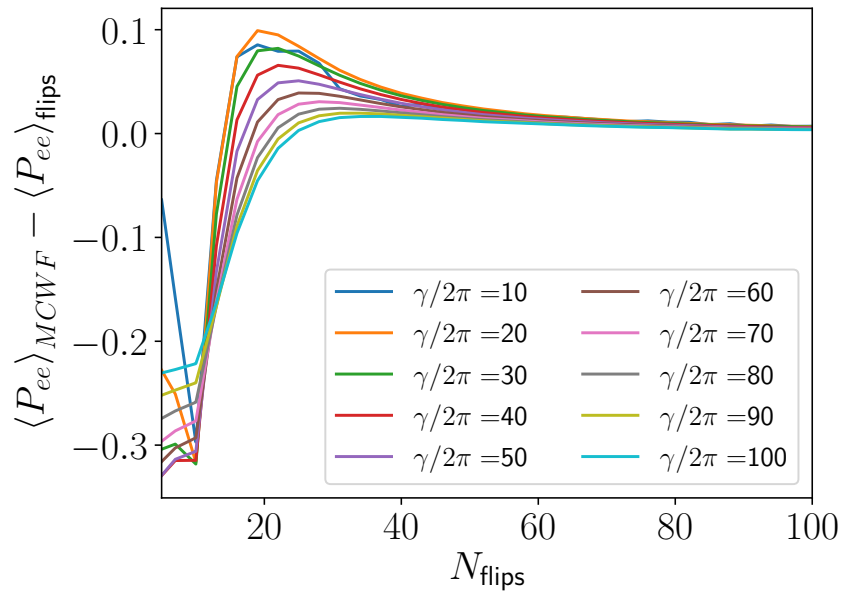


Figure 4.8.: Difference between the error correcting scheme and the solution without error over number of flips  $N_{flips}$  and for different decay rates  $\gamma$ .

of experiments surrounding the Ising model. A generalisation from two sites to  $N$  site should be possible because the protocol does not rely on the two-particle system and only applies global operations.

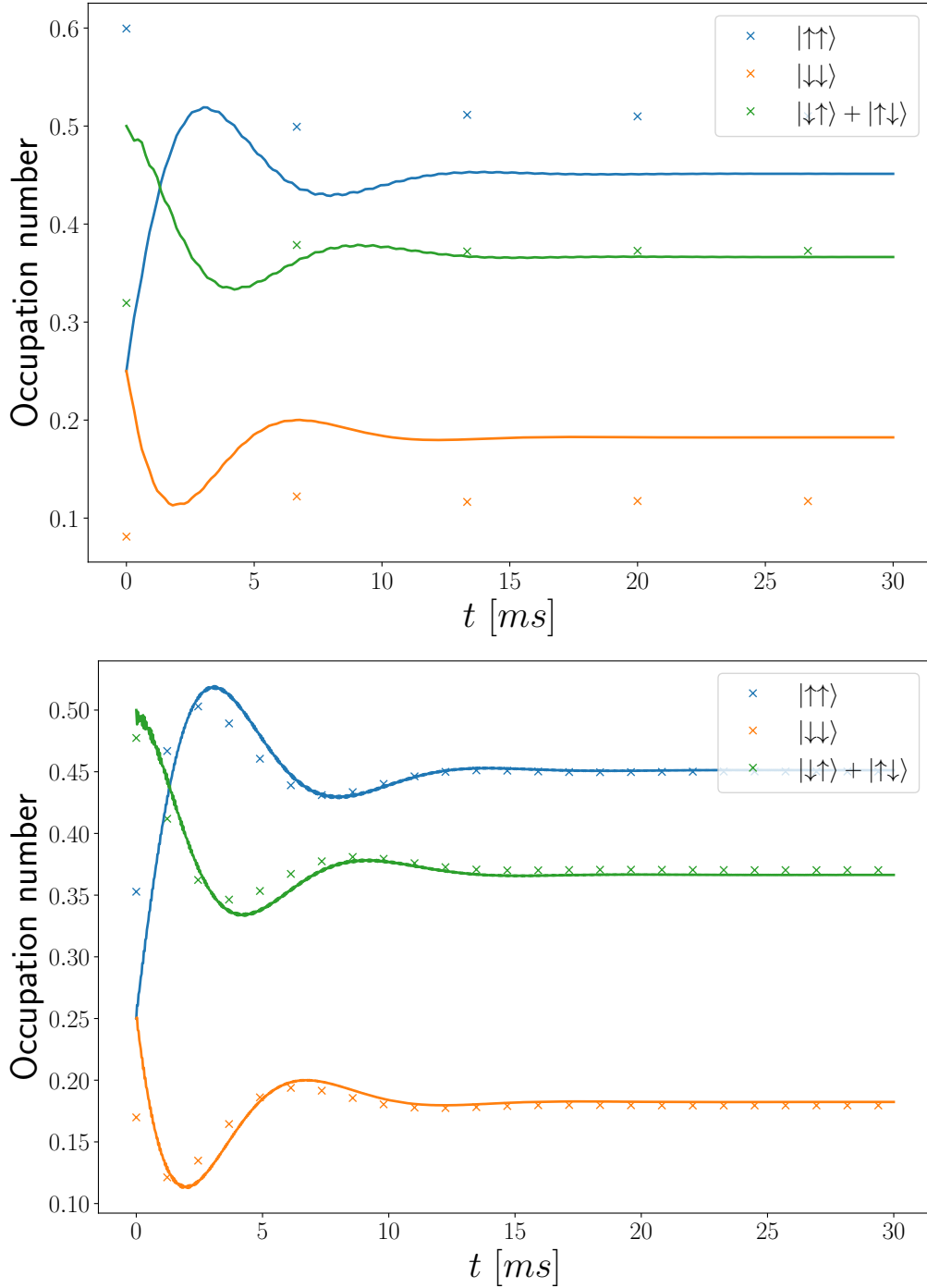


Figure 4.9.: Time evolution of the dissipative Ising model with implemented protocol to reduce influences of a detuning error  $\delta_1/2\pi = 50\text{Hz}$ . The solid lines indicate the solutions without any error in comparison. The upper plot shows the results for  $N = 10$  and the lower one with  $N = 50$  flips of the wanted detuning  $\Delta$  during the measurement. With a time of  $0.6\text{ms}$  between each flip in the second plot, the discrepancy between the solutions with and without errors is already down to  $\approx 0.003$ .



## 5. Summary

In this thesis, we studied the interaction between Rydberg atoms and photons in different systems. We presented an experimentally realisable and new approach to obtain single-photon emission without the usage of cavities. We used and expanded the variational principle for open quantum system to study different many-body systems.

In Chapter 2, we have demonstrated the possibility to treat large many-body systems of driven-dissipative systems of strongly interacting Rydberg polaritons using a variational approach. We used a setup in which we trapped Rubidium atoms in an optical lattice and used additional light fields to excite them to the Rydberg state. The obtained dispersion relation revealed the existence of two symmetrical dark-state polaritons for which we derived an extended Bose-Hubbard model with long-range hopping and interactions. We find that two counterpropagating probe light fields coupling to the same intermediate atomic level with the same polarisation allow for a linear dispersion around  $k \approx 0$  for the dark-state polaritons. We then studied the dynamics of the open quantum system via the Lindblad master equation in which we considered the often disregarded Rydberg decay. An adaptation of the Rydberg blockade into the variational approach yielded a good approximation for the dynamics, especially for larger system sizes. The blockade mechanism also led to a limit on the possible output intensity of the field. Furthermore, by measuring the two-time correlation function for emitted photons from the lattice, we observed that the propagation of photons through the lattice can yield in strong correlations between the particles. The work is an important first look into the driven-dissipative transport of Rydberg polariton and presents a novel theoretical analysis of polaritons in the many-body-regime. The setup we propose should also allow for an experimental realisation in the future.

In Chapter 3, we established a new way to integrate bosonic fields in the variational approach by representing the density matrix in terms of the quasi probability distributions. We used the convolution of different distribution functions to allow for a wide variety of possible states. We use the property of the P-distribution to allow for easy calculation of normal-ordered expectation values to reformulate the

## 5. Summary

variational principle also for equations of motion that we obtain from the Lindblad master equation.

We tested our method with the Jaynes-Cummings-model consisting of an atom inside the bosonic light field of a cavity. The bistability that is visible in the Maxwell-Bloch-equation, which corresponds to a mean-field approach, was not existing in our solution.

The investigation of an effective model to describe Rydberg atoms in an atom by the usage of three different bosonic fields revealed the necessity of correlation terms between different modes which were implemented by additional variational parameters. We used this to study the model in the polariton picture. The dynamics of the three polariton modes showed a dominating light polariton in the occupation numbers. On the other hand, we saw that the dark-state is heavily influenced by the Rydberg-Rydberg interaction, which leads to a strongly squeezed mode in comparison to the light modes.

In the end, we also gave an outlook on how to proceed with the new method which includes more exotic quantum states and also the possibility to use other quasiprobability distributions. In the future, the method should also allow a unique insight into the influences the individual state distributions have on the dynamics of different systems.

In Chapter 4 we focused on a different model that is often used to describe Rydberg atoms in the form of the Ising chain. We started by investigating the model by a combination of the variational and the mean-field method by inserting the mean-field solutions into the variational test density matrix. The goal was to see if traces of the full variational treatment of the model, which also include a first-order phase transition, can be found. Even though this was not the case, we still found that the treatment resolves the bistability of the mean-field solutions. Then we used the numerical integration of the master equation to see if signs of a phase transition are visible in finite lattices far away from the thermodynamic limit. We find that even for a lattice site of  $N = 2$ , the susceptibility of the system starts to show signs of divergence, which typically indicates a phase transition. The findings are especially important in the context of experiments. The Mølmer-Sørensen gate is often tested with the Ising model. Systematic error in the experimental setup of the ion traps in the gate can often lead to a departure from the theoretical prediction. We proposed a scheme that drastically reduces the influences of unwanted detuning terms by averaging them out over the measurement time. We found that the scheme can compensate for a large error span and is mostly independent of the other system parameters. We think that this scheme can be of great usage for future experiments



involving the transverse field Ising model.



# A. Pumping with a forward propagating wave

We assume that the coherent light we pump into the system create dark state polariton in all  $k$ -modes. The creation is expressed by the two creation operators  $a_{k_n}^\dagger$  and  $b_{k_n}^\dagger$ . Each operator can be written as the Fourier transform  $a_{k_n}^\dagger = \sum_{j=0}^N e^{i2\pi nj/N} a_j^\dagger$  in the real space. With that we can write the forward propagating part of the two bands as the sum  $\sum_{k_n=0}^{k_{N/2}} a_k^\dagger + \sum_{-k_{N/2}}^{k=0} b_k^\dagger$ . If we use the relation  $k_n = \frac{2\pi n}{L} = \frac{2\pi n}{Na}$  and  $r_i = aj$ ,  $j \in \mathbb{N}_+$ , we can write the two individual parts as

$$\sum_{k_n=0}^{k_{N/2}} a_k^\dagger = \frac{1}{\sqrt{N}} \sum_{n=1}^{N/2} \sum_{j=0}^N e^{i2\pi nj/N} a_j^\dagger + \frac{1}{\sqrt{2}} \sum_{j=0}^N a_j^\dagger$$

We singled out the mode for  $k = 0$  because this mode is formed through a superposition of both bands which we write as  $\frac{1}{\sqrt{2}}(a^\dagger + b^\dagger)$ . We can further simplify the expression in Eq. (A) to

$$\begin{aligned} &= \frac{1}{\sqrt{N}} \sum_{j=0}^N \left( \sum_{n=1}^{\tilde{N}} e^{i\pi nj/\tilde{N}} + \frac{1}{\sqrt{2}} \right) a_j^\dagger \\ &= \frac{1}{\sqrt{N}} \sum_{j=0}^N \left( \frac{N}{2} \delta_{j/2,0} + \frac{1}{\sqrt{2}} \right) a_j^\dagger \end{aligned}$$

If we use the summation representation of the kronecker delta  $\delta_m = \frac{1}{N} \sum_{k=1}^N e^{2\pi \frac{k}{N}(n-m)}$  with  $m = 0$ , we get as our final result

$$\sum_{k_n=0}^{k_{N/2}} a_k^\dagger = \frac{\sqrt{N}}{2} a_0^\dagger + \frac{1}{\sqrt{2N}} \sum_{j=0}^N a_j^\dagger \quad (\text{A.1})$$

A. *Pumping with a forward propagating wave*

and for the other band

$$\sum_{-k_{N/2}}^{k=0} b_k^\dagger = \frac{\sqrt{N}}{2} b_0^\dagger + \frac{1}{\sqrt{2N}} \sum_{j=0}^N b_j^\dagger.$$

## B. Fokker-Planck-equation for the damped harmonic oscillator

We want to give an example on how to obtain a Fokker-Planck-equation through the usage of the P-representation of the density matrix in the master equation in Lindblad form. Therefore, we follow the steps in [49] for the damped harmonic oscillator.

The coherent part of the Lindblad equation in 1.15 is given by the Hamiltonian of an harmonic oscillator

$$H = \omega_0 a^\dagger a \quad (\text{B.1})$$

with frequency  $\omega$ . We want to add two dissipation channels that results from coupling the oscillator to a reservoir. They can be described by the jump operators  $c_1 = \sqrt{\frac{\gamma}{2}}(\bar{n} + 1)a$  and  $c_2 = \sqrt{\bar{n}\frac{\gamma}{2}}a^\dagger$  with  $\bar{n} = \frac{e^{-\hbar\omega/k_b T}}{1 - e^{-\hbar\omega/k_b T}}$ . The constant  $k_b$  is the Boltzmann constant and  $T$  is the temperature.

If we substitute the density matrix by its P-representation Eq. (1.61), we obtain

$$\begin{aligned} \int d^2\alpha |\alpha\rangle \langle\alpha| \frac{\partial}{\partial t} P(\alpha, t) = & \\ \int d^2\alpha |\alpha\rangle \langle\alpha| P(\alpha, t) [-i\omega_0(a^\dagger a |\alpha\rangle \langle\alpha| - |\alpha\rangle \langle\alpha| a^\dagger a) & \\ + \frac{\gamma}{2}(2a |\alpha\rangle \langle\alpha| a^\dagger - a^\dagger a |\alpha\rangle \langle\alpha| - |\alpha\rangle \langle\alpha| a^\dagger a) & \\ + \gamma\bar{n}(a |\alpha\rangle \langle\alpha| a^\dagger + a^\dagger |\alpha\rangle \langle\alpha| a - a^\dagger a |\alpha\rangle \langle\alpha| - |\alpha\rangle \langle\alpha| a^\dagger a)]. & \end{aligned} \quad (\text{B.2})$$

At this point, we need to exchange the operators with the complex numbers  $\alpha, \alpha^*$ . With the definition of the coherent states in (1.44) and their derivatives

$$\frac{\partial}{\partial\alpha} |\alpha\rangle \langle\alpha| = (a^\dagger - \alpha^*) |\alpha\rangle \langle\alpha| \quad (\text{B.3})$$

$$\frac{\partial}{\partial\alpha^*} |\alpha\rangle \langle\alpha| = |\alpha\rangle \langle\alpha| (a - \alpha), \quad (\text{B.4})$$

*B. Fokker-Planck-equation for the damped harmonic oscillator*

we can rewrite (B.2) to

$$\begin{aligned} & \int d^2\alpha |\alpha\rangle \langle\alpha| \frac{\partial}{\partial t} P(\alpha, t) \\ &= \int d^2\alpha |\alpha\rangle \langle\alpha| \left[ \left( \frac{\gamma}{2} + i\omega_0 \right) \frac{\partial}{\partial\alpha} \alpha + \left( \frac{\gamma}{2} - i\omega_0 \right) \frac{\partial}{\partial\alpha^*} \alpha^* + \gamma\bar{n} \frac{\partial^2}{\partial\alpha\partial\alpha^*} \right] P(\alpha, t). \end{aligned} \quad (\text{B.5})$$

We used an integration by part to transfer the partial derivative from  $|\alpha\rangle \langle\alpha|$  to  $P(\alpha, t)$ . We also can drop the boundary terms if  $P(\alpha, t)$  vanished fast enough at infinity. The sufficient condition for (B.5) to be satisfied is the Fokker-Planck-equation for a damped harmonic oscillator:

$$\frac{\partial}{\partial t} P(\alpha, t) = \left[ \left( \frac{\gamma}{2} + i\omega_0 \right) \frac{\partial}{\partial\alpha} \alpha + \left( \frac{\gamma}{2} - i\omega_0 \right) \frac{\partial}{\partial\alpha^*} \alpha^* + \gamma\bar{n} \frac{\partial^2}{\partial\alpha\partial\alpha^*} \right] P(\alpha, t). \quad (\text{B.6})$$

At this point we could insert any test distribution  $P$  for our variational approach and minimize (B.6) in respect to the chosen variational parameters which we discussed in Sec. 3.1.

# Bibliography

- [1] M. Krenn, M. Malik, T. Scheidl, R. Ursin and A. Zeilinger, *Quantum Communication with Photons* (Springer International Publishing, Cham, 2016), pp. 455–482,  
URL: [https://doi.org/10.1007/978-3-319-31903-2\\_18](https://doi.org/10.1007/978-3-319-31903-2_18)
- [2] A. Imamoglu, H. Schmidt, G. Woods and M. Deutsch, *Strongly Interacting Photons in a Nonlinear Cavity*, Phys. Rev. Lett. **79** (1997), pp. 1467–1470,  
URL: <https://link.aps.org/doi/10.1103/PhysRevLett.79.1467>
- [3] S. E. Harris and L. V. Hau, *Nonlinear Optics at Low Light Levels*, Phys. Rev. Lett. **82** (1999), pp. 4611–4614,  
URL: <https://link.aps.org/doi/10.1103/PhysRevLett.82.4611>
- [4] D. E. Chang, V. Vuletić and M. D. Lukin, *Quantum nonlinear optics — photon by photon*, Nature Photonics **8** (2014) (9), pp. 685–694,  
URL: <https://doi.org/10.1038/nphoton.2014.192>
- [5] R. W. Boyd, *Nonlinear Optics, Third Edition*, 3rd ed. (Academic Press, Inc., USA, 2008)
- [6] Q. A. Turchette, C. J. Hood, W. Lange, H. Mabuchi and H. J. Kimble, *Measurement of Conditional Phase Shifts for Quantum Logic*, Phys. Rev. Lett. **75** (1995), pp. 4710–4713,  
URL: <https://link.aps.org/doi/10.1103/PhysRevLett.75.4710>
- [7] K. M. Birnbaum, A. Boca, R. Miller, A. D. Boozer, T. E. Northup and H. J. Kimble, *Photon blockade in an optical cavity with one trapped atom*, Nature **436** (2005) (7047), pp. 87–90,  
URL: <https://doi.org/10.1038/nature03804>
- [8] M. Fleischhauer and M. D. Lukin, *Dark-State Polaritons in Electromagnetically Induced Transparency*, Phys. Rev. Lett. **84** (2000), pp. 5094–5097,  
URL: <https://link.aps.org/doi/10.1103/PhysRevLett.84.5094>

## Bibliography

- [9] I. Friedler, D. Petrosyan, M. Fleischhauer and G. Kurizki, *Long-range interactions and entanglement of slow single-photon pulses*, Phys. Rev. A **72** (2005), p. 043803,  
URL: <https://link.aps.org/doi/10.1103/PhysRevA.72.043803>
- [10] M. D. Lukin, M. Fleischhauer, R. Côté, L. M. Duan, D. Jaksch, J. I. Cirac and P. Zoller, *Dipole Blockade and Quantum Information Processing in Mesoscopic Atomic Ensembles*, Phys. Rev. Lett. **87** (2001) (3), p. 037901
- [11] M. D. Lukin, S. F. Yelin and M. Fleischhauer, *Entanglement of Atomic Ensembles by Trapping Correlated Photon States*, Phys. Rev. Lett. **84** (2000), pp. 4232–4235,  
URL: <https://link.aps.org/doi/10.1103/PhysRevLett.84.4232>
- [12] D. F. Phillips, A. Fleischhauer, A. Mair, R. L. Walsworth and M. D. Lukin, *Storage of Light in Atomic Vapor*, Phys. Rev. Lett. **86** (2001), pp. 783–786,  
URL: <https://link.aps.org/doi/10.1103/PhysRevLett.86.783>
- [13] T. M. Weber, M. Honing, T. Niederprum, T. Manthey, O. Thomas, V. Guarnera, M. Fleischhauer, G. Barontini and H. Ott, *Mesoscopic Rydberg-blockaded ensembles in the superatom regime and beyond*, Nature Phys. **11** (2015), pp. 157–161
- [14] Y. O. Dudin and A. Kuzmich, *Strongly Interacting Rydberg Excitations of a Cold Atomic Gas*, Science **336** (2012), pp. 887–889
- [15] T. Peyronel, O. Firstenberg, Q.-Y. Liang, S. Hofferberth, A. V. Gorshkov, T. Pohl, M. D. Lukin and V. Vuletić, *Quantum nonlinear optics with single photons enabled by strongly interacting atoms*, Nature **488** (2012), pp. 57–60
- [16] J. Stanojevic, V. Parigi, E. Bimbard, A. Ourjoumtsev and P. Grangier, *Dispersive optical nonlinearities in a Rydberg electromagnetically-induced-transparency medium*, Phys. Rev. A **88** (2013), p. 053845,  
URL: <https://link.aps.org/doi/10.1103/PhysRevA.88.053845>
- [17] V. Parigi, E. Bimbard, J. Stanojevic, A. J. Hilliard, F. Nogrette, R. Tualle-Brouri, A. Ourjoumtsev and P. Grangier, *Observation and Measurement of Interaction-Induced Dispersive Optical Nonlinearities in an Ensemble of Cold Rydberg Atoms*, Phys. Rev. Lett. **109** (2012), p. 233602,  
URL: <https://link.aps.org/doi/10.1103/PhysRevLett.109.233602>



- [18] O. Firstenberg, T. Peyronel, Q.-Y. Liang, A. V. Gorshkov, M. D. Lukin and V. Vuletić, *A photon-photon quantum gate based on Rydberg interactions*, *Nature* **502** (2013), pp. 71–75,  
URL: <https://doi.org/10.1038/nature12512>
- [19] S. H. Cantu, A. V. Venkatramani, W. Xu, L. Zhou, B. Jelenković, M. D. Lukin and V. Vuletić, *Repulsive photons in a quantum nonlinear medium*, arXiv:1911.02586 (2019)
- [20] S. Baur, D. Tiarks, G. Rempe and S. Dürr, *Single-Photon Switch Based on Rydberg Blockade*, *Phys. Rev. Lett.* **112** (2014) (7), p. 073901
- [21] H. Gorniaczyk, C. Tresp, J. Schmidt, H. Fedder and S. Hofferberth, *Single-Photon Transistor Mediated by Interstate Rydberg Interactions*, *Phys. Rev. Lett.* **113** (2014) (5), p. 053601
- [22] D. Tiarks, S. Baur, K. Schneider, S. Dürr and G. Rempe, *Single-Photon Transistor Using a Förster Resonance*, *Phys. Rev. Lett.* **113** (2014) (5), p. 053602
- [23] D. Tiarks, S. Schmidt-Eberle, T. Stolz, G. Rempe and S. Däijrr, *A photon-photon quantum gate based on Rydberg interactions*, *Nature Physics* **15** (2019), pp. 124–126,  
URL: <https://doi.org/10.1038/s41567-018-0313-7>
- [24] A. V. Gorshkov, S. R. Manmana, G. Chen, J. Ye, E. Demler, M. D. Lukin and A. M. Rey, *Tunable Superfluidity and Quantum Magnetism with Ultracold Polar Molecules*, *Phys. Rev. Lett.* **107** (2011), p. 115301,  
URL: <http://link.aps.org/doi/10.1103/PhysRevLett.107.115301>
- [25] J. Otterbach, M. Moos, D. Muth and M. Fleischhauer, *Wigner Crystallization of Single Photons in Cold Rydberg Ensembles*, *Phys. Rev. Lett.* **111** (2013), p. 113001,  
URL: <https://link.aps.org/doi/10.1103/PhysRevLett.111.113001>
- [26] P. Bienias, S. Choi, O. Firstenberg, M. F. Maghrebi, M. Gullans, M. D. Lukin, A. V. Gorshkov and H. P. Büchler, *Scattering resonances and bound states for strongly interacting Rydberg polaritons*, *Phys Rev. A* **90** (2014) (5), p. 053804
- [27] M. J. Gullans, J. D. Thompson, Y. Wang, Q.-Y. Liang, V. Vuletić, M. D. Lukin and A. V. Gorshkov, *Effective Field Theory for Rydberg Polaritons*, *Phys. Rev. Lett.* **117** (2016), p. 113601,  
URL: <https://link.aps.org/doi/10.1103/PhysRevLett.117.113601>

## Bibliography

- [28] M. Müller, S. Diehl, G. Pupillo and P. Zoller, *Engineered Open Systems and Quantum Simulations with Atoms and Ions*, in P. Berman, E. Arimondo and C. Lin (eds.), *Advances in Atomic, Molecular, and Optical Physics* (Academic Press, 2012), vol. 61 of *Advances In Atomic, Molecular, and Optical Physics*, pp. 1 – 80,  
URL: <http://www.sciencedirect.com/science/article/pii/B9780123964823000016>
- [29] L. M. Sieberer, M. Buchhold and S. Diehl, *Keldysh field theory for driven open quantum systems*, Rep. Prog. Phys. **79** (2016) (9), p. 096001,  
URL: <http://stacks.iop.org/0034-4885/79/i=9/a=096001>
- [30] H. Weimer, A. Kshetrimayum and R. Orús, *Simulation methods for open quantum many-body systems*, arXiv:1907.07079 (2019)
- [31] V. R. Overbeck, M. F. Maghrebi, A. V. Gorshkov and H. Weimer, *Multicritical behavior in dissipative Ising models*, Phys. Rev. A **95** (2017), p. 042133,  
URL: <https://link.aps.org/doi/10.1103/PhysRevA.95.042133>
- [32] B. M. McCoy and T. T. Wu, *Theory of a Two-Dimensional Ising Model with Random Impurities. I. Thermodynamics*, Phys. Rev. **176** (1968), pp. 631–643,  
URL: <https://link.aps.org/doi/10.1103/PhysRev.176.631>
- [33] S. Sachdev, *Quantum Phase Transitions* (Cambridge University Press, Cambridge, 1999)
- [34] M. F. Maghrebi and A. V. Gorshkov, *Nonequilibrium many-body steady states via Keldysh formalism*, Phys. Rev. B **93** (2016), p. 014307,  
URL: <http://link.aps.org/doi/10.1103/PhysRevB.93.014307>
- [35] E. Schrödinger, *Quantisierung als Eigenwertproblem*, Annalen der Physik **384** (1926) (4), pp. 361–376,  
URL: <https://onlinelibrary.wiley.com/doi/abs/10.1002/andp.19263840404>
- [36] H.-P. Breuer and F. Petruccione, *The Theory of Open Quantum Systems* (Oxford University Press, Oxford, 2002)
- [37] M. Born, E. Wolf, A. B. Bhatia, P. C. Clemmow, D. Gabor, A. R. Stokes, A. M. Taylor, P. A. Wayman and W. L. Wilcock, *Principles of Optics: Electromagnetic Theory of Propagation, Interference and Diffraction of Light*, 7 ed. (Cambridge University Press, 1999)

- [38] W. R. Hamilton and F. Beaufort, *VII. Second essay on a general method in dynamics*, Philosophical Transactions of the Royal Society of London **125** (1835), pp. 95–144,  
URL: <https://royalsocietypublishing.org/doi/abs/10.1098/rstl.1835.0009>
- [39] C. Gignoux and B. Silvestre-Brac, *Hamilton's Principle* (Springer Netherlands, Dordrecht, 2009), pp. 111–164,  
URL: [https://doi.org/10.1007/978-90-481-2393-3\\_3](https://doi.org/10.1007/978-90-481-2393-3_3)
- [40] H. Weimer, *Variational Principle for Steady States of Dissipative Quantum Many-Body Systems*, Phys. Rev. Lett. **114** (2015), p. 040402
- [41] V. R. Overbeck, *Time evolution and steady states of dissipative quantum many-body systems*, Ph.D. thesis, Gottfried Wilhelm Leibniz Universität, Hannover (2018),  
URL: <https://www.repo.uni-hannover.de/handle/123456789/3508?show=full>
- [42] W. Nolting, *Grundkurs Theoretische Physik 3*, Grundkurs Theoretische Physik / Wolfgang Nolting (Springer, 2001)
- [43] D. F. Walls and G. J. Milburn, *Quantum Optics* (Springer, Berlin, 1994)
- [44] B. Varcoe, S. Brattke, B.-G. Englert and H. Walther, *Fock State Rabi Oscillations; A Building Block for the Observation of New Phenomena in Quantum Optics*, Fortschritte der Physik **48** (2000) (5), pp. 679–687,  
URL: <https://onlinelibrary.wiley.com/doi/abs/10.1002/%28SICI%291521-3978%28200005%2948%3A5%2F%3C679%3A%3AAID-PROP679%3E3.0.CO%3B2-L>
- [45] M. W. Reinsch, *A simple expression for the terms in the Baker-Campbell-Hausdorff series*, Journal of Mathematical Physics **41** (2000) (4), pp. 2434–2442,  
URL: <https://doi.org/10.1063/1.533250>
- [46] J. Aasi *et al.*, *Enhanced sensitivity of the LIGO gravitational wave detector by using squeezed states of light*, Nature Photonics **7** (2013) (8), pp. 613–619,  
URL: <https://doi.org/10.1038/nphoton.2013.177>

## Bibliography

- [47] R. J. Glauber, *Coherent and Incoherent States of the Radiation Field*, Phys. Rev. **131** (1963), pp. 2766–2788,  
URL: <https://link.aps.org/doi/10.1103/PhysRev.131.2766>
- [48] E. C. G. Sudarshan, *Equivalence of Semiclassical and Quantum Mechanical Descriptions of Statistical Light Beams*, Phys. Rev. Lett. **10** (1963), pp. 277–279,  
URL: <https://link.aps.org/doi/10.1103/PhysRevLett.10.277>
- [49] H. Carmichael, *Statistical Methods in Quantum Optics 1. Master Equations and Fokker-Planck Equations* (2002)
- [50] M. J. Lighthill, *An Introduction to Fourier Analysis and Generalised Functions*, Cambridge Monographs on Mechanics (Cambridge University Press, 1958)
- [51] H. Bremermann, *Distributions, complex variables, and Fourier transforms* (1965)
- [52] E. Wigner, *On the Quantum Correction For Thermodynamic Equilibrium*, Phys. Rev. **40** (1932), pp. 749–759,  
URL: <https://link.aps.org/doi/10.1103/PhysRev.40.749>
- [53] M. Hillery, R. O’Connell, M. Scully and E. Wigner, *Distribution functions in physics: Fundamentals*, Physics Reports **106** (1984) (3), pp. 121 – 167,  
URL: <http://www.sciencedirect.com/science/article/pii/0370157384901601>
- [54] S. Ryl, J. Sperling and W. Vogel, *Quantifying nonclassicality by characteristic functions*, Phys. Rev. A **95** (2017), p. 053825,  
URL: <https://link.aps.org/doi/10.1103/PhysRevA.95.053825>
- [55] J. Sperling and W. Vogel, *Quasiprobability distributions for quantum-optical coherence and beyond*, Physica Scripta **95** (2020) (3), p. 034007,  
URL: <https://doi.org/10.1088%2F1402-4896%2F95034007>
- [56] R. O’Connell and E. Wigner, *Some properties of a non-negative quantum-mechanical distribution function*, Physics Letters A **85** (1981) (3), pp. 121 – 126,  
URL: <http://www.sciencedirect.com/science/article/pii/0375960181908811>

- [57] A. N. Kolmogorov, *Foundations of the theory of probability.*, Foundations of the theory of probability. (Chelsea Publishing Co., Oxford, England, 1950)
- [58] U. Raitzsch, R. Heidemann, H. Weimer, B. Butscher, P. Kollmann, R. Löw, H. P. Büchler and T. Pfau, *Investigation of dephasing rates in an interacting Rydberg gas*, New J. Phys. **11** (2009) (5), p. 055014,  
URL: <http://stacks.iop.org/1367-2630/11/055014>
- [59] C. Carr, R. Ritter, C. G. Wade, C. S. Adams and K. J. Weatherill, *Nonequilibrium Phase Transition in a Dilute Rydberg Ensemble*, Phys. Rev. Lett. **111** (2013), p. 113901
- [60] N. Malossi, M. M. Valado, S. Scotto, P. Huillery, P. Pillet, D. Ciampini, E. Arimondo and O. Morsch, *Full Counting Statistics and Phase Diagram of a Dissipative Rydberg Gas*, Phys. Rev. Lett. **113** (2014), p. 023006
- [61] H. Schempp, G. Günter, M. Robert-de Saint-Vincent, C. S. Hofmann, D. Breyel, A. Komnik, D. W. Schönleber, M. Gärttner, J. Evers, S. Whitlock and M. Weidemüller, *Full Counting Statistics of Laser Excited Rydberg Aggregates in a One-Dimensional Geometry*, Phys. Rev. Lett. **112** (2014), p. 013002
- [62] A. Urvoy, F. Ripka, I. Lesanovsky, D. Booth, J. P. Shaffer, T. Pfau and R. Löw, *Strongly Correlated Growth of Rydberg Aggregates in a Vapor Cell*, Phys. Rev. Lett. **114** (2015), p. 203002,  
URL: <http://link.aps.org/doi/10.1103/PhysRevLett.114.203002>
- [63] E. A. Goldschmidt, T. Boulier, R. C. Brown, S. B. Koller, J. T. Young, A. V. Gorshkov, S. L. Rolston and J. V. Porto, *Anomalous Broadening in Driven Dissipative Rydberg Systems*, Phys. Rev. Lett. **116** (2016), p. 113001,  
URL: <http://link.aps.org/doi/10.1103/PhysRevLett.116.113001>
- [64] T. E. Lee, H. Häffner and M. C. Cross, *Antiferromagnetic phase transition in a nonequilibrium lattice of Rydberg atoms*, Phys. Rev. A **84** (2011), p. 031402,  
URL: <http://link.aps.org/doi/10.1103/PhysRevA.84.031402>
- [65] J. Honer, R. Löw, H. Weimer, T. Pfau and H. P. Büchler, *Artificial Atoms Can Do More Than Atoms: Deterministic Single Photon Subtraction from Arbitrary Light Fields*, Phys. Rev. Lett. **107** (2011), p. 093601
- [66] A. W. Glaetzle, R. Nath, B. Zhao, G. Pupillo and P. Zoller, *Driven-dissipative dynamics of a strongly interacting Rydberg gas*, Phys. Rev. A **86** (2012), p.

## Bibliography

- 043403,  
URL: <http://link.aps.org/doi/10.1103/PhysRevA.86.043403>
- [67] C. Ates, B. Olmos, W. Li and I. Lesanovsky, *Dissipative Binding of Lattice Bosons through Distance-Selective Pair Loss*, Phys. Rev. Lett. **109** (2012), p. 233003,  
URL: <http://link.aps.org/doi/10.1103/PhysRevLett.109.233003>
- [68] M. Lemeshko, N. Y. Yao, A. V. Gorshkov, H. Weimer, S. D. Bennett, T. Momose and S. Gopalakrishnan, *Controllable quantum spin glasses with magnetic impurities embedded in quantum solids*, Phys. Rev. B **88** (2013), p. 014426,  
URL: <http://link.aps.org/doi/10.1103/PhysRevB.88.014426>
- [69] A. Hu, T. E. Lee and C. W. Clark, *Spatial correlations of one-dimensional driven-dissipative systems of Rydberg atoms*, Phys. Rev. A **88** (2013), p. 053627,  
URL: <http://link.aps.org/doi/10.1103/PhysRevA.88.053627>
- [70] M. Hoening, W. Abdussalam, M. Fleischhauer and T. Pohl, *Antiferromagnetic long-range order in dissipative Rydberg lattices*, Phys. Rev. A **90** (2014), p. 021603,  
URL: <http://link.aps.org/doi/10.1103/PhysRevA.90.021603>
- [71] J. Otterbach and M. Lemeshko, *Dissipative Preparation of Spatial Order in Rydberg-Dressed Bose-Einstein Condensates*, Phys. Rev. Lett. **113** (2014), p. 070401,  
URL: <http://link.aps.org/doi/10.1103/PhysRevLett.113.070401>
- [72] J. Sanders, R. van Bijnen, E. Vredenbregt and S. Kokkelmans, *Wireless Network Control of Interacting Rydberg Atoms*, Phys. Rev. Lett. **112** (2014), p. 163001,  
URL: <http://link.aps.org/doi/10.1103/PhysRevLett.112.163001>
- [73] M. Marcuzzi, E. Levi, S. Diehl, J. P. Garrahan and I. Lesanovsky, *Universal Nonequilibrium Properties of Dissipative Rydberg Gases*, Phys. Rev. Lett. **113** (2014), p. 210401,  
URL: <http://link.aps.org/doi/10.1103/PhysRevLett.113.210401>
- [74] R. Löw, H. Weimer, J. Nipper, J. B. Balewski, B. Butscher, H. P. Büchler and T. Pfau, *An Experimental and Theoretical Guide to Strongly Interacting Rydberg Gases*, J. Phys. B: At. Mol. Opt. Phys. (2012)

- [75] T. F. Gallagher, *Rydberg Atoms* (Cambridge University Press, Cambridge, 1994)
- [76] R. J. LeRoy, *Long-Range Potential Coefficients From RKR Turning Points:  $C_6$  and  $C_8$  for  $B(3\Pi_{O_u}^+)$ -State  $\text{Cl}_2$ ,  $\text{Br}_2$ , and  $\text{I}_2$* , Can. J. Phys. **52** (1974), pp. 246–256
- [77] R. Grimm, M. WeidemÄijller and Y. B. Ovchinnikov, *Optical Dipole Traps for Neutral Atoms* (Academic Press, 2000), vol. 42 of *Advances In Atomic, Molecular, and Optical Physics*, pp. 95 – 170,  
URL: <http://www.sciencedirect.com/science/article/pii/S1049250X0860186X>
- [78] S. Peil, J. V. Porto, B. L. Tolra, J. M. Obrecht, B. E. King, M. Subbotin, S. L. Rolston and W. D. Phillips, *Patterned loading of a Bose-Einstein condensate into an optical lattice*, Phys. Rev. A **67** (2003), p. 051603,  
URL: <https://link.aps.org/doi/10.1103/PhysRevA.67.051603>
- [79] Z. Hadzibabic, S. Stock, B. Battelier, V. Bretin and J. Dalibard, *Interference of an Array of Independent Bose-Einstein Condensates*, Phys. Rev. Lett. **93** (2004), p. 180403,  
URL: <https://link.aps.org/doi/10.1103/PhysRevLett.93.180403>
- [80] T. Pistorius, J. Kazemi and H. Weimer, *Quantum many-body dynamics of driven-dissipative Rydberg polaritons* (in print)
- [81] I. Iakoupov, J. R. Ott, D. E. Chang and A. S. Sørensen, *Dispersion relations for stationary light in one-dimensional atomic ensembles*, Phys. Rev. A **94** (2016) (5), p. 053824
- [82] D. Jaksch, C. Bruder, J. I. Cirac, C. W. Gardiner and P. Zoller, *Cold Bosonic Atoms in Optical Lattices*, Phys. Rev. Lett. **81** (1998) (15), pp. 3108–3111
- [83] M. Mašalas and M. Fleischhauer, *Scattering of dark-state polaritons in optical lattices and quantum phase gate for photons*, Phys. Rev. A **69** (2004), p. 061801(R),  
URL: <https://link.aps.org/doi/10.1103/PhysRevA.69.061801>
- [84] D. B. Branden, T. Juhasz, T. Mahlokozera, C. Vesa, R. O. Wilson, M. Zheng, A. Kortyna and D. A. Tate, *Radiative lifetime measurements of rubidium Rydberg states*, Journal of Physics B: Atomic, Molecular and Optical Physics **43**

## Bibliography

- (2009) (1), p. 015002,  
URL: <https://doi.org/10.1088%2F0953-4075%2F43%2F1%2F015002>
- [85] T. Caneva, M. T. Manzoni, T. Shi, J. S. Douglas, J. I. Cirac and D. E. Chang, *Quantum dynamics of propagating photons with strong interactions: a generalized input–output*, New Journal of Physics **17** (2015) (11), p. 113001
- [86] C. W. Gardiner and M. J. Collett, *Input and output in damped quantum systems: Quantum stochastic differential equations and the master equation*, Physical Review A **31** (1985) (6), p. 3761
- [87] M. Moos, M. Hönig, R. Unanyan and M. Fleischhauer, *Many-body physics of Rydberg dark-state polaritons in the strongly interacting regime*, PhyPhys. Rev. A, **92** (2015) (5), p. 053846
- [88] M. Viteau, M. G. Bason, J. Radogostowicz, N. Malossi, D. Ciampini, O. Morsch and E. Arimondo, *Rydberg atoms in one-dimensional optical lattices* (2011)
- [89] J. Johansson, P. Nation and F. Nori, *QuTiP: An open-source Python framework for the dynamics of open quantum systems*, Comp. Phys. Comm. **183** (2012) (8), pp. 1760 – 1772,  
URL: <http://www.sciencedirect.com/science/article/pii/S0010465512000835>
- [90] J. Johansson, P. Nation and F. Nori, *QuTiP 2: A Python framework for the dynamics of open quantum systems*, Comp. Phys. Comm. **184** (2013) (4), pp. 1234–1240,  
URL: <http://www.sciencedirect.com/science/article/pii/S0010465512003955>
- [91] K. Mølmer, Y. Castin and J. Dalibard, *Monte Carlo wave-function method in quantum optics*, J. Opt. Soc. Am. B **10** (1993) (3), pp. 524–538
- [92] V. R. Overbeck and H. Weimer, *Time evolution of open quantum many-body systems*, Phys. Rev. A **93** (2016), p. 012106,  
URL: <http://link.aps.org/doi/10.1103/PhysRevA.93.012106>
- [93] H. Weimer, R. Löw, T. Pfau and H. P. Büchler, *Quantum critical behavior in strongly interacting Rydberg gases*, Phys. Rev. Lett. **101** (2008), p. 250601
- [94] M. Raghunandan, J. Wrachtrup and H. Weimer, *High-density quantum sensing with dissipative first order transitions*, arXiv:1703.07358 (2017)



- [95] M. Fleischhauer, A. Imamoglu and J. P. Marangos, *Electromagnetically induced transparency: Optics in coherent media*, Rev. Mod. Phys. **77** (2005) (2), pp. 633–673
- [96] M. O. Scully and M. S. Zubairy, *Quantum Optics* (Cambridge University Press, 1997)
- [97] C. W. Gardiner and P. Zoller, *Quantum Noise*, second ed. (Springer, 2000)
- [98] C. Gardiner and P. Zoller, *Quantum Noise* (Springer-Verlag, Berlin Heidelberg, 2004)
- [99] E. Zeuthen, M. J. Gullans, M. F. Maghrebi and A. V. Gorshkov, *Correlated Photon Dynamics in Dissipative Rydberg Media*, Phys. Rev. Lett. **119** (2017), p. 043602,  
URL: <https://link.aps.org/doi/10.1103/PhysRevLett.119.043602>
- [100] E. T. Jaynes and F. W. Cummings, *Comparison of quantum and semiclassical radiation theories with application to the beam maser*, Proc. IEEE **51** (1963) (1), pp. 89–109
- [101] R. Bonifacio, L. M. Narducci and E. Montaldi, *Conditions for Existence of a Diagonal Representation for Quantum Mechanical Operators*, Phys. Rev. Lett. **16** (1966), pp. 1125–1127,  
URL: <https://link.aps.org/doi/10.1103/PhysRevLett.16.1125>
- [102] P. Marian and T. A. Marian, *Destruction of higher-order squeezing by thermal noise*, Journal of Physics A: Mathematical and General **29** (1996) (19), pp. 6233–6245,  
URL: <https://doi.org/10.1088%2F0305-4470%2F29%2F19%2F009>
- [103] A. Isar, W. Scheid and A. Sandulescu, *Quasiprobability distributions for open quantum systems within the Lindblad theory*, Journal of Mathematical Physics **32** (1991) (8), pp. 2128–2134,  
URL: <https://doi.org/10.1063/1.529185>
- [104] T. Kiesel, W. Vogel, B. Hage, J. DiGuglielmo, A. Sambrowski and R. Schnabel, *Experimental test of nonclassicality criteria for phase-diffused squeezed states*, Phys. Rev. A **79** (2009), p. 022122,  
URL: <https://link.aps.org/doi/10.1103/PhysRevA.79.022122>

## Bibliography

- [105] H. J. Carmichael, *Breakdown of Photon Blockade: A Dissipative Quantum Phase Transition in Zero Dimensions*, Phys. Rev. X **5** (2015), p. 031028, URL: <https://link.aps.org/doi/10.1103/PhysRevX.5.031028>
- [106] T. K. Mavrogordatos, *Quantum phase transitions in the driven dissipative Jaynes-Cummings oscillator: From the dispersive regime to resonance*, EPL (Europhysics Letters) **116** (2016) (5), p. 54001, URL: <https://doi.org/10.1209%2F0295-5075%2F116%2F54001>
- [107] C. Di Castro and R. Raimondi, *Statistical Mechanics and Applications in Condensed Matter* (Cambridge University Press, 2015)
- [108] S. Ryl, J. Sperling, E. Agudelo, M. Mraz, S. Köhnke, B. Hage and W. Vogel, *Unified nonclassicality criteria*, Phys. Rev. A **92** (2015), p. 011801, URL: <https://link.aps.org/doi/10.1103/PhysRevA.92.011801>
- [109] M. Bohmann, E. Agudelo and J. Sperling, *Probing nonclassicality with matrices of phase-space distributions* (2020)
- [110] J. J. Sanchez-Mondragon, N. B. Narozhny and J. H. Eberly, *Theory of Spontaneous-Emission Line Shape in an Ideal Cavity*, Phys. Rev. Lett. **51** (1983), pp. 550–553, URL: <https://link.aps.org/doi/10.1103/PhysRevLett.51.550>
- [111] Y. Zhu, D. J. Gauthier, S. E. Morin, Q. Wu, H. J. Carmichael and T. W. Mossberg, *Vacuum Rabi splitting as a feature of linear-dispersion theory: Analysis and experimental observations*, Phys. Rev. Lett. **64** (1990), pp. 2499–2502, URL: <https://link.aps.org/doi/10.1103/PhysRevLett.64.2499>
- [112] Y.-Y. Zhang, Q.-H. Chen and S.-Y. Zhu, *Vacuum Rabi Splitting and Dynamics of the Jaynes—Cummings Model for Arbitrary Coupling*, Chinese Physics Letters **30** (2013) (11), p. 114203, URL: <https://doi.org/10.1088%2F0256-307x%2F30%2F11%2F114203>
- [113] G. S. Agarwal, *Vacuum-Field Rabi Splittings in Microwave Absorption by Rydberg Atoms in a Cavity*, Phys. Rev. Lett. **53** (1984), pp. 1732–1734, URL: <https://link.aps.org/doi/10.1103/PhysRevLett.53.1732>
- [114] G. S. Agarwal, *Vacuum-field Rabi oscillations of atoms in a cavity*, J. Opt. Soc. Am. B **2** (1985) (3), pp. 480–485, URL: <http://josab.osa.org/abstract.cfm?URI=josab-2-3-480>

- [115] A. Grankin, E. Brion, E. Bimbard, R. Boddeda, I. Usmani, A. Ourjoumtsev and P. Grangier, *Quantum statistics of light transmitted through an intracavity Rydberg medium*, New Journal of Physics **16** (2014) (4), p. 043020,  
URL: <https://doi.org/10.1088%2F1367-2630%2F16%2F4%2F043020>
- [116] A. Grankin, E. Brion, E. Bimbard, R. Boddeda, I. Usmani, A. Ourjoumtsev and P. Grangier, *Quantum-optical nonlinearities induced by Rydberg-Rydberg interactions: A perturbative approach*, Phys. Rev. A **92** (2015), p. 043841,  
URL: <https://link.aps.org/doi/10.1103/PhysRevA.92.043841>
- [117] H. A. M. Leymann, A. Foerster and J. Wiersig, *Expectation value based cluster expansion*, physica status solidi c **10** (2013) (9), pp. 1242–1245,  
URL: <https://onlinelibrary.wiley.com/doi/abs/10.1002/pssc.201200711>
- [118] H. A. M. Leymann, A. Foerster and J. Wiersig, *Expectation value based equation-of-motion approach for open quantum systems: A general formalism*, Phys. Rev. B **89** (2014), p. 085308,  
URL: <https://link.aps.org/doi/10.1103/PhysRevB.89.085308>
- [119] H. Schoeller, *A New Transport Equation for Single-Time Green's Functions in an Arbitrary Quantum System. General Formalism*, Annals of Physics **229** (1994) (2), pp. 273 – 319,  
URL: <http://www.sciencedirect.com/science/article/pii/S0003491684710098>
- [120] P. Marian, *Higher-order squeezing properties and correlation functions for squeezed number states*, Phys. Rev. A **44** (1991), pp. 3325–3330,  
URL: <https://link.aps.org/doi/10.1103/PhysRevA.44.3325>
- [121] M. S. Kim, F. A. M. de Oliveira and P. L. Knight, *The Squeezing of Fock and Thermal Field States*, in J. H. Eberly, L. Mandel and E. Wolf (eds.), *Coherence and Quantum Optics VI* (Springer US, Boston, MA, 1989), pp. 601–605
- [122] M. S. Kim, F. A. M. de Oliveira and P. L. Knight, *Properties of squeezed number states and squeezed thermal states*, Phys. Rev. A **40** (1989), pp. 2494–2503,  
URL: <https://link.aps.org/doi/10.1103/PhysRevA.40.2494>
- [123] P. Marian and T. A. Marian, *Squeezed states with thermal noise. I. Photon-number statistics*, Phys. Rev. A **47** (1993), pp. 4474–4486,  
URL: <https://link.aps.org/doi/10.1103/PhysRevA.47.4474>

## Bibliography

- [124] R. A. Brewster and J. D. Franson, *Generalized delta functions and their use in quantum optics*, Journal of Mathematical Physics **59** (2018) (1), p. 012102, URL: <https://doi.org/10.1063/1.4985938>
- [125] M. Hillery, *Amplitude-squared squeezing of the electromagnetic field*, Phys. Rev. A **36** (1987), pp. 3796–3802, URL: <https://link.aps.org/doi/10.1103/PhysRevA.36.3796>
- [126] J. A. Bergou, M. Hillery and D. Yu, *Minimum uncertainty states for amplitude-squared squeezing: Hermite polynomial states*, Phys. Rev. A **43** (1991) (1), pp. 515–520
- [127] T. R. Tan, J. P. Gaebler, Y. Lin, Y. Wan, R. Bowler, D. Leibfried and D. J. Wineland, *Multi-element logic gates for trapped-ion qubits*, Nature **528** (2015) (7582), pp. 380–383, URL: [http://www.nature.com/nature/journal/v528/n7582/full/nature16186.html?WT.ec\\_id=NATURE-20151217&spMailingID=50271052&spUserID=MjA1NTA5MDEyMwS2&spJobID=822569676&spReportId=ODIyNTY5Njc2S0](http://www.nature.com/nature/journal/v528/n7582/full/nature16186.html?WT.ec_id=NATURE-20151217&spMailingID=50271052&spUserID=MjA1NTA5MDEyMwS2&spJobID=822569676&spReportId=ODIyNTY5Njc2S0)
- [128] G. S. Agarwal and K. Tara, *Nonclassical character of states exhibiting no squeezing or sub-Poissonian statistics*, Phys. Rev. A **46** (1992), pp. 485–488, URL: <https://link.aps.org/doi/10.1103/PhysRevA.46.485>
- [129] A. Zavatta, V. Parigi and M. Bellini, *Experimental nonclassicality of single-photon-added thermal light states*, Phys. Rev. A **75** (2007), p. 052106, URL: <https://link.aps.org/doi/10.1103/PhysRevA.75.052106>
- [130] S. M. Barnett, G. Ferenczi, C. R. Gilson and F. C. Speirits, *Statistics of photon-subtracted and photon-added states*, Phys. Rev. A **98** (2018), p. 013809, URL: <https://link.aps.org/doi/10.1103/PhysRevA.98.013809>
- [131] N. Syassen, D. M. Bauer, M. Lettner, T. Volz, D. Dietze, J. J. García-Ripoll, J. I. Cirac, G. Rempe and S. Dürr, *Strong Dissipation Inhibits Losses and Induces Correlations in Cold Molecular Gases*, Science **320** (2008) (5881), pp. 1329–1331, URL: <http://www.sciencemag.org/content/320/5881/1329.abstract>
- [132] K. Baumann, C. Guerlin, F. Brennecke and T. Esslinger, *Dicke quantum phase transition with a superfluid gas in an optical cavity*, Nature **464** (2010), pp. 1301–1306

- [133] J. T. Barreiro, M. Müller, P. Schindler, D. Nigg, T. Monz, M. Chwalla, M. Hennrich, C. F. Roos, P. Zoller and R. Blatt, *An open-system quantum simulator with trapped ions*, Nature **470** (2011), p. 486
- [134] H. Krauter, C. A. Muschik, K. Jensen, W. Wasilewski, J. M. Petersen, J. I. Cirac and E. S. Polzik, *Entanglement Generated by Dissipation and Steady State Entanglement of Two Macroscopic Objects*, Phys. Rev. Lett. **107** (2011), p. 080503,  
URL: <http://link.aps.org/doi/10.1103/PhysRevLett.107.080503>
- [135] G. Barontini, R. Labouvie, F. Stubenrauch, A. Vogler, V. Guarrera and H. Ott, *Controlling the Dynamics of an Open Many-Body Quantum System with Localized Dissipation*, Phys. Rev. Lett. **110** (2013), p. 035302,  
URL: <http://link.aps.org/doi/10.1103/PhysRevLett.110.035302>
- [136] S. Diehl, A. Micheli, A. Kantian, B. Kraus, H. P. Büchler and P. Zoller, *Quantum states and phases in driven open quantum systems with cold atoms*, Nature Phys. **4** (2008), pp. 878–883
- [137] A. Sørensen and K. Mølmer, *Quantum Computation with Ions in Thermal Motion*, Phys. Rev. Lett. **82** (1999), pp. 1971–1974,  
URL: <https://link.aps.org/doi/10.1103/PhysRevLett.82.1971>
- [138] G. Zarantonello, H. Hahn, J. Morgner, M. Schulte, A. Bautista-Salvador, R. F. Werner, K. Hammerer and C. Ospelkaus, *Robust and Resource-Efficient Microwave Near-Field Entangling  ${}^9\text{Be}^+$  Gate*, Phys. Rev. Lett. **123** (2019), p. 260503,  
URL: <https://link.aps.org/doi/10.1103/PhysRevLett.123.260503>
- [139] A. Bautista-Salvador, G. Zarantonello, H. Hahn, A. Preciado-Grijalva, J. Morgner, M. Wahnschaffe and C. Ospelkaus, *Multilayer ion trap technology for scalable quantum computing and quantum simulation*, New Journal of Physics **21** (2019) (4), p. 043011,  
URL: <https://doi.org/10.1088%2F1367-2630%2F190404301>
- [140] A. Mitra, M. J. Martin, G. W. Biedermann, A. M. Marino, P. M. Poggi and I. H. Deutsch, *Robust Mølmer-Sørensen gate for neutral atoms using rapid adiabatic Rydberg dressing*, Phys. Rev. A **101** (2020), p. 030301,  
URL: <https://link.aps.org/doi/10.1103/PhysRevA.101.030301>
- [141] V. R. Overbeck, M. F. Maghrebi, A. V. Gorshkov and H. Weimer, *Multicritical behavior in dissipative Ising models*, arXiv:1606.08863 (2016)

## Bibliography

- [142] L. Landau, *On the Theory of Phase Transitions*, Ukr. J. Phys. **53** (2008), pp. 25–35, originally published in Zh. Eksp. Teor. Fiz. 7, 19–32 (1937)
- [143] N. Goldenfeld, *Lectures on Phase Transitions and the Renormalization Group* (Perseus Books, Reading, 1992)
- [144] P. Ehrenfest, *Phasenumwandlungen im ueblichen und erweiterten Sinn, clasifiziert nach den entsprechenden Singularitaeten des thermodynamischen Potentiales* (NV Noord-Hollandsche Uitgevers Maatschappij, 1933)
- [145] J. I. Cirac and P. Zoller, *Quantum Computations with Cold Trapped Ions*, Phys. Rev. Lett. **74** (1995), pp. 4091–4094,  
URL: <https://link.aps.org/doi/10.1103/PhysRevLett.74.4091>
- [146] H. Hahn, G. Zarantonello, M. Schulte, A. Bautista-Salvador, K. Hammerer and C. Ospelkaus, *Integrated  $9\text{Be}+$  multi-qubit gate device for the ion-trap quantum computer*, npj Quantum Information **5** (2019) (1), p. 70,  
URL: <https://doi.org/10.1038/s41534-019-0184-5>
- [147] M. H. Levitt and R. Freeman, *NMR population inversion using a composite pulse*, Journal of Magnetic Resonance (1969) **33** (1979) (2), pp. 473 – 476,  
URL: <http://www.sciencedirect.com/science/article/pii/0022236479902658>
- [148] L. Viola, E. Knill and S. Lloyd, *Dynamical Decoupling of Open Quantum Systems*, Phys. Rev. Lett. **82** (1999), pp. 2417–2421,  
URL: <https://link.aps.org/doi/10.1103/PhysRevLett.82.2417>
- [149] T. Ruster, C. T. Schmiegelow, H. Kaufmann, C. Warschburger, F. Schmidt-Kaler and U. G. Poschinger, *A long-lived Zeeman trapped-ion qubit*, Applied Physics B **122** (2016) (10), p. 254,  
URL: <https://doi.org/10.1007/s00340-016-6527-4>

## Acknowledgement

Ich möchte dieses letztes Kapitel dazu nutzen, meine Dankbarkeit den Menschen gegenüber auszusprechen, ohne die diese These nicht möglich gewesen wäre. Zu allererst muss hier Hendrik Weimer genannt werden. Ohne ihn hätte ich dies hier nicht verwirklichen können. Seine Einsichten in die Physik waren von unschätzbaren Wert in den vergangenen Jahren. Sein Umgang mit schwierigen Situationen finde ich bewunderswert und hat mich aus manch schwieriger Lage gerettet, wofür ich ihm nochmal im besonderen Rahmen danken möchte.

Mein Dank geht auch an meine beiden Referees, Michael Fleischhauer und Klemens Hammerer, raus, die sich extra Zeit genommen haben um diese Arbeit zu evaluieren. Hierbei sei auch Christian Ospelkaus genannt, der sich bereit erklärt hatte die Chairperson für die Verteidigung zu sein. Die finanzielle Unterstützung durch die Volkswagen Foundation und des SFB DQ-mat sollen an dieser Stelle auch nicht unerwähnt bleiben, da sie meine Forschungen ermöglichten.

Die großartige Zusammenarbeit mit klugen Köpfen wie Jingtao Fan und Dr. Zaran-tonello erweiterten mein Wissen über die theoretische aber auch der experimentellen Welt der Physik. Insbesondere sei hier mein Besuch in Stuttgart bei Prof. Dr. Hans Peter Büchler erwähnt und die daraus resultierenden Diskussionen. Viele Menschen am Institut wurden im Laufe der Jahre zu mehr als Kollegen mit denen man über die Physik diskutiert sondern auch zu Freunden mit denen Mann anstoßen kann oder von denen man bei bestimmten Spielen feststellt wie erschreckend gut sie lügen können. Insbesondere aus den Arbeitsgruppen Weimer/Santos werden mir viele Menschen in Erinnerung bleiben wie Vincent, Maryam, Lorenzo, Javad, Amit, Arya, Lars und noch viele Weitere. Die Freundschaften außerhalb des Instituts sind mir auch immer sehr wichtig gewesen, da sie mir immer wieder den benötigten Abstand zu meiner Arbeit erlaubten. Meiner Office Kollegin Meghana gilt ein besonderer Dank, da sie mich nicht nur mit einer Engelsgeduld die letzten Jahre ertragen hat, sondern mir auch immer mit Rat und Tat zur Seite stand.

Ich werde niemals in der Lage meinen Eltern die Erkenntlichkeit zukommen zu lassen, die sie verdient haben für ihre Unterstützung und Liebe. Ich weiß, dass mein Bruder und meine Eltern immer für mich da sein werden, was mir eine unbezahlbare Sicherheit in meinem Leben gab und geben wird.

Meine Abschlussworte möchte ich der Person widmen, die während der ganzen Zeit an meiner Seite war, egal ob es gut oder schlecht lief. Martha hat mich die letzten 5 Jahre bei allem begleitet und unterstützt, was auch immer auf mich zu kam. Sie war nicht nur immer wissbegierig, was genau ich hier gemacht habe, sondern hatte auch immer ein Ohr für auftretende Probleme. Ich bin dankbar diese Frau an meiner

## *Bibliography*

Seite zu wissen und das auch für die nächsten Etappen unseres Lebens.



# Publications

Parts of the content of this thesis has been published previously in the following manuscripts:

- Tim Pistorius, Javad Kazemi and Hendrik Weimer  
"Quantum many-body dynamics of driven-dissipative Rydberg polaritons"  
arXiv: 2003.10463, in print, Phys Rev. Lett.
  
- Tim Pistorius and Hendrik Weimer  
"Variational analysis of driven-dissipative bosonic fields"  
arXiv: 2011.13746, submitted to Phys, Rev. A



# Curriculum vitae

## Personal details

Tim Pistorius

Innersteweg 2, 30419 Hannover

Date of birth: 28.01.1991 in Schönebeck

E-mail: pistorius.tim@gmail.com

Mobile: +(49) 1573/7984841

## Education

10/2015 -04/2020: Doctoral student in Physics, Leibniz University Hannover

10/2009 - 09/2015: Diploma in Physics, Otto-von-Guericke-University, Magdeburg

2003 - 2009: Abitur, Dr.-Carl-Hermann-Gymnasium, Schönebeck



# Selbstständigkeitserklärung

Hiermit erkläre ich, dass ich die vorliegende Arbeit selbstständig und ohne fremde Hilfe verfasst und keine anderen Hilfsmittel als angegeben verwendet habe. Insbesondere versichere ich, dass ich alle wörtlichen und sinngemäßen Übernahmen aus anderen Werken als solche kenntlich gemacht habe.

Hannover, April 8, 2021  
Tim Pistorius